UNIVERSIDADE ESTADUAL PAULISTA ‘‘JÚLIO DE MESQUITA FILHO’’
FACULDADE DE ENGENHARIA DE ILHA SOLTEIRA
DEPARTAMENTO DE ENGENHARIA MECÂNICA

Oscar Scussel

ON THE USE OF VOLTERRA SERIES IN STRUCTURAL DYNAMICS: CONTRIBUTIONS FROM INPUT-OUTPUT TO OUTPUT-ONLY ANALYSIS AND IDENTIFICATION

ILHA SOLTEIRA
2017

OSCAR SCUSSEL

ON THE USE OF VOLTERRA SERIES IN STRUCTURAL DYNAMICS: CONTRIBUTIONS FROM INPUT-OUTPUT TO OUTPUT-ONLY ANALYSIS AND IDENTIFICATION

Thesis presented to the Faculdade de Engenharia de Ilha Solteira - UNESP as a part of the requirements for obtaining the Doctorate in Mechanical Engineering.
Knowledge area: Solid Mechanics.

Prof. Dr. Samuel da Silva
Advisor

ILHA SOLTEIRA

2017

FICHA CATALOGRÁFICA
Desenvolvido pelo Serviço Técnico de Biblioteca e Documentação

Scussel, Oscar.
S437u On the use of Volterra series in structural dynamics: contributions from input-output to output-only analysis and identification / Oscar Scussel. -- Ilha Solteira: [s.n.], 2017
141 f. : il.

Tese (doutorado) - Universidade Estadual Paulista. Faculdade de Engenharia de Ilha Solteira. Área de conhecimento: Mecânica dos Sólidos, 2017

Orientador: Samuel da Silva
Inclui bibliografia

1. Nonlinear systems. 2. Structural dynamics. 3. Volterra series. 4. Output-only identification. 5. Modal analysis. 6. Higher-Order Frequency Response Functions (HOFRFS).

unesp

UNIVERSIDADE ESTADUAL PAULISTA

Câmpus de Ilha Solteira

CERTIFICADO DE APROVAÇÃO

TÍTULO DA TESE: On the Use of Volterra Series in Structural Dynamics: Contributions From Input-Output to Output-Only Analysis and Identification

AUTOR: OSCAR SCUSSEL
ORIENTADOR: SAMUEL DA SILVA

Aprovado como parte das exigências para obtenção do Título de Doutor em ENGENHARIA MECÂNICA, área: MECANICA DOS SÓLIDOS pela Comissão Examinadora:

Prof. Dr. SAMUEL DA SILVA
Departamento de Engenharia Mecânica / Faculdade de Engenharia de Ilha Solteira

Prof. Dr. JOAO ANTONIO PEREIRA
Departamento de Engenharia Mecânica / Faculdade de Engenharia de Ilha Solteira

Prof. Dr. MILTON DIAS JUNIOR
Departamento de Sistemas Integrados / Universidade Estadual de Campinas - UNICAMP

Prof. Dr. AMERICO BARBOSA DA CUNHA JUNIOR
Instituto de Matemática e Estatística / Universidade do Estado do Rio de Janeiro - UERJ

Prof. Dr. JOSÉ ROBERTO DE FRANÇA ARRUDA
Departamento de Mecanica Computacional / Universidade Estadual de Campinas - UNICAMP

Ilha Solteira, 27 de março de 2017

To my family and friends.

Acknowledgments

I will give thanks to Prof. Samuel da Silva for his helpful guidance throughout the PhD thesis and the last 6 years of friendship. I am grateful for this opportunity, and the new encountered knowledge for modelling, identification and design of nonlinear system in structural dynamics problems has been educational and challenging.

To my mother Lucila Gonçalves and my siblings, Benhur, Carmelita, Lohaine and João Paulo that provided constant support for motivating me to go ahead and to achieve my goals even if they seem to be too far.

I have received generous support from Profs. Michael J. Brennan and João Antonio Pereira from UNESP/Ilha Solteira who contributed to this thesis with many advices and questions, which is highly appreciated. Thanks for your open door and willingness to help.

Equally, I would like to thank professors Spilios D. Fassois and John S. Sakellariou from Univestity of Patras for the period of research internship in the Laboratory of Stochastic Mechanical Systems & Automation (SMSA) and for the advices and support. An additional thanks are going to the colleagues in SMSA lab and Ms. Toula Katopodi, who provided support and reports I needed. I appreciated your fast email answers and willingness to help. Also, I would like to thank all my friends from Greece who made my Stay in Patras so special.

I would also like to thank fellow students and colleagues from the Group of Intelligent Materials and Systems (GMSInt), the Mechanical Engineering Department and to all the technical staff from UNESP/Ilha Solteira. A special word of thanks to all my friends from the "República Monte Olimpo".

Finally, I would also like to thank the São Paulo Research Foundation (FAPESP) by grant number 12/09135-3 and National Council for Scientific and Technological Development (CNPq) under grants numbers 47058/2012-0 and 203610/2014-8 (my research internship abroad in Patras, Greece.). Furthermore, I would like to thank the scholarship and financial support from the Coordination for the Improvement of Higher Education Personnel (CAPES).


FAPESP


CNPq
Conselho Nacional de Desenvolvimento
Científico e Tecnológico


inct
institutos nacionais
de ciência e tecnologia


CIÊNCIA
SEM FRONTEIRAS


SMSA
Stochastic Mechanical Systems & Automation


ΠΑΝΕΠΙΣΤΗΜΙΟ
ΠΑΤΡΩΝ
UNIVERSITY OF PATRAS


unesp
UNIVERSIDADE ESTADUAL PAULISTA
"JÚLIO DE MESQUITA FILHO"


GMSINT
GRUPO DE MATERIAIS E SISTEMAS INTELIGENTES

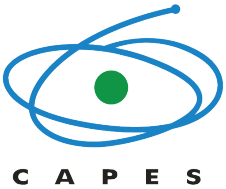
CAPES

One thing I have learned in a long life: that all our science, measured against reality, is primitive and childlike - and yet is the most precious thing we have.

Albert Einstein (1879-1955)

Abstract

Most recent engineering applications involve structures essentially nonlinear where several techniques have been recently studied and investigated by many researchers. Among them, the methods based on Volterra series expansion have presented powerful properties to provide a better understanding for identification and analysis. In this context, the present thesis proposes new contributions in how to use Volterra series for characterization, identification and dynamical analysis of nonlinear systems based on input and output signals and output-only signals. Initially, a methodology for analysis of nonlinear mechanical systems through higher-order frequency response functions (HOFRFs) is presented and the concept of extended HOFRFs based on output-only is introduced and described in detail. Afterwards, an approach for identification of nonlinear systems based on Volterra series through the expansion onto orthonormal Kautz basis is proposed. This technique allows to identify the Volterra kernels easily and enable to split the contribution of the linear and nonlinear terms using input-output as well as output-only signals. Furthermore, a methodology for modal analysis of weakly nonlinear systems under multilevel excitation is also proposed. The contribution of this new approach lies in the fact that HOFRFs are simply computed as functions of the linear FRFs. Basically, it extends the conventional experimental modal analysis methods in order to characterize and treat nonlinear effects. The results based on numerical and experimental examples presented along the thesis show the contributions, benefits and effectiveness of the proposal.

Keywords: Nonlinear systems. Structural dynamics. Volterra series. Output-only identification. Modal analysis. Higher-order Frequency Response Functions (HOFRFs).

Resumo

Muitas aplicações da engenharia envolvem estruturas essencialmente não-lineares onde várias técnicas têm sido recentemente estudadas e investigadas por muitos pesquisadores. Dentre as várias abordagems, as que usam séries de Volterra têm apresentado propriedades úteis para fornecer um melhor entendimento para identificação e análise. Neste contexto, a presente tese propõem novas contribuições em como usar as séries de Volterra para caracterização, identificação e análise dinâmica de sistemas não-lineares usando sinais de entrada e saída e sinais somente de saída. Inicialmente, apresenta-se uma metodologia para análise de sistemas mecânicos não-lineares através das funções de resposta em frequência de alta-ordem (HOFRFs) e o conceito de HOFRFs estendidas com dados apenas de saída é introduzido e descrito em detalhes. Após isso, uma abordagem para identificação de sistemas não-lineares com base nas séries de Volterra através da expansão na base ortonormal de Kautz é proposta. Essa técnica permite identificar os seus núcleos mais facilmente e permite separar as contribuições dos termos lineares e não-lineares usando somente sinais de saída. Além disso, uma metodologia para análise modal de sistemas fracamente não-lineares sujeito a excitações com vários níveis de amplitude é também apresentada. A contribuição desse novo método reside no fato de que as HOFRFs são simplesmente estimadas como função das FRFs lineares. Basicamente, essa metodologia estende o conceito de métodos convencionais de analise modal experimental para caracterizar e tratar efeitos não-lineares. Os resultados via exemplos numéricos e experimentais apresentados ao longo da tese mostram as contribuições, benefícios e eficácia da proposta.

Palavras-chave: Sistemas não-lineares. Dinâmica estrutural. Séries de Volterra. Identificação com dados somente de saída. Análise modal. FRFs de alta ordem (HOFRFs).

List of Symbols

$\ddot{y}$ Acceleration output vector

$\dot{y}$ Velocity output vector

y Displacement output vector

$F(\boldsymbol{\Theta}')$ Objective function of output prediction of Volterra-Kautz models based on output-only signals

$F(\boldsymbol{\Theta})$ Objective function of output prediction of conventional Volterra-Kautz models

$\bar{\boldsymbol{\mathcal{F}}}(\boldsymbol{u})$ Vector of external modal force

$\bar{\boldsymbol{\mathcal{F}}}_{nl}(\boldsymbol{\Phi}\mathbf{q})$ Internal nonlinear feedback modal forces

$\boldsymbol{\mathcal{F}}(\mathbf{u})$ Set of input force vectors

$\boldsymbol{f}_{nl}(\Delta(t))$ Nonlinear components of restoring forces

$\boldsymbol{Z}$ Damping factor matrix

$\bar{\mathbf{M}}$ Matrix of modal mass

$\mathbf{C}$ Damping matrix

$\mathbf{K}$ stiffness matrix

$\mathbf{M}$ Mass matrix

$\mathbf{q}$ Vector of generelized coordinates (modal model)

$\mathbf{u}$ Set force excitation vectors

$\mathbf{y}$ Set of output/displacement vectors

$\mathcal{G}_1(n_1)$ Discrete-time extended Voltera kernel of first order

$\mathcal{G}_2(n_1, n_2)$ Discrete-time extended Voltera kernel of second order

$\mathcal{G}_3(n_1, n_2, n_3)$ Discrete-time extended Voltera kernel of third order

$\mathcal{G}_\eta(n_1, n_2, \ldots, n_\eta)$ Discrete-time extended Volterra kernels of ηth order

$\mathcal{G}_\eta^{(p)}(\omega, \omega, \ldots, \omega)$ Extended HOFRF of ηth order related to the pth output signal

$\mathcal{H}_1(\omega_1)$ Voltera kernel transform of first order

$\mathcal{H}_1(n_1)$ Discrete-time Voltera kernel of first order

$\mathcal{H}_2(\omega_1, \omega_2)$ Voltera kernel transform of second order

$\mathcal{H}_2(n_1, n_2)$ Discrete-time Voltera kernel of second order

$\mathcal{H}_3(\omega_1, \omega_2, \omega_3)$ Voltera kernel transform of third order

$\mathcal{H}_3(n_1, n_2, n_3)$ Discrete-time Voltera kernel of third order

$\mathcal{H}_\eta(\omega_1, \omega_2, \ldots, \omega_\eta)$ Voltera kernel transform of ηth order

$\mathcal{H}_\eta(n_1, n_2, \ldots, n_\eta)$ Discrete-time Volterra kernels of ηth order

$\mathcal{H}_\eta^{(p)}(\omega, \omega, \ldots, \omega)$ HOFRF of ηth order related to the pth output signal

$\mathcal{F}_{nl}(\mathbf{y})$ Nonlinear functional of the set of output vectors $\mathbf{y}$

$\mathcal{Q}_1^{(i)}(\omega)$ Modal frequency response functions of first order related to the ith output

$\mathscr{H}_\eta(z_1, \ldots, z_\eta)$ Multidimensional z transform of the discrete-time Volterra kernel $\mathcal{H}_\eta(n_1, \ldots, n_\eta)$

$\mathscr{B}_\eta(i_1, i_2, \ldots, i_\eta)$ Coefficients of the orthonormal Kautz basis expansion of the conventional Volterra kernels of ηth order

$\mathscr{V}_\eta(i_1, i_2, \ldots, i_\eta)$ Coefficients of the orthonormal Kautz basis expansion of the extended Volterra kernels of ηth order

A forcing level amplitude

c viscous damping

f excitation frequency in Hz

$g_1^{(p)}(\tau_1)$ Extended Voltera kernel of first order of the pth output

$g_2^{(p)}(\tau_1, \tau_2)$ Extended Voltera kernel of second order the pth output

$g_3^{(p)}(\tau_1, \tau_2, \tau_3)$ Extended Voltera kernel of third order the pth output

$H'_\eta(n_1, n_2 \ldots, n_\eta)$ Discrete-time Volterra kernel of ηth order relate to the output $y'(k)$

$h_1(\tau_1)$ Voltera kernel of first order

$h_2(\tau_1, \tau_2)$ Voltera kernel of second order

$h_3(\tau_1, \tau_2, \tau_3)$ Voltera kernel of third order

$h_\eta(\tau_1, \tau_2, \ldots, \tau_\eta)$ Voltera kernel of ηth order

J_η Number of functions of the truncated the Volterra kernel of ηth order expanded into Katuz basis

k_1 linear damping

$l_{i_j}(k; \theta'_j)$ Denotes the convolution between the Kautz filters with the output signal $y'(k)$

m mass coefficient

n_1 Time delay for the first order Voltera kernel in the discrete-time domain

n_2 Time delay for the second order Voltera kernel in the discrete-time domain

n_3 Time delay for the third order Voltera kernel in the discrete-time domain

N_η Number of functions of the discrete-time Volterra kernel of ηth order

n_η Time delay for the ηth order Voltera kernel in the continuous-time domain

$P_u(\omega)$ Power spectrum of the input signal

$P_{y^{(P)}}(\omega)$ Power spectrum of the pth output signal

$P_{y_\eta(k;\Theta'_\eta)}(\omega)$ Power spectral density of the total output predited by the Volterra-Kautz model based on output-only signals.

$P_{y_\eta(k;\theta'_\eta)}(\omega)$ Frequency contribution of the output components predited by the Volterra-Kautz model based on output-only signals.

$P_{y_\eta(k;\Theta_\eta)}(\omega)$ Power spectral density of the total output predited by the conventional Volterra-Kautz model.

$P_{y_\eta(k;\theta_\eta)}(\omega)$ Frequency contribution of the output components predited by the conventional Volterra-Kautz model.

s_η Kautz filters complex parameter of related to the Volterra kernel of ηth order in the discrete-time

$u(k)$ Discrete-time input signal

$u(t)$ Continuous-time input signal

$y'(k)$ Discrete-time output signal measured in a different location of $y(k)$

$y(k)$ Discrete-time output signal

$y(k;\boldsymbol{\Theta}')$ Output predicted by discrete-time Volterra-Kautz filters via output-only method

$y(k;\boldsymbol{\Theta})$ Output predicted by discrete-time Volterra-Kautz filters via conventional method

$y(t)$ Continuous-time output signal

$y_1(k)$ Discrete-time linear contribution of Volterra series response

$y_2(k)$ Discrete-time quadratic contribution of Volterra series response

$y_3(k)$ Discrete-time cubic contribution of Volterra series response

y_η Contribution of ηth order of the total output predicted by Volterra series

$y_\eta(k;\boldsymbol{\Theta}')$ Contribution of ηth order computed by discrete-time Volterra-Kautz filters via output-only method

$y_\eta(k;\boldsymbol{\Theta})$ Contribution of ηth order computed by discrete-time Volterra-Kautz filters via conventional method

z_η Kautz filters complex parameter of related to the Volterra kernel of ηth order in the continuous-time

Greek Letters

α coefficient of quadratic stiffness

β coefficient of cubic stiffness

$\boldsymbol{\Lambda}$ Matrix containing the regressors terms $l_{i_j}(k)$ of inputs filtered by Kautz functions

$\boldsymbol{\Omega}$ Spectal matrix

$\boldsymbol{\Phi}$ Vector with unknown coefficients of the orthonormal Kautz basis expansion of the extended Volterra kernels

$\mathbf{\Phi}$ Matrix of eigenvectors (mode shapes)

$\mathbf{\Theta'}$ Vector with Kautz filters parameters of the model via output-only method

$\mathbf{\Theta}$ Vector with Kautz filters parameters of the model via conventional method

ϵ Stopping criteria of the objective function

ω_1 Frequency vector for the first order Voltera kernel in the continuous-time domain

ω_2 Frequency vector the second order Voltera kernel in the continuous-time domain

ω_3 Frequency vector for the third order Voltera kernel in the continuous-time domain

ω_η Frequency vector for the ηth order Voltera kernel in the continuous-time domain

ψ_{i_j} Kautz functions

τ_1 Time delay for the first order Voltera kernel in the continuous-time domain

τ_2 Time delay for the second order Voltera kernel in the continuous-time domain

τ_3 Time delay for the third order Voltera kernel in the continuous-time domain

τ_η Time delay for the ηth order Voltera kernel in the continuous-time domain

θ_η Vector with Kautz filters complex conjugate parameters z_η and $\bar{z}_\eta$

ϖ_η Frequency factor associated to the Kautz filters describing the Volterra kernel of ηth order

ϱ Nonlinear stiffness term of quadratic order

ς Nonlinear stiffness term of cubic order

ξ_η Damping factor associated to the Kautz filters describing the Volterra kernel of ηth order

List of abbreviations

ARX autoregressive model with exogenous inputs

BSI blind system identification

BSS blind source separation

DFMs Discrete frequency models

DOF Degree-of-freedom

FRF Frequency response function

HOFRF Higher-order frequency response function

HOIRF Higher-order impuslse response function

IRF Impulse response function

MAC modal assurance criterion

MARMAX Modal nonlinear auto regressive moving average with exogenous inputs

MIMO Multi-input and multi-output

NARMAX Nonlinear auto regressive moving average with exogenous inputs

NFRFs Nonlinear frequency response functions

NMPC nonlinear model predictive control

NMSE Normalized mean square error

NNMs Nonlinear normal modes

NRMSE Normalised root mean square error

POD Principal orthogonal decomposition

PSD Power Spectrum Density

SIMO Single-input multi-output

SISO Single-input single-output

SQP Sequential Quadratic Programming

TFs transmissibility functions

List of Figures

List of Tables

Contents

1 Introduction

This chapter presents the introduction pointing out the problem statement, topics and subjects that cover the present thesis. The motivation and main challenging issues are presented in Section 1.1. Section 1.2 presents the main objective of this thesis. In Section 1.3 are presented the contributions, and the outline of this thesis is described in Section 1.4.

1.1 Motivation

The development of methods to analyze nonlinear vibrations has been a topic of interest during recent years in system identification and structural dynamics applications. Normally, vibrating engineering structures can present some nonlinear regime of motion depending on several conditions. For instance, in lightweight and flexible structures these effects are caused by several mechanisms such as friction, level of excitation, gaps, geometry, nonlinear stress-strain or even complex materials, etc (WORDEN; TOMLINSON, 2001; KERSCHEN et al., 2006; FALCO et al., 2014; PASQUALI et al., 2014). Consequently, a wide variety of dynamical phenomena can appear: harmonics, modal interactions, jumps between coexisting solutions, limit cycles, chaos, etc. (VIRGIN, 2000; MANKTELOW et al., 2014; NOËL; KERSCHEN, 2017). The identification of problems characterized by such complex effects becomes a difficult challenge once the algebraic solution is not well established and does not exist in some cases. In a modern engineering design is fundamental to predict and to have deep knowledge about this possible behavior. Thus, several tools can be used for detection and identification of nonlinearities in structural dynamics to overcome these challenging issues (ADAMS, 2002; LENAERTS et al., 2003; DA SILVA et al., 2009a; ISASA et al., 2011).

It is important to point out that the classical system identification techniques based on the input and output data can be effectively used to characterize nonlinearities (MASRI; CAUGHEY, 1979; BILLINGS, 1980; SJÖBERG et al., 1995; LJUNG, 2007; WORDEN

et al., 2009). Many approaches have been developed, for instance, Wiener-Hammerstein models (WILLS et al., 2013; BILLINGS; FAKHOURI, 1977), polynomial representation through NARX/NARMAX models (CHEN; BILLINGS, 1989; MOHAMED; M'HIRI, 2008), frequency domain subspace models (NOËL; KERSCHEN, 2013; NOËL et al., 2014a), principal component analysis (HOT et al., 2012), neural networks (IBNKAHLA, 2002; IBNKAHLA, 2003; JAFARIAN et al., 2015), Volterra series (WORDEN et al., 1997; NOVÁK, 2007; TANG et al., 2010; DA SILVA et al., 2010), machine learning approaches (WORDEN; GREEN, 2017) and others. Among the several methods existing to deal with this kind of problem, the Volterra series theory has been extensively used with satisfactory results (RUGH, 1981; DA SILVA, 2011a; SHIKI et al., 2014a; XIA et al., 2016). The Volterra series allow to represent the output of nonlinear systems as a polynomial power series expansion in the time domain through the multi-dimensional convolutions between the input signal and the higher-order Volterra kernels (SCHETZEN, 1980).

The multi-dimensional Fourier transform of the Volterra kernels generates the higher-order frequency response functions (HOFRFs) that are used to describe the conventional harmonic probing method (BILLINGS; TSANG, 1989a; BILLINGS; TSANG, 1989b; CARASSALE; KAREEM, 2010; BILLINGS, 2013; RIJLAARSDAM et al., 2017). It is a natural extension of the usual procedure for obtaining the linear transfer functions and has been used in several mechanical applications involving output prediction (STORER; TOMLINSON, 1993; CAFFERTY; TOMLINSON, 1997; WORDEN et al., 1997; KIM, 2015), nonlinear parameter estimation (CHATTERJEE; VYAS, 2004; CHATTERJEE, 2010a), modal analysis (TAWFIQ; VINH, 2003) and structural health monitoring (CHATTERJEE, 2010b). Besides that, criteria for the response convergence of the Volterra series by using the HOFRFs have been investigated as well (TOMLINSON et al., 1996; THOUVEREZ, 1998; CHATTERJEE; VYAS, 2000; PENG; LANG, 2007).

Although the conventional harmonic probing method is very useful for problems of structural dynamics, the requirement of this tool lies in the knowledge of the equations of motion, known as white box modeling. Moreover, the input and output data must be available. Thus, the analysis in operational conditions becomes very limited in several real world engineering applications once they are driven by unknown inputs. In order to overcome these limitations involving problems where the input signal is not directly available or totally unknown in their environmental operating, many concepts and techniques of blind system identification (BSI) have been developed and employed (ABED-MERAIN, 1997; KALOUPTSIDIS; KOUKOULAS, 2003). In such cases, the Volterra series theory

has been extensively used mainly in areas such as signal processing and communications (TAN et al., 2008; CHERIF et al., 2012). Although these blind methods based on Volterra series allow to identify nonlinear systems, it would be very welcome a simple extension of the conventional harmonic probing method in order to deal directly with problems of structural dynamics through the extended HOFRFs and the respective nonlinear parameters.

In this context, the first part of the present thesis is aimed in to propose a new version of the conventional harmonic probing method. The analytical expressions of the extended HOFRFs are presented and the theoretical aspects as well as its significance are discussed. Thus, the first part of this thesis brings new benefits of Volterra series for analysis of weakly nonlinear systems. The main advantage of this new method lies in its ability to treat nonlinearities in applications where only the output signals are available.

The second part of the present thesis is concerned with the characterization and identification of nonlinear mechanical systems based on the extended kernels presented in the first part of this thesis. Once the convergence of Volterra kernels is warranted, it is possible to split the total response into linear and nonlinear contributions. However, several numerical drawbacks are associated with overparametrizations in ill-posed problems due to the large number of samples to identify the kernels. Fortunately, an orthonormal expansion can overcome these drawbacks (WIENER, 1958). The Kautz filters compose a convenient orthonormal basis to expand the Volterra series in order to identify vibrating systems (KAUTZ, 1954; WAHLBERG, 1994; BJÖRSELL et al., 2010; SHIKI et al., 2012; HANSEN et al., 2014). In this context, the contribution of the second part of this thesis is concerned with the development of a novel approach to identify a model based on Volterra series, Kautz filters and output-only signals to apply in nonlinear mechanical systems. The main idea is to describe the multiple convolutions by using output-only and through the model identified to predict the response in several different conditions and to detect the linear or nonlinear behavior associated with the data. In the proposed method, the Kautz filters parameters are obtained through the sequential quadratic programming algorithm (SQP) minimizing the normalized mean square error-prediction (NMSE) as objective function. The unknown kernels coefficients are identified using the classical least squares approach.

The development of methods for system identification and modal analysis has grown significantly during the last decades due to the increased number of industrial applications in aerospace, mechanical, electrical and civil engineering and many other areas (PLATTEN et al., 2009; ZWOLSKI; BIEŃ, 2011; NOËL et al., 2014b; BROWNJOHN et al.,

2015; OZBEK; RIXEN, 2016). The main goal of modal analysis is to characterize the behaviour of a testing structure in terms of its natural characteristics and modes of vibration (CAUGHEY; O'KELLY, 1965; MAYBEE, 1966; MAIA; SILVA, 1997; EWINS, 2000). In linear systems the modal parameters can be extracted using classical experimental modal analysis methods. Several commercial softwares are able to identify these parameters. However, the nonlinear behavior is still not well developed and included in such kind of softwares and packages. In this sense, the main contribution of the third part of this thesis is to propose the identification of HOFRFs through an alternative methodology under multilevel excitation signals. Basically, this part shows how the Volterra series can be extremely useful in applications of structural dynamics and modal analysis of weakly nonlinear systems.

1.2 Objective

The main goal of the present thesis is to propose a new method to identify nonlinear systems described by Volterra series considering output-only signals and modal parameters involving the conventional linear FRFs.

1.3 Main contributions

The main contributions of the present thesis are:

- To review of state-of-art covering topics on modelling and dynamical analysis, identification, parameter estimation and modal analysis of nonlinear engineering structural systems.
- To propose a full description of an alternative methodology based on multidimensional Fourier transform of continuous-time Voterra series and output-only signals. These contributions were published recently in Scussel and da Silva (2017).
- To provide a new method to identify nonlinear mechanical systems based on output-only signals and the discrete-time Volterra kernels. These results can be found in Scussel and da Silva (2016b).
- To apply HOFRFs computed as functions of the conventional FRFs and modal properties estimated by conventional modal analysis approaches in order to analyze nonlinear behaviour and output-prediction.

1.4 Outline

This thesis is organized as follows:

- **Chapter 1 - Introduction**: motivations, main objective, contributions and the scope of the present thesis.

- **Chapter 2 - From input-output to output-only dynamical analysis based on Volterra Series**: is concerned with analysis of nonlinear vibrating systems via continuous-time Volterra Series based on the harmonic probing algorithm by using input-output and output-only methodologies. An extended version of the harmonic probing method is proposed in order to deal with applications where only the outputs are available. Consequently, this initial part of the thesis is aimed in providing the algebraic expressions of the extended Volterra kernels transform and their theoretical properties for vibration analysis. The main advantages, novelties and drawbacks are discussed and compared with the conventional approach. It is verified that the new kernels can be expressed as a combination of the conventional ones. Numerical tests based on a classical two degrees-of-freedom (2DOF) Duffing oscillator are carried out and the results reveal the effectiveness and potentialities of the extended harmonic probing method.

- **Chapter 3 - From input-output to output-only system identification based on Volterra Series**: presents the development of a system identification approach based on discrete-time Volterra series expanded onto orthonormal Kautz basis using output-only data. In the conventional Volterra series, the outputs of the system are computed by multiple convolutions between the excitation force and the Volterra kernels. However, in this approach at least two output signals measured in different placements are used to compute the multiple convolutions and the excitation signals are not required. The novel kernels identified can be used to characterize the nonlinear behavior through a model using output-only data. A numerical example based on a Duffing oscillator with 2DOF and experimental vibration data are used to illustrate the proposed method. A comparison has shown that the prediction results using output-only data are similar to the conventional Volterra kernels based on input and output data.

- **Chapter 4 - Applications of Volterra Series in modal analysis**: this chapter is concerned with applications of the Volterra kernels and their respective multidimensional Fourier transforms, called as higher-order frequency response functions

(HOFRFs), to analyse the inherent properties and natural characteristics of systems with mild nonlinearity characterized by polynomial restoring force functions. The contribution of this study lies in a practical way of describing these HOFRFs through an algorithm structured in a multi-step way. Firstly, the conventional FRFs of the linear part are identified when the system operates in linear regime, at low level of excitation. Afterwards, the HOFRFs are computed as a function of the conventional ones at higher forcing levels. This fact shows the potentialities and practicability of this alternative approach that can be used for problems in structural dynamics. The results based on numerical and experimental cases have shown the applicability of the method for nonlinearity identification, output prediction, analysis and design of vibrating tests.

- **Chapter 5 - Final remarks**: presents the conclusions and some challenging issues as well as suggestions for further researches are carried out.

2 From Input-Output to Output-Only Dynamical Analysis Based on Volterra Series

This chapter presents an extended version of the harmonic probing method via Volterra series expansion to deal with applications where only output signals are available. Section 2.1 is dedicated to a brief critical review of the state-of-the-art and motivations pointing out recent trends covering dynamical analysis of nonlinear systems based on harmonic probing method and Volterra series expansion. In Section 2.2 is reviewed the Volterra series theory for single-input and single-output (SISO) systems and the conventional harmonic probing method to compute the higher-order frequency response functions (HOFRFs). Afterwards, in Section 2.3 is reviewed the concept of HOFRFs for single-input and multi-output (SIMO) systems. In Section 2.4 is provided the algebraic expressions of the extended Volterra kernels transform and their theoretical properties for vibration analysis. A new theorem is derived to prove the existence of the extended HOFRFs for continuous nonlinear systems. Additionally, an alternative procedure based on the conventional harmonic probing method is presented to obtain the analytical expressions of these new HOFRFs. In Section 2.5, numerical tests based on a classical two degrees-of-freedom (2DOF) Duffing oscillator are carried out and the results have shown the effectiveness and potentialities of the extended harmonic probing method for structural dynamic analysis. Theoretical aspects of the model based on output-only as well as its significance are addressed. The results are compared with the conventional approach through the HOFRFs up until the third order. Finally, the conclusions are presented in Section 2.6.

2.1 A brief state-of-the-art on Volterra series

A large number of methods and research efforts are described in the literature directed towards detection and quantification of structural dynamics applications (WOR-

DEN; TOMLINSON, 2001; KERSCHEN et al., 2006; ZHANG; BILLINGS, 2017; NOËL; KERSCHEN, 2017). Among them, the Volterra series have been widely used and applied in many different fields of engineering science involving nonlinear problems (CHENG et al., 2017). Cheng et al. (2017) summarized the achievements and status of Volterra Series as well as their powerful vigor and broad application in areas as biomedical engineering, fluid dynamics, electrical engineering, mechanical engineering, etc.

The Volterra series theory is very useful to describe the relationship between the input and output of the system through higher-order Volterra kernels, called also as higher-order impulse response function (HOIRFs) represented in the time domain or higher-order frequency response functions (HOFRFs) represented in the frequency domain (VOLTERRA, 1959; BILLINGS, 1980; SCHETZEN, 1980; RUGH, 1981). In particular, the framework of the HOFRFs is very important to characterize the nonlinear part of the system and their analytical expressions are very useful allowing a better insight of the phenomenon (CAFFERTY; TOMLINSON, 1997; PENG et al., 2008; CHATTERJEE, 2010a; CHATTERJEE; VYAS, 2003). In order to provide the analytical expressions of the HOFRFs, Bedrosian and Rice (1971) have proposed the harmonic probing method for continuous-time nonlinear systems.

A few years later, Billings and Tsang (1989a) and Billings and Tsang (1989b) extended this method for the discrete-time case. Furthermore, Frachebourg et al. (1988) used the Volterra series to the special case subjected to an impulse excitation for modal analysis of a two degrees-of-freedom system with nonlinear springs. The results showed the useful properties of the Volterra kernels of higher-order for giving a better insight of the mode shapes and their useful properties to capture effects (phase decay) that the linear model based on the classical transfer function of first order is not enough to reach. Furthermore, the approach allows to localize the nonlinear spring component when the system has weakly coupled modes. Gifford and Tomlinson (1989) applied a curve fitting method to compute the HOFRFs up to third order of nonlinear multi-degrees-of-freedom systems. The HOFRFs can predict aspects and an appropriate way to extract a parametric model for systems with weak nonlinearities. Afterwards, Worden et al. (1997) proposed an extension of the harmonic probing method for both continuous and discrete-time cases subject to multiple sinusoidal inputs. The algebraic expressions revealed that the higher-order and the cross-kernel transforms are directly related with the first order kernel and function of the nonlinear parameters described by polynomial representation.

Although this representation provides a useful tool for the study of nonlinear behavior, it may present convergence problems (TOMLINSON et al., 1996; THOUVEREZ, 1998;

CHATTERJEE; VYAS, 2000; PENG; LANG, 2007). Tomlinson et al. (1996) proposed a criterion to determine the upper limit to the sinusoidal excitation level at the natural frequency. This strategy provides an estimation of the magnitude amplitude at which the output starts to diverge. The results obtained through single degree-of-freedom (SDOF) and 2DOF Duffing oscillators with cubic stiffness revealed the accuracy of the method to establish the magnitude of the harmonic input and the number of terms required in the Volterra series expansion to predict the response of systems described by polynomial nonlinearities. In addition, Thouverez (1998) provided an alternative procedure to estimate an upper limit of the convergence radius of the Volterra series by using the dynamical equations in terms of the harmonic balance method. Furthermore, the complex variable properties with Rouché's theorem and Lagrange's expansion are applied to obtain the convergence criterion. The examples using Duffing oscillators with nonlinear springs showed that the approximation due to the harmonic balance approach does not affect the estimation of the convergence radius. An improved method to analyse the convergence threshold of the Volterra series response was proposed by Chatterjee and Vyas (2000). The contribution lies in a procedure based on critical values of the non-dimensional nonlinear parameters for the response convergence over a wide range of excitation frequencies. This critical limit value is described as a function of the number of the Volterra series terms that added to the approximation of the response predicted. The results based on a 2DOF nonlinear system showed that the critical values are found to be directly dependent on the nonlinear stiffness as well as on the linear coupling stiffness coefficients.

Throughout the past few decades, it can be noted that the Volterra series theory and the transfer functions of higher order (HOFRFs) have been increasingly investigated and widely applied in several problems of structural dynamics for mechanical nonlinear detection, characterization, identification and design (CAMBRAIA, 1990; TOMLINSON et al., 1996; LEE, 1997; WORDEN; MANSON, 2005; PENG et al., 2008; BILLINGS, 2013). For instance, the HOFRFs were applied in modal testing by Storer and Tomlinson (1993) showing that the higher-order transfer functions up to third order can be measured through sine excitation on a practical case involving a nonlinear beam rig. The paper illustrated the possibility of detecting nonlinear effects by using the HOFRFs. However, the method studied suffers some limitations once the HOFRFs can not be well measured due to the bend resonant peaks and it requires curve-fitting procedures based on an priori model. Furthermore, Cafferty and Tomlinson (1997) applied the frequency domain technique using the HOFRFs in order to investigate the energy transfer properties and to characterize a Monroe automotive damper. In the same year, Lee (1997) developed a

method to compute the higher-order kernel transforms using a component separation technique that allowed to extract the linear response component. The nonlinear parameters were estimated by a relationship between the first order and the higher-order kernel transform. The nonlinear parameter estimation method was applied in simulated systems with nonlinear stiffness and nonlinear damping. The method presented a few disadvantages and problems of convergence of the response predicted under high level of amplitude excitation. Additionally, the application of HOFRFs in modal analysis of mechanical problems inherently nonlinear was addressed by Tawfiq and Vinh (2003). The authors concluded that the HOFRFs as well as the Volterra kernels constitute the bases of nonlinear modal analysis. The utilization of the quotient of polynomials for transfer functions and impulse response functions revealed a great importance allowing to interpret physical phenomena (dampings, eigenvalues, etc.).

An interesting method based on modal coordinates was presented by Thouverez and Jezequel (1996). The authors developed a method to identify MARMAX models that represent an alternative version of the conventional NARMAX (nonlinear auto regressive moving average with exogenous inputs) in modal space. The main drawbacks of the NARMAX models, overparametrization and huge number of terms, can be reduced by using modal expansion. Although, the truncated modal problem is more convenient to analyse, some undesirable effects arise during the identification of the eigenvector matrix. The incorrect identification of the eigenvector matrix leads to cases where the linear part of the NARMAX model identified might not be uncoupled. Numerical tests involving nonlinear oscillator with quadratic nonlinearity and a beam (multi-dimensional case) undergoing tension and compression have demonstrated the accuracy of this technique and its potential features.

After a few years, Adams (2002) proposed an alternative technique using multi-harmonic FRF estimators via frequency domain autoregressive models with exogenous inputs (ARX) that are identified through the HOFRFs and the discrete frequency models (DFMs). A combination of parametric and non-parametric ARX models is used to compute the multi-harmonic FRFs. The idea behind this method lies in the fact that the multi-harmonic estimator relates the forced response to the input and output at harmonics of the excitation frequency. Numerical and experimental real-world data show the applicability of the ARX models in frequency domain to deal with nonlinear systems subjected to broadband excitations involving frequency interactions and amplitude variations. Chatterjee and Vyas (2003) investigated an alternative approach where the nonlinear parameters along with the first order kernel transforms are obtained by us-

ing recursive iteration technique. The number of terms of the response series and the excitation amplitude over a wide range of frequencies are driven by the convergence criterion. The procedure is investigated through numerical simulation involving a Duffing oscillator and the robustness is also tested against random measurement noise. Subsequently, the recursive iteration procedure proposed by Chatterjee and Vyas (2003) was extended by Chatterjee and Vyas (2004) for multi-degrees-of-freedom systems with multiple inputs based on higher-order and cross-kernel transforms. The method was tested through numerical simulation for rotor-bearing system characterized by square and cubic stiffness nonlinearities. Analysis of error and convergence were also made and the results illustrated the accuracy of the method for nonlinear system analysis under multi-input harmonic excitations.

Additionally, it is important to emphasize that the Volterra series expansion as well as the HOFRFs have been a topic of interest in applications of vibration-based structural health monitoring since the mechanical or structural damage eventually leads to nonlinear effects. Chatterjee (2010c) investigated the use of HOFRFs for damage detection problems on nonlinear response characteristics of a cantilever beam with a breathing crack. This study employed Volterra series for developing a quantitative damage assessment in order to investigate the response harmonic amplitudes for the benchmark studied.

Although the conventional harmonic probing method presents benefits for structural dynamics problems, this tool requires the knowledge of the equations of motion, known as white box modelling. Moreover, the input and output data must be available. Thus, the analysis in operational conditions becomes very limited in several real world engineering applications once they are driven by unknown inputs.

In order to overcome these limitations involving problems where the input signal is not directly available or totally unknown in their environmental operating, many concepts and techniques of blind system identification (BSI) have been developed and employed (ABED-MERAIN, 1997; KALOUPTSIDIS; KOUKOULAS, 2003). A vast number of methods based on blind source separation (BSS) techniques have been widely used due to their potential in modal analysis based on output-only signals (YANG; NAGARAJAIAH, 2013; GROSEL et al., 2014; LI et al., 2016). In such cases, the Volterra series theory has been extensively used mainly in areas such as signal processing and communications (TAN et al., 2008; CHERIF et al., 2012), damage detection and location in multi-degree-of-freedom (MDOF) systems based on the transmissibility of nonlinear output frequency response functions (NOFRFs) (LANG et al., 2011; ZHAO et al., 2015).

It would be very desirable to show a simple extension of the conventional harmonic probing method in order to deal directly with problems of structural dynamics through the extended HOFRFs and the respective nonlinear parameters in the continuous-time domain.

In this context, the present chapter is aimed in to propose a new version of the conventional harmonic probing method based on the following contributions:

(i) A new theorem is derived to prove the existence of the extended HOFRFs for continuous nonlinear systems.

(ii) An alternative procedure based on the conventional harmonic probing method is presented to obtain the analytical expressions of extended HOFRFs.

(iii) Theoretical aspects of the model based on output-only as well as its significance are addressed in a practical example.

2.2 Single-input and single-output (SISO) Volterra series theory

The Volterra series is a powerful tool to describe the relationship of input and output of nonlinear dynamical systems through multidimensional convolutions. This representation allows to describe the output of a single-input and single-output (SISO) system as the following mapping (VOLTERRA, 1959):

$$y(t) = \sum_{\eta=1}^{+\infty} y_\eta(t) = y_1(t) + y_2(t) + y_3(t) + \dots \tag{1}$$

where the respective polynomial contributions are given by:

$$y_\eta(t) = \int_{-\infty}^{+\infty} \int_{-\infty}^{+\infty} \dots \int_{-\infty}^{+\infty} h_\eta(\tau_1, \tau_2, \dots, \tau_\eta) \prod_{i=1}^{\eta} u(t-\tau_i) d\tau_i \tag{2}$$

where $h_\eta(\tau_1, \tau_2, \dots, \tau_\eta)$ is called the Volterra kernel of ηth order and is a generalization of the well know impulse response function (IRF) (SCHETZEN, 1980). The terms τ_i are the lags related to the input and this fact shows that the Volterra series is basically a generalization of the concept of Taylor series expansion since it involves the effect of memory (MILANESE, 2009). Although the Volterra series theory seems to be an abstract mathematical tool, it can be a useful instrument to identify and characterise certain nonlinear effects (RUGH, 1981; STORER, 1991). The property of separating the total output of the

system in linear and nonlinear components brings great benefits for nonlinear vibration analysis. It can be seen also as odd/even separation to provide a better understanding into the eventual symmetries of the nature of the system nonlinearity (OGUNFUNMI, 2007). In addition, the Volterra kernel $h_\eta(\tau_1, \tau_2, \ldots, \tau_\eta)$ can be computed in an symmetric way, for instance $h_2(\tau_1, \tau_2) = h_2(\tau_2, \tau_1)$. For causal systems $h_\eta(\tau_1, \tau_2, \ldots, \tau_\eta) = 0 \ \forall \tau_\eta < 0$ and the statement

$$\lim_{\tau_1, \tau_2, \ldots, \tau_\eta \longrightarrow \infty} h_\eta(\tau_1, \tau_2, \ldots, \tau_\eta) = 0 \tag{3}$$

for the model with finite length memory.

Furthermore, applying the multi-dimensional Fourier transforms of the Volterra kernels generates the higher-order frequency response functions (HOFRFs) given as (CHATTERJEE, 2010a):

$$\mathcal{H}_\eta(\omega_1, \omega_2, \ldots, \omega_\eta) = \int_{-\infty}^{+\infty} \int_{-\infty}^{+\infty} \ldots \int_{-\infty}^{+\infty} h_\eta(\tau_1, \tau_2, \ldots, \tau_\eta) \prod_{i=1}^{\eta} e^{-j\omega_i \tau_i} d\tau_1 d\tau_2 \ldots d\tau_\eta \tag{4}$$

In this context, if is considered a single-tone harmonic force excitation $u(t) = A\cos(\omega t) = \frac{A}{2}e^{j\omega t} + \frac{A}{2}e^{-j\omega t}$ the polynomial contributions of the output $y(t)$ are calculated as (TOMLINSON et al., 1996)

$$\begin{aligned}
y_1(t) &= \int_{-\infty}^{+\infty} h_1(\tau_1) u(t-\tau_1) d\tau_1 = \int_{-\infty}^{+\infty} h_1(\tau_1) \left\{ \frac{A}{2} e^{j\omega(t-\tau_1)} + \frac{A}{2} e^{-j\omega(t-\tau_1)} \right\} d\tau_1 \\
&= \frac{A}{2} \int_{-\infty}^{+\infty} h_1(\tau_1) e^{-j\omega\tau_1} d\tau_1 e^{j\omega t} + \frac{A}{2} \int_{-\infty}^{+\infty} h_1(\tau_1) e^{j\omega\tau_1} d\tau_1 e^{-j\omega t} \\
&= \frac{A}{2} \mathcal{H}_1(\omega) e^{j\omega t} + \frac{A}{2} \mathcal{H}_1(-\omega) e^{-j\omega t} \\
y_2(t) &= \int_{-\infty}^{+\infty} \int_{-\infty}^{+\infty} h_2(\tau_1, \tau_2) u(t-\tau_1) u(t-\tau_2) d\tau_1 d\tau_2 \\
&= \int_{-\infty}^{+\infty} \int_{-\infty}^{+\infty} h_2(\tau_1, \tau_2) \left\{ \frac{A}{2} e^{j\omega(t-\tau_1)} + \frac{A}{2} e^{-j\omega(t-\tau_1)} \right\} \left\{ \frac{A}{2} e^{j\omega(t-\tau_2)} + \frac{A}{2} e^{-j\omega(t-\tau_2)} \right\} d\tau_1 d\tau_2 \\
&= \frac{A^2}{4} \mathcal{H}_2(\omega, \omega) e^{j2\omega t} + \frac{A^2}{4} \mathcal{H}_2(-\omega, \omega) + \frac{A^2}{4} \mathcal{H}_2(\omega, -\omega) + \frac{A^2}{4} \mathcal{H}_2(-\omega, -\omega) e^{-j2\omega t} \\
y_3(t) &= \int_{-\infty}^{+\infty} \int_{-\infty}^{+\infty} \int_{-\infty}^{+\infty} h_3(\tau_1, \tau_2, \tau_3) u(t-\tau_1) u(t-\tau_2) u(t-\tau_3) d\tau_1 d\tau_2 d\tau_3 \\
&= \frac{A^3}{8} \mathcal{H}_3(\omega, \omega, \omega) e^{j3\omega t} + \frac{A^3}{8} \mathcal{H}_3(-\omega, \omega, \omega) e^{j\omega t} + \frac{A^3}{8} \mathcal{H}_3(\omega, -\omega, \omega) e^{j\omega t} \\
&+ \frac{A^3}{8} \mathcal{H}_3(\omega, \omega, -\omega) e^{j\omega t} + \frac{A^3}{8} \mathcal{H}_3(-\omega, -\omega, \omega) e^{-j\omega t} + \frac{A^3}{8} \mathcal{H}_3(-\omega, \omega, -\omega) e^{-j\omega t} \\
&+ \frac{A^3}{8} \mathcal{H}_3(\omega, -\omega, -\omega) e^{-j\omega t} + \frac{A^3}{8} \mathcal{H}_3(-\omega, -\omega, -\omega) e^{-j3\omega t} \\
&\quad \text{and so on contributions.}
\end{aligned}$$

By using the property of symmetry

$$\begin{aligned}
&\mathcal{H}_2(-\omega,\omega) = \mathcal{H}_2(\omega,-\omega),\\
&\mathcal{H}_3(-\omega,\omega,\omega) = \mathcal{H}_3(\omega,-\omega,\omega) = \mathcal{H}_3(\omega,\omega,-\omega),\\
&\mathcal{H}_3(-\omega,-\omega,\omega) = \mathcal{H}_3(\omega,-\omega,-\omega) = \mathcal{H}_3(-\omega,\omega,-\omega),\\
&\vdots
\end{aligned}$$

the expression for the output predicted in Eq. (1) is given by:

$$\begin{aligned}
y(t) &= \frac{A}{2}\mathcal{H}_1(\omega)e^{j\omega t} + \frac{A}{2}\mathcal{H}_1(-\omega)e^{-j\omega t}\\
&+ \frac{A^2}{4}\mathcal{H}_2(\omega,\omega)e^{j2\omega t} + \frac{A^2}{2}\mathcal{H}_2(-\omega,\omega) + \frac{A^2}{4}\mathcal{H}_2(-\omega,-\omega)e^{-j2\omega t}\\
&+ \frac{A^3}{8}\mathcal{H}_3(\omega,\omega,\omega)e^{j3\omega t} + \frac{3A^3}{8}\mathcal{H}_3(-\omega,\omega,\omega)e^{j\omega t}\\
&+ \frac{3A^3}{8}\mathcal{H}_3(-\omega,-\omega,\omega)e^{-j\omega t} + \frac{A^3}{8}\mathcal{H}_3(-\omega,-\omega,-\omega)e^{-j3\omega t}\\
&+ \ldots, \qquad (5)
\end{aligned}$$

Thus, Eq. (5) shows a way to compute the response through HOFRFs when the nonlinear system is subjected to a single-tone harmonic force excitation. Now, a procedure known as harmonic probing algorithm will be used to obtain the expressions for the conventional HOFRFs up until third order. In order to attend this purpose, consider without loss of generality a single degree-of-freedom (SDOF) Duffing oscillator under harmonic input $u(t)$ characterized by quadratic and cubic stiffness as follows (KOVACIC IVANA; BRENNAN, 2011):

$$m\ddot{y}(t) + c\dot{y}(t) + k_1 y(t) + \alpha y^2(t) + \beta y^3(t) = u(t) \qquad (6)$$

where m [kg] is the mass coefficient, c is the viscous damping [Ns/m], k_1 [N/m] is the linear damping, α [N/m^2] and β [N/m^3] are the quadratic and cubic stiffnesses, respectively. Additionally, $\ddot{y}$, $\dot{y}$ and y represent the acceleration [m/s^2], velocity [m/s] and displacement [m], respectively, and $u(t) = Ae^{j\omega t}$ [N] is the input with A as forcing level of amplitude and frequency of excitation ω [rad/s]. Usually, Eq. (6) is a classical model to represent apparently many nonlinear physical systems described by phenomena such as geometric nonlinearities in lightly damped thin beans and plates (KHOUAJA et al., 2004; KOVACIC IVANA; BRENNAN, 2011).

Based on Volterra series expansion, the output in Eq. (1) can be rewritten as:

$$\begin{aligned} y(t) &= Ae^{j\omega t}\int_{-\infty}^{+\infty} h_1(\tau_1)e^{-j\omega\tau_1}d\tau_1 + A^2e^{j2\omega t}\int_{-\infty}^{+\infty}\int_{-\infty}^{+\infty} h_2(\tau_1,\tau_2)e^{-j\omega(\tau_1+\tau_2)}d\tau_1 d\tau_2 + \ldots \\ &+ A^\eta e^{\eta}\int_{-\infty}^{+\infty}\int_{-\infty}^{+\infty}\ldots\int_{-\infty}^{+\infty} h_\eta(\tau_1,\tau_2,\ldots,\tau_\eta)e^{-j\omega(\tau_1+\tau_2+\ldots+\tau_\eta)}d\tau_1 d\tau_2\ldots d\tau_\eta, \end{aligned}$$

with $\eta \to \infty$. From Eq. (4) the output $y(t)$ is alternatively rewritten as a combination of the HOFRFs:

$$y(t) = \mathcal{H}_1(\omega)Ae^{j\omega t} + \mathcal{H}_2(\omega,\omega)A^2e^{j2\omega t} + \mathcal{H}_3(\omega,\omega,\omega)A^3e^{j3\omega t} + \ldots + \mathcal{H}_\eta(\omega,\ldots,\omega)A^\eta e^{j\eta\omega t}.$$

By differentiating $y(t)$ for the velocity and the acceleration yields

$$\begin{aligned} \dot{y}(t) &= j\omega\mathcal{H}_1(\omega)Ae^{j\omega t} + j2\omega\mathcal{H}_2(\omega,\omega)A^2e^{j2\omega t} + j3\omega\mathcal{H}_3(\omega,\omega,\omega)A^3e^{j3\omega t} + \ldots, \\ \ddot{y}(t) &= -\omega^2\mathcal{H}_1(\omega)Ae^{j\omega t} - (2\omega)^2\mathcal{H}_2(\omega,\omega)A^2e^{j2\omega t} - (3\omega)^2\mathcal{H}_3(\omega,\omega,\omega)A^3e^{j3\omega t} + \ldots, \end{aligned}$$

For simplicity, it is considered $\mathcal{H}_1(\omega) = \mathcal{H}_1$, $\mathcal{H}_2(\omega,\omega) = \mathcal{H}_2$ and $\mathcal{H}_3(\omega,\omega,\omega) = \mathcal{H}_3$ in order to obtain the algebraic expressions of HOFRFs through an easier and compact way. Thus, by substituting the terms $y(t)$, $\dot{y}(t)$ and $\ddot{y}(t)$ into Eq. (6) gives

$$\begin{aligned} Ae^{j\omega t} &= m[-\omega^2\mathcal{H}_1Ae^{j\omega t} - (2\omega)^2\mathcal{H}_2A^2e^{j2\omega t} - (3\omega)^2\mathcal{H}_3A^3e^{j3\omega t} + \ldots] \\ &+ c[j\omega\mathcal{H}_1Ae^{j\omega t} + j2\omega\mathcal{H}_2A^2e^{j2\omega t} + j3\omega\mathcal{H}_3A^3e^{j3\omega t} + \ldots] \\ &+ k_1[\mathcal{H}_1Ae^{j\omega t} + \mathcal{H}_2A^2e^{j2\omega t} + \mathcal{H}_3A^3e^{j3\omega t} + \ldots] \\ &+ \alpha\underbrace{[H_1Ae^{j\omega t} + \mathcal{H}_2A^2e^{j2\omega t} + \mathcal{H}_3A^3e^{j3\omega t} + \ldots]^2}_{\text{(I)}} \\ &+ \beta\underbrace{[\mathcal{H}_1Ae^{j\omega t} + \mathcal{H}_2A^2e^{j2\omega t} + \mathcal{H}_3A^3e^{j3\omega t} + \ldots]^3}_{\text{(II)}}, \end{aligned} \tag{7}$$

where

$$\begin{aligned} \text{(I)} &= [\mathcal{H}_1Ae^{j\omega t} + \mathcal{H}_2A^2e^{j2\omega t} + \mathcal{H}_3A^3e^{j3\omega t} + \ldots][\mathcal{H}_1Ae^{j\omega t} + \mathcal{H}_2A^2e^{j2\omega t} + \mathcal{H}_3A^3e^{j3\omega t} + \ldots] \\ &= \mathcal{H}_1^2A^2e^{j2\omega t} + \mathcal{H}_2^2A^4e^{j4\omega t} + \mathcal{H}_3^2A^6e^{j6\omega t} + 2\mathcal{H}_1\mathcal{H}_2A^3e^{j3\omega t} + 2\mathcal{H}_1\mathcal{H}_3A^4e^{j4\omega t} + 2\mathcal{H}_2\mathcal{H}_3A^5e^{j5\omega t} + \ldots \end{aligned}$$

and

$$\text{(II)} = \text{(I)}[\mathcal{H}_1Ae^{j\omega t} + \mathcal{H}_2A^2e^{j2\omega t} + \mathcal{H}_3A^3e^{j3\omega t} + \ldots] = \mathcal{H}_1^3A^3e^{3j\omega t} + \mathcal{H}_1\mathcal{H}_2^2A^5e^{j5\omega t} + \ldots,$$

From Eq. (7) it is possible to equate the terms with $Ae^{j\omega t}$ that provides the FRF:

$$[-m\omega^2 + j\omega c + k_1]\mathcal{H}_1(\omega) - 1 = 0 \Leftrightarrow \mathcal{H}_1(\omega) = \frac{1}{k_1 - m\omega^2 + cj\omega} \tag{8}$$

The FRF of second order $\mathcal{H}_2(\omega,\omega)$ is obtained equating the terms with $A^2e^{j2\omega t}$

$$[-(2\omega)^2 m + j2\omega c + k_1]H_2(\omega,\omega) + \alpha H_1^2(\omega) = 0 \Leftrightarrow \mathcal{H}_2(\omega,\omega) = -\alpha\mathcal{H}_1^2(\omega)\mathcal{H}_1(2\omega) \tag{9}$$

To determine an algebraic expression for $\mathcal{H}_3(\omega,\omega,\omega)$ the coefficients with $A^3e^{j3\omega t}$ are equated

$$\begin{aligned}[-(3\omega)^2 m + j3\omega c + k_1]\mathcal{H}_3(\omega,\omega,\omega) + 2\alpha\mathcal{H}_1(\omega)\mathcal{H}_2(\omega,\omega) + \beta\mathcal{H}_1^3(\omega) = 0 \\ \Leftrightarrow \mathcal{H}_3(\omega,\omega,\omega) = 2\alpha^2\mathcal{H}_1^3(\omega)\mathcal{H}_1(2\omega)H_1(3\omega) - \beta\mathcal{H}_1^3(\omega)\mathcal{H}_1(3\omega)\end{aligned} \tag{10}$$

It is worth noting that the term $\mathcal{H}_1(\omega)$ is the linear transfer function described in terms of physical parameters from equation of motion. It shows that the harmonic probing method is a white-box methodology since it is necessary the knowledge of the system (BEDROSIAN; RICE, 1971). Moreover, the transfer functions of second and third order $\mathcal{H}_2(\omega,\omega)$ and $\mathcal{H}_3(\omega,\omega,\omega)$, respectively, are functions of $\mathcal{H}_1(\omega)$ and they allow to provide an insight into the nonlinear behavior of the system once they are functions of the nonlinear parameters as well (BILLINGS; TSANG, 1989a; BILLINGS; TSANG, 1989b). The theory briefly reviewed in this section will be extended for the case with multiple outputs in the next Section.

2.3 Single-input and multi-output (SIMO) Volterra series theory

The functionals of Volterra series for single-input and multi-output (SIMO) systems with pth output and the input are described by (WORDEN et al., 1997):

$$y^{(p)}(t) = \sum_{\eta=1}^{+\infty} y_\eta^{(p)}(t) = y_1^{(p)}(t) + y_2^{(p)}(t) + y_3^{(p)}(t) + \dots \tag{11}$$

where the respective polynomial contributions of ηth order are given by the following mapping:

$$y_\eta^{(p)}(t) = \int_{-\infty}^{+\infty} \dots \int_{-\infty}^{+\infty} h_\eta^{(p)}(\tau_1, \tau_2, \dots, \tau_\eta) \prod_{i=1}^{\eta} u(t-\tau_i) d\tau_i \tag{12}$$

The term $h_\eta^{(p)}(\tau_1,\ldots,\tau_\eta)$ is the Volterra kernel of ηth order related with the pth output and is a generalization of the well known impulse response function (IRF). The multi-dimensional Fourier transform of the Volterra kernels is computed as follows:

$$\mathcal{H}_\eta^{(p)}(\omega_1,\omega_2,\ldots,\omega_\eta) = \int_{-\infty}^{+\infty}\int_{-\infty}^{+\infty}\ldots\int_{-\infty}^{+\infty} h_\eta^{(p)}(\tau_1,\tau_2,\ldots,\tau_\eta)\prod_{i=1}^{\eta} e^{-j\omega_i\tau_i} d\tau_1 d\tau_2\ldots d\tau_\eta \quad (13)$$

Now, by considering the property of symmetry of the kernels, as can be found in Cafferty and Tomlinson (1997), and a single-tone input $u(t) = \frac{A}{2}e^{j\omega t} + \frac{A}{2}e^{-j\omega t}$, the output in Eq. (11) is given as:

$$\begin{aligned} y^{(p)}(t) &= \frac{A}{2}\mathcal{H}_1^{(p)}(\omega)e^{j\omega t} + \frac{A}{2}\mathcal{H}_1^{(p)}(-\omega)e^{-j\omega t} \\ &+ \frac{A^2}{4}\mathcal{H}_2^{(p)}(\omega,\omega)e^{j2\omega t} + \frac{A^2}{2}\mathcal{H}_2^{(p)}(-\omega,\omega) + \frac{A^2}{4}\mathcal{H}_2^{(p)}(-\omega,-\omega)e^{-j2\omega t} \\ &+ \frac{A^3}{8}\mathcal{H}_3^{(p)}(\omega,\omega,\omega)e^{j3\omega t} + \frac{3A^3}{8}\mathcal{H}_3^{(p)}(-\omega,\omega,\omega)e^{j\omega t} \\ &+ \frac{3A^3}{8}\mathcal{H}_3^{(p)}(-\omega,-\omega,\omega)e^{-j\omega t} + \frac{A^3}{8}\mathcal{H}_3^{(p)}(-\omega,-\omega,-\omega)e^{-j3\omega t} \\ &+ \ldots, \end{aligned} \quad (14)$$

where A is the forcing level amplitude and ω is the excitation frequency.

Without loss of generality to illustrate the method, a classical two degrees-of-freedom (2DOF) Duffing oscillator, as can be seen in Fig. 1, with quadratic and cubic nonlinearity is used. Furthermore, at the end of this section the framework of the conventional HOFRFs as a function of the physical parameters of mass, damping and stiffness is reviewed.

Figure 1 – Duffing oscillator with 2DOF and nonlinearities involving quadratic and cubic stiffnesses.

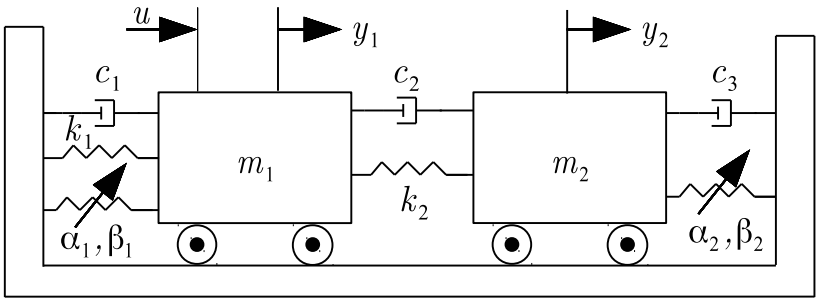

Source: Prepared by the author.

The system in Fig. 1 is described by the following equations of motion:

$$\mathbf{M}\ddot{\mathbf{y}} + \mathbf{C}\dot{\mathbf{y}} + \mathbf{K}\mathbf{y} + \mathcal{F}_{nl}(\mathbf{y}) = \mathbf{u}, \tag{15}$$

where $\mathbf{M}, \mathbf{C}$ and $\mathbf{K}$ are the mass, damping and stiffness matrices, respectively, described as:

$$\mathbf{M} = \begin{bmatrix} m_1 & 0 \\ 0 & m_2 \end{bmatrix}, \ \mathbf{K} = \begin{bmatrix} k_1 + k_2 & -k_2 \\ -k_2 & k_2 \end{bmatrix} \text{ and } \mathbf{C} = \begin{bmatrix} c_1 + c_2 & -c_2 \\ -c_2 & c_2 + c_3 \end{bmatrix} \tag{16}$$

The term $\mathbf{u}$ is the set force excitation vector and $\mathbf{y}$ is the set of output vectors:

$$\mathbf{u} = \begin{Bmatrix} u(t) & 0 \end{Bmatrix}^T \text{ and } \mathbf{y} = \begin{Bmatrix} y^{(1)}(t) & y^{(2)}(t) \end{Bmatrix}^T,$$

where the superscript ^{T} denotes the transpose and $\mathcal{F}_{nl}(\mathbf{y})$ denotes the nonlinear functional given by:

$$\mathcal{F}_{nl}(\mathbf{y}) = \begin{Bmatrix} \alpha_1[y^{(1)}(t)]^2 + \beta_1[y^{(1)}(t)]^3 & \alpha_2[y^{(2)}(t)]^2 + \beta_2[y^{(2)}(t)]^3 \end{Bmatrix}^T.$$

where α_1 and β_1 are the components of quadratic and cubic stiffnesses, respectively, connected to the first mass. The terms α_2 and β_2 are the components of quadratic and cubic stiffnesses connected to the second mass. From the Volterra expansion in Eq. (11) with $\eta = 3$, the displacement of the first mass can be represented as:

$$\begin{aligned} y^{(1)}(t) &= \underbrace{\int_{-\infty}^{\infty} h_1^{(1)}(\tau_1)u(t-\tau_1)d\tau_1}_{y_1^{(1)}(t)} \\ &+ \underbrace{\int_{-\infty}^{\infty}\int_{-\infty}^{\infty} h_2^{(1)}(\tau_1,\tau_2)u(t-\tau_1)u(t-\tau_2)d\tau_1 d\tau_2}_{y_2^{(1)}(t)} \\ &+ \underbrace{\int_{-\infty}^{\infty}\int_{-\infty}^{\infty}\int_{-\infty}^{\infty} h_3^{(1)}(\tau_1,\tau_2,\tau_3)u(t-\tau_1)u(t-\tau_2)u(t-\tau_3)d\tau_1 d\tau_2 d\tau_3}_{y_3^{(1)}(t)} \end{aligned} \tag{17}$$

where $y_1^{(1)}(t)$ is the linear contribution, $y_2^{(1)}(t)$ is the quadratic contribution and $y_3^{(1)}(t)$ denotes the cubic polynomial contribution. By assuming a harmonic input $u(t) = Ae^{j\omega t}$ applied to the first mass, the output can be rewritten as a function of the HOFRFs:

$$y^{(1)}(t) = Ae^{j\omega t}\mathcal{H}_1^{(1)}(\omega) + A^2e^{j2\omega t}\mathcal{H}_2^{(1)}(\omega,\omega) + A^3e^{j3\omega t}\mathcal{H}_3^{(1)}(\omega,\omega,\omega) \tag{18}$$

Differentiating $y^{(1)}(t)$ for the velocity and the acceleration yields

$$\begin{aligned}\dot{y}^{(1)}(t) &= j\omega A e^{j\omega t}\mathcal{H}_1^{(1)}(\omega) + j2\omega A^2 e^{j2\omega t}\mathcal{H}_2^{(1)}(\omega,\omega) + j3\omega A^3 e^{j3\omega t}\mathcal{H}_3^{(1)}(\omega,\omega,\omega),\\ \ddot{y}^{(1)}(t) &= -\omega^2 A e^{j\omega t}\mathcal{H}_1^{(1)}(\omega) - 4\omega^2 A^2 e^{j2\omega t}\mathcal{H}_2^{(1)}(\omega,\omega) - 9\omega^2 A^3 e^{j3\omega t}\mathcal{H}_3^{(1)}(\omega,\omega,\omega).\end{aligned}$$

By substituting the terms $y^{(1)}(t)$, $\dot{y}^{(1)}(t)$ and $\ddot{y}^{(1)}(t)$ into the Eq. (15) and equating the coefficients of $Ae^{j\omega t}$ generates the following expressions for the FRFs of first order:

$$\mathcal{H}_1^{(1)}(\omega) = \frac{1}{-m_1\omega^2 + (k_1 + k_2) + j\omega(c_1 + c_2)} \tag{19}$$

$$\mathcal{H}_1^{(2)}(\omega) = \frac{1}{-k_2 - j\omega c_2} \tag{20}$$

the FRFs of second order are obtained by equating the coefficients of $A^2e^{j2\omega t}$:

$$\mathcal{H}_2^{(1)}(\omega,\omega) = -\alpha_1[\mathcal{H}_1^{(1)}(\omega)]^2\mathcal{H}_1^{(1)}(2\omega) \tag{21}$$

Now, equating the coefficients of $A^3e^{j3\omega t}$ yields the FRF of third order:

$$\mathcal{H}_3^{(1)}(\omega,\omega,\omega) = [\mathcal{H}_1^{(1)}(\omega)]^3\mathcal{H}_1^{(1)}(3\omega)\Big[2\alpha_1^2\mathcal{H}_1^{(1)}(2\omega) - \beta_1\Big] \tag{22}$$

Nevertheless, the conventional harmonic probing method briefly reviewed in this section is applicable only in cases where the input signal is known. Thus, this formulation is quite limited for applications under operational conditions where the excitation force is unmeasured. Consequently, an extended version of the conventional method to treat such cases through output-only is very welcome. Thus, the next Section presents one of the contributions of this thesis, an extension of the harmonic probing method and the algebraic expressions of the extended HOFRFs based on output-only data. These results were published in Scussel and da Silva (2017).

2.4 Harmonic probing method based on output-only signals

This section presents a theorem for the existence of extended HOFRFs. In order to provide the analytical expressions of extended HOFRFs, an alternative procedure based on the conventional harmonic probing method is proposed. Furthermore, theoretical aspects of the model based on output-only signals as well as its significance, benefits and

possible limitations are addressed.

Initially, the following assumptions are made:

i) For the SIMO system described in Eq. (15), a single-tone harmonic force excitation $u(t) = \cos(\omega t) = \frac{A}{2}(e^{j\omega t} + e^{-j\omega t})$ is applied to the first mass.

ii) Without loss of generality, suppose that the system has a convergent polynomial expansion truncated up to third-order based on the conventional Volterra kernels as in Eq. (17).

Theorem 1 *By assuming i) and ii), then the output signal can be expressed as a multi-dimensional convolution between the extended Volterra kernels and the linear contribution of another output as follows:*

$$\begin{aligned} y^{(1)}(t) &= \int_{-\infty}^{\infty} g_1^{(1)}(\tau_1) y_1^{(2)}(t-\tau_1) d\tau_1 \\ &+ \int_{-\infty}^{\infty}\int_{-\infty}^{\infty} g_2^{(1)}(\tau_1,\tau_2) y_1^{(2)}(t-\tau_1) y_1^{(2)}(t-\tau_2) d\tau_1 d\tau_2 \\ &+ \int_{-\infty}^{\infty}\int_{-\infty}^{\infty}\int_{-\infty}^{\infty} g_3^{(1)}(\tau_1,\tau_2,\tau_3) y_1^{(2)}(t-\tau_1) y_1^{(2)}(t-\tau_2) y_1^{(2)}(t-\tau_3) d\tau_1 d\tau_2 d\tau_3 \end{aligned} \tag{23}$$

where $g_1^{(1)}(\tau_1)$, $g_2^{(1)}(\tau_1,\tau_2)$ and $g_3^{(1)}(\tau_1,\tau_2,\tau_3)$ are the extended kernels of first, second and third-order, respectively.

Proof: Initially, it is considered the harmonic input as $u(t) = Ae^{j\omega t}$ from i) applied to the first mass of the system in Eq. (15). The part with $e^{-j\omega t}$ is neglected in order to simplify the expressions presented. Thus, from Eq. (17), the linear polynomial contribution of the output $y^{(1)}(t)$ is given by:

$$\begin{aligned} y_1^{(1)}(t) &= \int_{-\infty}^{\infty} h_1^{(1)}(\tau_1) u(t-\tau_1) d\tau_1 = Ae^{j\omega t}\mathcal{H}_1^{(1)}(\omega) \\ \Leftrightarrow y_1^{(1)}(t) &= Ae^{j\omega t}\mathcal{H}_1^{(2)}(\omega)\mathcal{H}_1^{(1)}(\omega)\left[\mathcal{H}_1^{(2)}(\omega)\right]^{-1}, \end{aligned}$$

Assuming that $\mathcal{G}_1^{(1)}(\omega) = \mathcal{H}_1^{(1)}(\omega)\left[\mathcal{H}_1^{(2)}(\omega)\right]^{-1}$ yields:

$$\begin{aligned} y_1^{(1)}(t) &= Ae^{j\omega t}\mathcal{H}_1^{(2)}(\omega)\mathcal{G}_1^{(1)}(\omega) \\ \Leftrightarrow y_1^{(1)}(t) &= Ae^{j\omega t}\mathcal{H}_1^{(2)}(\omega)\int_{-\infty}^{\infty} g_1^{(1)}(\tau_1) e^{-j\omega\tau_1} d\tau_1 \\ \Leftrightarrow y_1^{(1)}(t) &= \int_{-\infty}^{\infty} g_1^{(1)}(\tau_1) Ae^{j\omega(t-\tau_1)}\mathcal{H}_1^{(2)}(\omega) d\tau_1 \\ \Leftrightarrow y_1^{(1)}(t) &= \int_{-\infty}^{\infty} g_1^{(1)}(\tau_1) y_1^{(2)}(t-\tau_1) d\tau_1. \end{aligned}$$

The quadratic contribution of the output $y^{(1)}(t)$ is calculated to be:

$$\begin{aligned}
y_2^{(1)}(t) &= A^2 e^{j2\omega t}\mathcal{H}_2^{(1)}(\omega,\omega)\\
\Leftrightarrow y_2^{(1)}(t) &= A^2 e^{j2\omega t}[\mathcal{H}_1^{(2)}(\omega)]^2\Big[-\alpha_1[\mathcal{H}_1^{(1)}(\omega)]^2\mathcal{H}_1^{(1)}(2\omega)\Big][\mathcal{H}_1^{(2)}(\omega)]^{-2}\\
\Leftrightarrow y_2^{(1)}(t) &= A^2 e^{j2\omega t}[\mathcal{H}_1^{(2)}(\omega)]^2\mathcal{G}_2^{(1)}(\omega,\omega)\\
\Leftrightarrow y_2^{(1)}(t) &= A^2 e^{j2\omega t}[\mathcal{H}_1^{(2)}(\omega)]^2\int_{-\infty}^{\infty}\int_{-\infty}^{\infty} g_2^{(1)}(\tau_1,\tau_2)e^{-j\omega\tau_1}e^{-j\omega\tau_2}d\tau_1 d\tau_2\\
\Leftrightarrow y_2^{(1)}(t) &= \int_{-\infty}^{\infty}\int_{-\infty}^{\infty} g_2^{(1)}(\tau_1,\tau_2)y_1^{(2)}(t-\tau_1)y_1^{(2)}(t-\tau_2)d\tau_1 d\tau_2.
\end{aligned}$$

Now, the cubic contribution of $y^{(1)}(t)$ is computed as:

$$\begin{aligned}
y_3^{(1)}(t) &= A^3 e^{j3\omega t}\mathcal{H}_3^{(1)}(\omega,\omega,\omega)\\
\Leftrightarrow y_3^{(1)}(t) &= A^3 e^{j3\omega t}[\mathcal{H}_1^{(2)}(\omega)]^3[\mathcal{H}_1^{(1)}(\omega)]^3[\mathcal{H}_1^{(2)}(\omega)]^{-3}\mathcal{H}_1^{(1)}(3\omega)\Big[2\alpha_1^2\mathcal{H}_1^{(1)}(2\omega)-\beta_1\Big]\\
\Leftrightarrow y_3^{(1)}(t) &= A^3 e^{j3\omega t}[\mathcal{H}_1^{(2)}(\omega)]^3\mathcal{G}_3^{(1)}(\omega,\omega,\omega)\\
\Leftrightarrow y_3^{(1)}(t) &= A^3 e^{j3\omega t}[\mathcal{H}_1^{(2)}(\omega)]^3\int_{-\infty}^{\infty}\int_{-\infty}^{\infty}\int_{-\infty}^{\infty} g_3^{(1)}(\tau_1,\tau_2,\tau_3)e^{-j\omega(\tau_1+\tau_2+\tau_3)}d\tau_1 d\tau_2 d\tau_3\\
\Leftrightarrow y_3^{(1)}(t) &= \int_{-\infty}^{\infty}\int_{-\infty}^{\infty}\int_{-\infty}^{\infty} g_3^{(1)}(\tau_1,\tau_2,\tau_3)y_1^{(2)}(t-\tau_1)y_1^{(2)}(t-\tau_2)y_1^{(2)}(t-\tau_3)d\tau_1 d\tau_2 d\tau_3.
\end{aligned}$$

From assumption ii) implies directly in $y^{(1)}(t) = y_1^{(1)}(t) + y_2^{(1)}(t) + y_3^{(1)}(t)$. Thus, the theorem 1 is proved. □

It is important to emphasize that the theorem and the procedure presented in this section can be generalized for any arbitrary polynomial order η by simply taking into account the framework of the extended FRF $G_\eta^{(p)}(\omega,\ldots,\omega)$ related to the pth output signal.

Now, in order to obtain the analytical expressions of the extended HOFRFs, a simple procedure based on the conventional harmonic probing is applied. From Theorem 1, Eq. (23) can be rewritten as:

$$\begin{aligned}
y^{(1)}(t) &= \int_{-\infty}^{\infty} g_1^{(1)}(\tau_1)Ae^{j\omega(t-\tau_1)}\mathcal{H}_1^{(2)}(\omega)d\tau_1\\
&+ \int_{-\infty}^{\infty}\int_{-\infty}^{\infty} g_2^{(1)}(\tau_1,\tau_2)Ae^{j\omega(t-\tau_1)}\mathcal{H}_1^{(2)}(\omega)Ae^{j\omega(t-\tau_2)}\mathcal{H}_1^{(2)}(\omega)d\tau_1 d\tau_2\\
&+ \int_{-\infty}^{\infty}\int_{-\infty}^{\infty}\int_{-\infty}^{\infty} g_3^{(1)}(\tau_1,\tau_2,\tau_3)Ae^{j\omega(t-\tau_1)}\mathcal{H}_1^{(2)}(\omega)Ae^{j\omega(t-\tau_2)}\mathcal{H}_1^{(2)}(\omega)\\
&\times\ Ae^{j\omega(t-\tau_3)}\mathcal{H}_1^{(2)}(\omega)d\tau_1 d\tau_2 d\tau_3,
\end{aligned}$$

$$\begin{aligned}
\Leftrightarrow y^{(1)}(t) &= Ae^{j\omega(t)}\mathcal{H}_1^{(2)}(\omega)\int_{-\infty}^{\infty} g_1^{(1)}(\tau_1)e^{-j\omega\tau_1}d\tau_1 \\
&+ A^2e^{j2\omega t}[\mathcal{H}_1^{(2)}(\omega)]^2\int_{-\infty}^{\infty}\int_{-\infty}^{\infty} g_2^{(1)}(\tau_1,\tau_2)e^{-j\omega(\tau_1+\tau_2)}d\tau_1 d\tau_2 \\
&+ A^3e^{j3\omega t}[\mathcal{H}_1^{(2)}(\omega)]^3\int_{-\infty}^{\infty}\int_{-\infty}^{\infty}\int_{-\infty}^{\infty} g_3^{(1)}(\tau_1,\tau_2,\tau_3)e^{-j\omega(\tau_1+\tau_2+\tau_3)}d\tau_1 d\tau_2 d\tau_3.
\end{aligned}$$

Thus, from Eq. (13) the output is given as:

$$\begin{aligned}
y^{(1)}(t) &= Ae^{j\omega t}\mathcal{H}_1^{(2)}(\omega)\mathcal{G}_1^{(1)}(\omega) + A^2e^{j2\omega t}[\mathcal{H}_1^{(2)}(\omega)]^2\mathcal{G}_2^{(1)}(\omega,\omega) \\
&+ A^3e^{j3\omega t}[\mathcal{H}_1^{(2)}(\omega)]^3\mathcal{G}_3^{(1)}(\omega,\omega,\omega) \qquad (24)
\end{aligned}$$

By differentiating $y^{(1)}(t)$ in Eq. (24) yields expressions for the respective velocity and acceleration as:

$$\begin{aligned}
\dot{y}^{(1)}(t) &= j\omega Ae^{j\omega t}\mathcal{H}_1^{(2)}(\omega)\mathcal{G}_1^{(1)}(\omega) + j2\omega A^2e^{j2\omega t}[\mathcal{H}_1^{(2)}(\omega)]^2\mathcal{G}_2^{(1)}(\omega,\omega) \\
&+ j3\omega A^3e^{j3\omega t}[\mathcal{H}_1^{(2)}(\omega)]^3\mathcal{G}_3^{(1)}(\omega,\omega,\omega), \\
\ddot{y}^{(1)}(t) &= -\omega Ae^{j\omega t}\mathcal{H}_1^{(2)}(\omega)\mathcal{G}_1^{(1)}(\omega) - 4\omega^2A^2e^{j2\omega t}[\mathcal{H}_1^{(2)}(\omega)]^2\mathcal{G}_2^{(1)}(\omega,\omega) \\
&- 9\omega^2A^3e^{j3\omega t}[\mathcal{H}_1^{(2)}(\omega)]^3\mathcal{G}_3^{(1)}(\omega,\omega,\omega),
\end{aligned}$$

By substituting the terms $y^{(1)}(t)$, $\dot{y}^{(1)}(t)$ and $\ddot{y}^{(1)}(t)$ into Eq. (15) provides

$$\begin{aligned}
Ae^{j\omega t} &= m_1\Big[-\omega^2Ae^{j\omega t}\mathcal{H}_1^{(2)}(\omega)\mathcal{G}_1^{(1)}(\omega) - 4\omega^2A^2e^{j2\omega t}[\mathcal{H}_1^{(2)}(\omega)]^2\mathcal{G}_2^{(1)}(\omega,\omega) \\
&- 9\omega^2A^3e^{j3\omega t}[\mathcal{H}_1^{(2)}(\omega)]^3\mathcal{G}_3^{(1)}(\omega,\omega,\omega)\Big] + (k_1+k_2)\Big[Ae^{j\omega t}\mathcal{H}_1^{(2)}(\omega)\mathcal{G}_1^{(1)}(\omega) \\
&+ A^2e^{j2\omega t}[\mathcal{H}_1^{(2)}(\omega)]^2\mathcal{G}_2^{(1)}(\omega,\omega) + A^3e^{j3\omega t}[\mathcal{H}_1^{(2)}(\omega)]^3\mathcal{G}_3^{(1)}(\omega,\omega,\omega)\Big] \\
&+ (c_1+c_2)\Big[j\omega Ae^{j\omega t}\mathcal{H}_1^{(2)}(\omega)\mathcal{G}_1^{(1)}(\omega) + j2\omega A^2e^{j2\omega t}[\mathcal{H}_1^{(2)}(\omega)]^2\mathcal{G}_2^{(1)}(\omega,\omega) \\
&+ j3\omega A^3e^{j3\omega t}[\mathcal{H}_1^{(2)}(\omega)]^3\mathcal{G}_3^{(1)}(\omega,\omega,\omega)\Big] + \alpha_1\Big[Ae^{j\omega t}\mathcal{H}_1^{(2)}(\omega)\mathcal{G}_1^{(1)}(\omega) \\
&+ A^2e^{j2\omega t}[\mathcal{H}_1^{(2)}(\omega)]^2\mathcal{G}_2^{(1)}(\omega,\omega) + A^3e^{j3\omega t}[\mathcal{H}_1^{(2)}(\omega)]^3\mathcal{G}_3^{(1)}(\omega,\omega,\omega)\Big]^2 \\
&+ \beta_1\Big[Ae^{j\omega t}\mathcal{H}_1^{(2)}(\omega)\mathcal{G}_1^{(1)}(\omega) + A^2e^{j2\omega t}[\mathcal{H}_1^{(2)}(\omega)]^2\mathcal{G}_2^{(1)}(\omega,\omega) \\
&+ A^3e^{j3\omega t}[\mathcal{H}_1^{(2)}(\omega)]^3\mathcal{G}_3^{(1)}(\omega,\omega,\omega)\Big]^3,
\end{aligned}$$

Equating the coefficients of $Ae^{j\omega t}$ yields:

$$\begin{aligned}
1 &= \mathcal{G}_1^{(1)}(\omega)\mathcal{H}_1^{(2)}(\omega)[-\omega^2m_1 + (k_1+k_2) + (c_1+c_2)j\omega] \\
\Leftrightarrow \mathcal{G}_1^{(1)}(\omega) &= \frac{-k_2 - c_2j\omega}{-\omega^2m_1 + (k_1+k_2) + (c_1+c_2)j\omega} \qquad (25)
\end{aligned}$$

Consequently, the extended FRF in Eq. (25) can be rewritten as

$$\mathcal{G}_1^{(1)}(\omega) = \frac{\mathcal{H}_1^{(1)}(\omega)}{\mathcal{H}_1^{(2)}(\omega)} \tag{26}$$

Now, by equating the coefficients of $A^2 e^{j2\omega t}$ provides:

$$0 = [\mathcal{H}_1^{(2)}(\omega)]^2 \mathcal{G}_2^{(1)}(\omega,\omega)\Big[-4\omega^2 m_1 + (k_1+k_2) + (c_1+c_2)j2\omega\Big] + \alpha_1[\mathcal{H}_1^{(2)}(\omega)\mathcal{G}_1^{(1)}(\omega)]^2$$

$$\Leftrightarrow \mathcal{G}_2^{(1)}(\omega,\omega) = -\alpha_1[\mathcal{G}_1^{(1)}(\omega)]^2 \mathcal{H}_1^{(1)}(2\omega) \tag{27}$$

From Eq. (26), the extended FRF of second order can be expressed as:

$$\mathcal{G}_2^{(1)}(\omega,\omega) = -\alpha_1\left[\frac{\mathcal{H}_1^{(1)}(\omega)}{\mathcal{H}_1^{(2)}(\omega)}\right]^2 \mathcal{H}_1^{(1)}(2\omega) \tag{28}$$

Furthermore, by equating the coefficients of $A^3 e^{j3\omega t}$ yields:

$$\begin{aligned} 0 &= [\mathcal{H}_1^{(2)}(\omega)]^3 \mathcal{G}_3^{(1)}(\omega,\omega,\omega)\Big[-9\omega^2 m_1 + (k_1+k_2) + (c_1+c_2)j3\omega\Big] \\ &+ 2\alpha_1[\mathcal{H}_1^{(2)}(\omega)]^3 \mathcal{G}_1^{(1)}(\omega)\mathcal{G}_2^{(1)}(\omega,\omega) + \beta_1[\mathcal{H}_1^{(2)}(\omega)\mathcal{G}_1^{(1)}(\omega)]^3 \\ \mathcal{G}_3^{(1)}(\omega,\omega,\omega) &= 2\alpha_1^2 \mathcal{G}_1^{(1)}(\omega)^3 \mathcal{H}_1^{(1)}(2\omega)\mathcal{H}_1^{(1)}(3\omega) - \beta_1 \mathcal{G}_1^{(1)}(\omega)^3 \mathcal{H}_1^{(1)}(3\omega), \end{aligned}$$

Thus, the extended FRF of third order can be computed alternatively as:

$$\mathcal{G}_3^{(1)}(\omega,\omega,\omega) = \left[\frac{\mathcal{H}_1^{(1)}(\omega)}{\mathcal{H}_1^{(2)}(\omega)}\right]^3 \mathcal{H}_1^{(1)}(3\omega)\left[2\alpha_1^2 \mathcal{H}_1^{(1)}(2\omega) - \beta_1\right] \tag{29}$$

The extended FRF $\mathcal{G}_1^{(1)}(\omega)$ from Eq. (26) shows an important result which describes itself as a ratio between the conventional FRFs from Eqs. (19) and (20). Basically, it represents a simple ratio between two output spectra of the structure of interest and defines the concept of transmissibility that has been widely studied used for damage detection and fault diagnosis (MAIA et al., 2001; WEIJTJENS et al., 2014; CHESNÉ; DERAEMAEKER, 2013; ZHAO et al., 2015; ALJANAIDEH; BERNSTEIN, 2017). Thus, this new concept of extended FRF presents similar characteristics to the concept of transmissibility since the function $\mathcal{G}_1^{(1)}(\omega)$ behaves and it is computed in a similar way as the transmissibility functions (TFs) .

Moreover, it can be seen in Eqs. (28) and (29) that the second and third order ex-

tended FRFs, $\mathcal{G}_2^{(1)}(\omega,\omega)$ and $G_3^{(1)}(\omega,\omega,\omega)$, are also related to the conventional FRFs and the nonlinear parameters as well. It is important to point out that the extended HOFRFs introduced here have a similar definition as the transmissibility funtions of NOFRFs presented by Lang et al. (2011) and Zhao et al. (2015). Thus, the extended version of the harmonic probing method may present potential features for further applications in transmissibility for damage detection, location and fault diagnosis of nonlinear systems.

Although the extended HOFRFs reveal great features and benefits for prediction of nonlinear vibrating systems based on output-only, the method might present some drawbacks and limitations such as the convergence of the series, the order of the Volterra kernels and number of parameters to be estimated. Usually, the convergence problems are directly related to the amplitude of excitation, discontinuities and complex nonlinearities. The Volterra series representation might not be appropriate to deal with systems characterized by effects, such as strong jump phenomena, limit-cycles, chaos, etc (TOMLINSON et al., 1996; THOUVEREZ, 1998; CHATTERJEE; VYAS, 2000; PENG; LANG, 2007). In order to deal with problems involving strong nonlinearities it will be necessary to consider more terms in the Volterra series expansion. Despite the limitations discussed, the advantage of the method presented lies in its ability to treat weakly nonlinear systems through the extended HOFRFs up until third order as stated in Scussel and da Silva (2017). In Section 2.5, the method is applied in a Duffing oscillator system with 2DOF characterized by restoring force involving quadratic and cubic nonlinearities associated to the stiffness. The results reached by the extended method are compared with the results found by the conventional harmonic probing method.

2.5 Numerical analysis

In order to illustrate the approaches, conventional and extended harmonic probing, the system described in Eq. (15) is used. The main goal is to show how the extended HOFRFs are able to compute the response as well as the conventional HOFRFs. Additionally, the possibility of analysing the polynomial contributions (linear, quadratic and cubic) of the total output predicted is also a mighty property investigated. The physical parameters showed in the Tab. 1 are adopted.

A harmonic input $u(t) = A\cos(2\pi\omega t)$ with amplitude of $A = 0.48$ N and the excitation frequency close to $f = 11$ Hz is applied to the first mass. The outputs are obtained by solving numerically the equations of motion through Newmark method combined with Newton-Raphson procedure and initial conditions $(y^{(1)}(0), y^{(2)}(0)) = (0,0)$

Table 1 – Parameters of the Duffing oscillator with 2DOF and restoring force characterized by quadratic and cubic stiffnesses.

Parameter	Value
m_1	1 [kg]
m_2	1 [kg]
k_1	10^4 [N/m]
k_2	9×10^4 [N/m]
c_1	10 [N.s/m]
c_2	10 [N.s/m]
c_3	10 [N.s/m]
α_1	10^5 [N/m^2]
α_2	10^5 [N/m^2]
β_1	10^9 [N/m^3]
β_2	10^9 [N/m^3]

Source: Prepared by the author.

and $(\dot{y}^{(1)}(0), \dot{y}^{(2)}(0)) = (0.0240, 0.0240)$ in order to obtain the transient and steady-state regimes in the response apparently with the same amplitude. A sampling rate of 500 Hz corresponding approximately to 45 times the first fundamental resonance and 8 times the second one is used to avoid aliasing effects. Furthermore, it is important to note that the nonlinear system adopted here is characterized by the linear resonances for the first and second linear modes close to 11 Hz and 68.5 Hz, respectively.

The simulation is performed with a time duration of 10 seconds and by using 5001 samples. Additionally, the power spectral density (PSD) function of the reference dataset is calculated. In order to attain this purpose, Welch's periodogram is adopted with Hanning window. However, Fig. 2 shows a zoom of the PSDs over a frequency range of 5-40 Hz in order to provide a better visual inspection of the curves. Figure 2(a) shows the PSD of the force excitation, denoted as $P_u(\omega)$, where it is possible to note the peak that correspond to the first fundamental frequency of resonance at approximately 11 Hz. Furthermore, in Fig. 2(b) is showed the PSD of the first mass displacement, denoted as $P_{y^{(1)}}(\omega)$ is shown. It can be seen in such curve the presence of even and odd harmonics at 22 Hz and 33 Hz, respectively. These harmonics in the output spectrum point out the nonlinear effects of the system characterized by quadratic and cubic stiffnesses.

The physical parameters described in Tab. 1 were used to compute the FRF of first order (the linear transfer function) $\mathcal{H}_1^{(1)}(\omega)$ from Eq. (19) and $\mathcal{G}_1^{(1)}(\omega)$ from Eq. (25) over a frequency range of 0-90 with increment step of 0.1 Hz. In general, Fig. 3 shows the comparison between the conventional FRF and extended FRF of first-order. Figures 3(a) and 3(b) show the magnitude and phase of the FRF $\mathcal{H}_1^{(1)}(\omega)$. The resonances peaks of

Figure 2 – Analysis of the harmonics in the response signal $y^{(1)}(t)$ subjected to a sinusoidal input applied to the first mass with excitation frequency close to 11 Hz and amplitude level of 0.48 N.

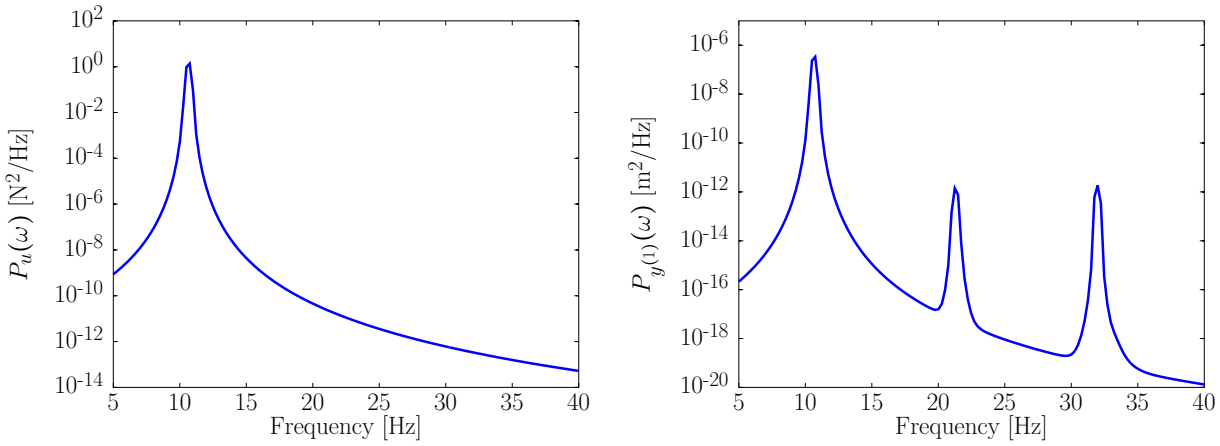

(a) PSD of the harmonic input applied to the first mass.

(b) PSD of the output $y^{(1)}(t)$ (displacement of the first mass).

Source: Prepared by the author.

the first mode (11 Hz) and the second mode (68.5 Hz) associated with the linear dynamic of the model can be seen. Figures 3(c) and 3(d) show the magnitude and phase of the extended FRF $\mathcal{G}_1^{(1)}(\omega)$ as well. In such case, it can be noted that only the anti-resonance peak (close to 48 Hz) appears and the figure presents characteristics of the transmissibility curve as can be verified in Eq. (26).

It is important to emphasize that extended FRF and the conventional one differ values in magnitude and phase because of their different framework. Moreover, the extended FRF has an additional term $-k_2 - c_2 j$. Although they present different behavior as discussed, they are used in a similar way to predict the linear contribution $y_1^{(1)}(t)$ of the output.

Figure 4 shows the frequency response functions of second order $\mathcal{H}_2^{(1)}(\omega,\omega)$ and $\mathcal{G}_2^{(1)}(\omega,\omega)$ in magnitude and phase. It is clearly possible to see in Fig. 4(a) the resonances at 11 Hz and 68.5 Hz and their secondary resonances at 5.50 Hz and 34.25 Hz, respectively. Thus, the framework of the conventional FRF of second-order characterizes the quadratic polynomial nolinearities and is used to predict the quadratic contribution of the total output of the model. On the other hand, the extended FRF of second order contains only the secondary resonances shown in Fig. 4(c). This effect is due to the framework of the function $\mathcal{G}_2^{(1)}(\omega,\omega)$ as in Eq. (28).

Figure 5 illustrates the frequency response functions of third order $\mathcal{H}_3^{(1)}(\omega,\omega,\omega)$ and

Figure 3 – First-order frequency response functions.

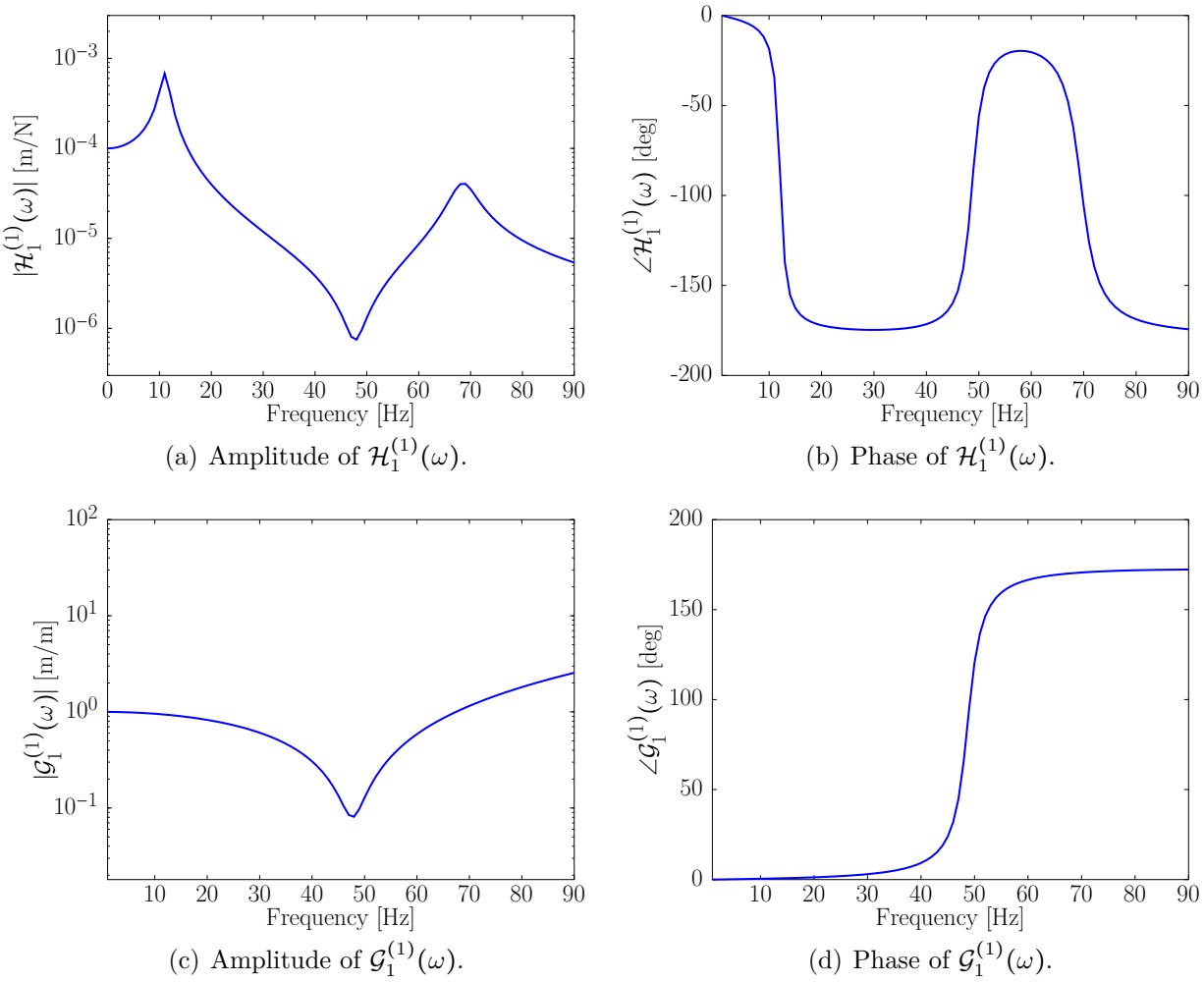

(a) Amplitude of $\mathcal{H}_1^{(1)}(\omega)$.

(b) Phase of $\mathcal{H}_1^{(1)}(\omega)$.

(c) Amplitude of $\mathcal{G}_1^{(1)}(\omega)$.

(d) Phase of $\mathcal{G}_1^{(1)}(\omega)$.

Source: Prepared by the author.

$\mathcal{G}_3^{(1)}(\omega,\omega,\omega)$ calculated by the algebraic expressions from Eqs. (22) and (29) in magnitude and phase. The conventional FRF of third order provides information about cubic nolinearities and is used to compute the cubic contribution of the total output of the model.

In Figure 5(a), it is possible to see that the conventional FRF exhibits the resonances at 11 Hz and 68.5 Hz and their tertiary resonances at 3.67 Hz and 22.8 Hz, approximately. However, it is worthing to mention that the secondary resonances do not appear due to the low contribution of quadratic stiffness terms α_1 and α_2 adopted. Cafferty and Tomlinson (1997) presented an example where the peaks referred to the second order are present in the conventional FRF of third order once the terms of quadratic stiffness have significant contribution.

Moreover, it can be observed in Fig. 5(c) the extended FRF showing that the tertiary

Figure 4 – Principal diagonal of the second order frequency response functions.

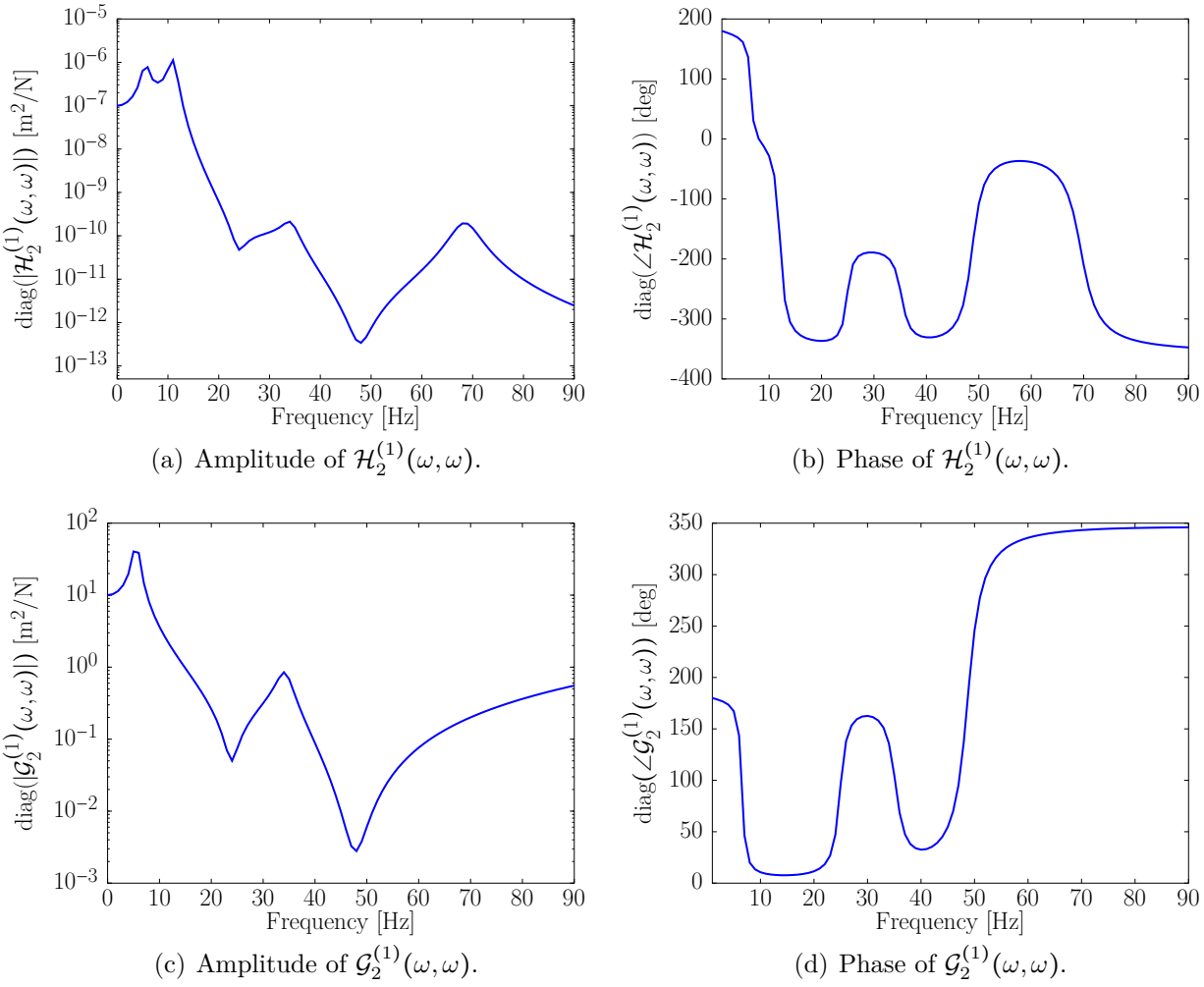

(a) Amplitude of $\mathcal{H}_2^{(1)}(\omega,\omega)$.

(b) Phase of $\mathcal{H}_2^{(1)}(\omega,\omega)$.

(c) Amplitude of $\mathcal{G}_2^{(1)}(\omega,\omega)$.

(d) Phase of $\mathcal{G}_2^{(1)}(\omega,\omega)$.

Source: Prepared by the author.

resonances arise only due the framework of $\mathcal{G}_3^{(1)}(\omega,\omega,\omega)$ from Eq. (29). In general, the extended kernels can be useful in applications of identification and transmissibility of nonlinear systems (SCUSSEL; da Silva, 2017).

The HOFRFs of each method are used to predict the respective polynomial contributions $y_1^{(1)}(t)$, $y_2^{(1)}(t)$ and $y_3^{(1)}(t)$. The possibility of splitting the total response predicted in polynomial contributions reveals one powerful benefit of using Volterra series expansion to describe weakly nonlinear systems. Although the framework of the functions $\mathcal{H}_\eta^{(1)}(\omega_1,\ldots,\omega_\eta)$ and $\mathcal{G}_\eta^{(1)}(\omega_1,\ldots,\omega_\eta)$ present different behavior as verified previously, they can be used to predict the response in a similar way. While the conventional one uses the input excitation, the extended one is based on another output measured.

Figure 6 shows the linear, quadratic and cubic contributions of the total output pre-

Figure 5 – Principal diagonal of the third order frequency response functions.

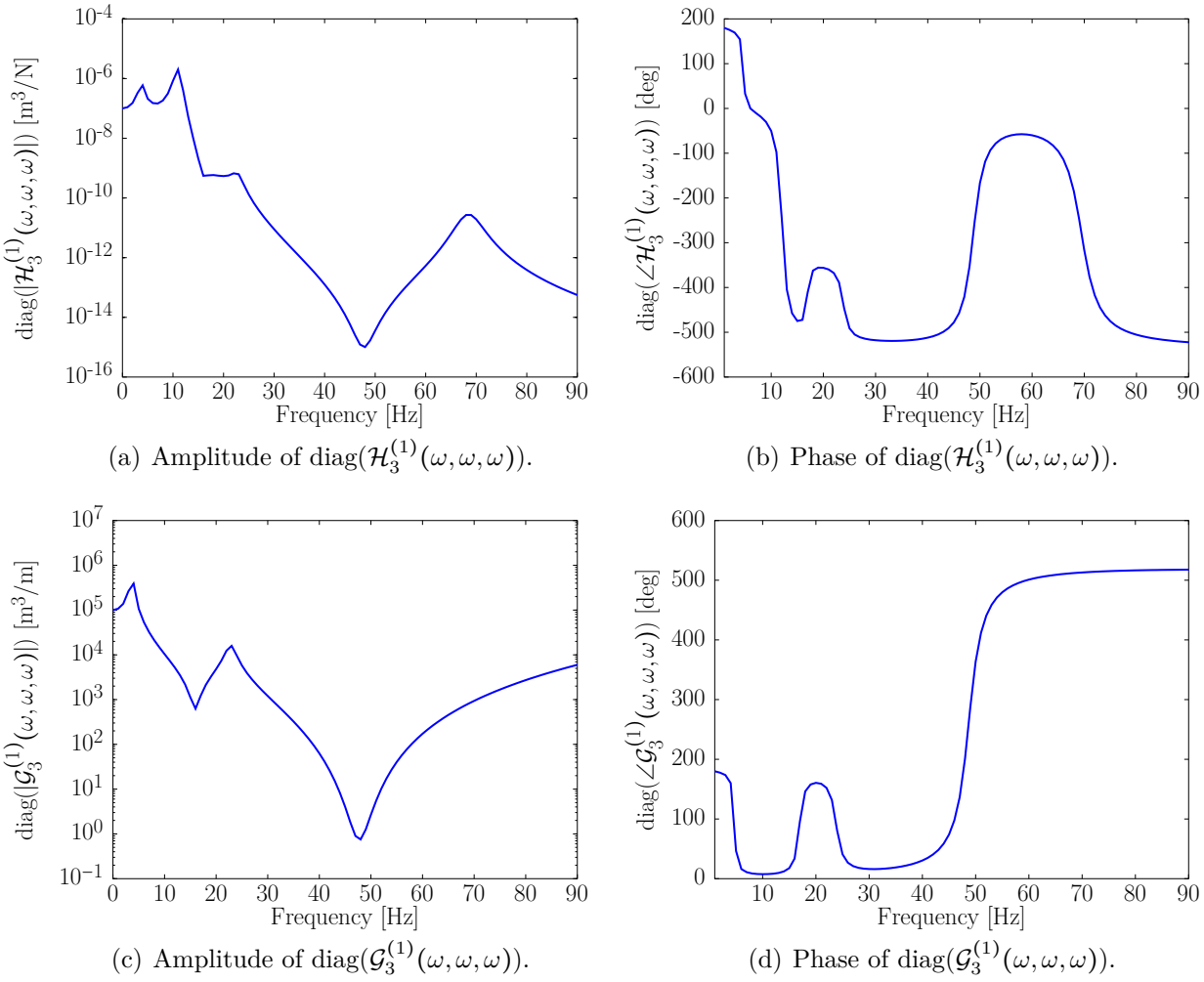

(a) Amplitude of diag($\mathcal{H}_3^{(1)}(\omega,\omega,\omega)$).

(b) Phase of diag($\mathcal{H}_3^{(1)}(\omega,\omega,\omega)$).

(c) Amplitude of diag($\mathcal{G}_3^{(1)}(\omega,\omega,\omega)$).

(d) Phase of diag($\mathcal{G}_3^{(1)}(\omega,\omega,\omega)$).

Source: Prepared by the author.

dicted by each method as well as their spectra where it can be noted that there is agreement. In this example, the temporal contribution of second order is quite low due to the terms α_1 and α_2 chosen. Additionally, it can be noted the asymmetric behavior of the contribution $y_2^{(1)}(t)$.

Figure 7 shows the comparison between the output simulated by the Newmark method and the outputs predicted by the conventional and extended harmonic probing method obtained by summing the contributions $y_1^{(1)}(t) + y_2^{(1)}(t) + y_3^{(1)}(t)$. In both cases, it is possible to see good agreement demonstrating the accuracy of the approaches for output prediction. Figure 8 shows response spectrum through the PSD function where is possible to note that the models were able to detect the presence of the fundamental frequency resonance at 11 Hz and the second and third harmonics, at 22 Hz at 33 Hz, called also

Figure 6 – Comparison between the results obtained by using the harmonic probing method (–) and the results reached by the method based on output-only data (∗).

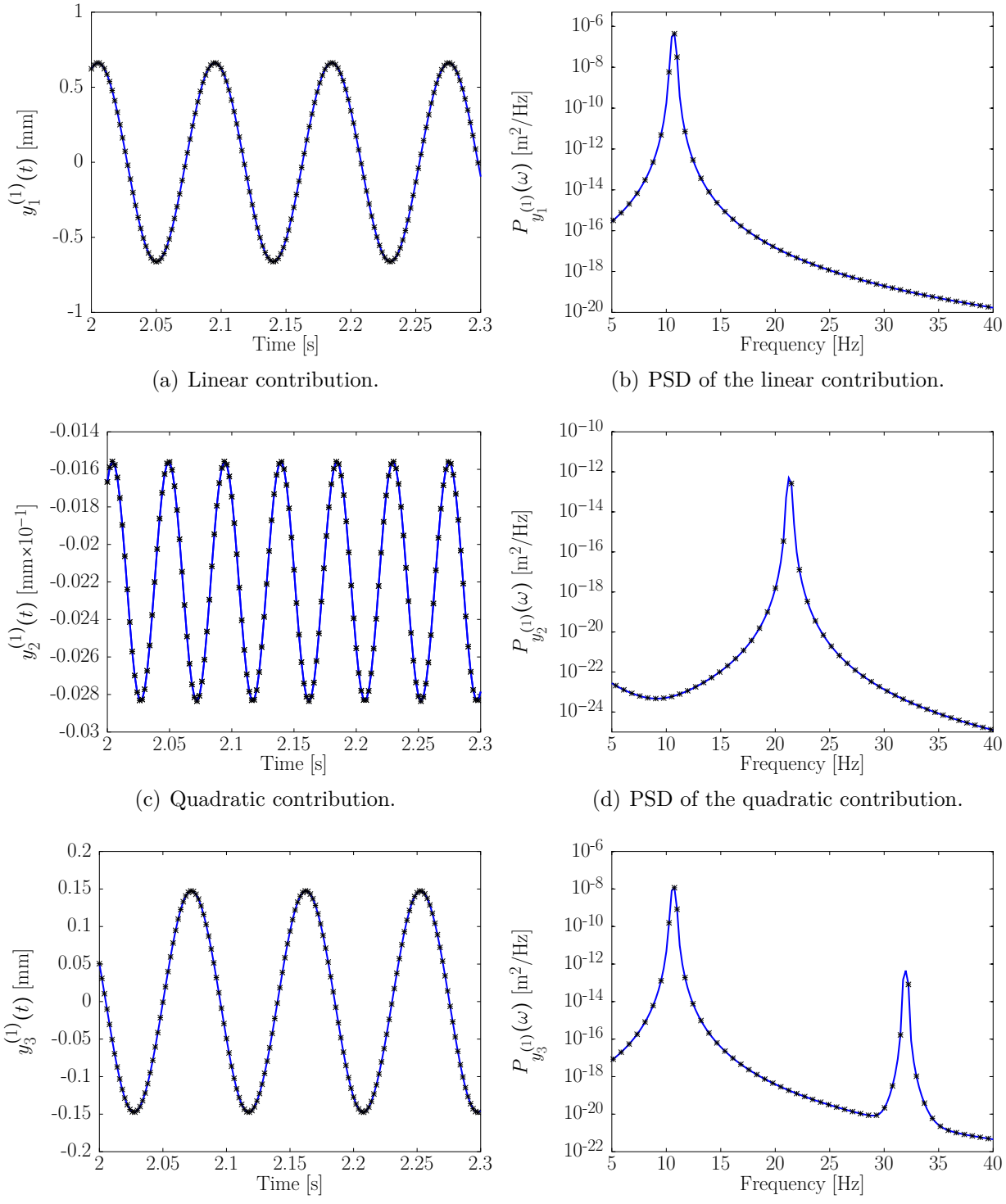

(a) Linear contribution.

(b) PSD of the linear contribution.

(c) Quadratic contribution.

(d) PSD of the quadratic contribution.

(e) Cubic contribution.

(f) PSD of the cubic contribution.

Source: Prepared by the author.

even and odd harmonics.

Figure 7 – Comparison of the output simulated by Newmark method (–) with the outputs predicted by the conventional and extended harmonic probing method (∗).

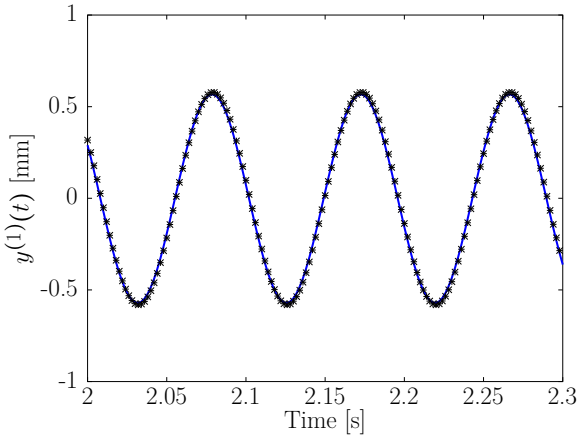

(a) Output simulated (–) and predicted by conventional harmonic probing method (∗).

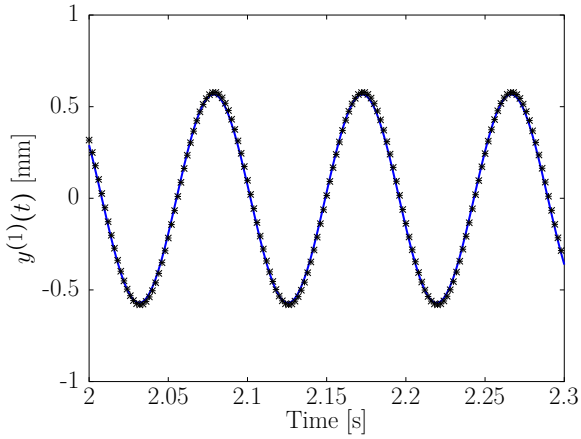

(b) Output simulated (–) and predicted by extended harmonic probing method (∗).

Source: Prepared by the author.

Figure 8 – Analysis of the outputs spectra simulated by Newmark method (–) and the outputs predicted by the conventional and extended harmonic probing method (∗).

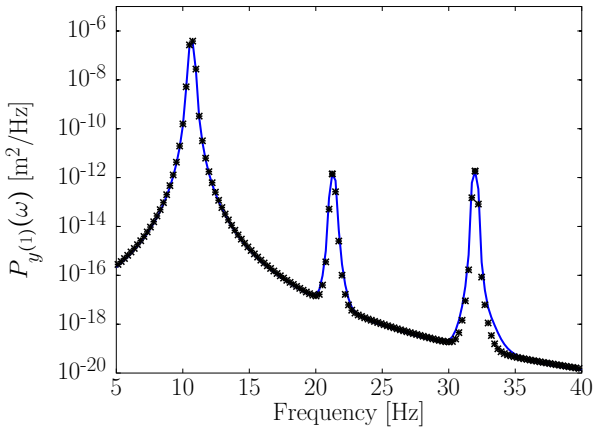

(a) Output spectrum simulated (–) and predicted by conventional harmonic probing method (∗).

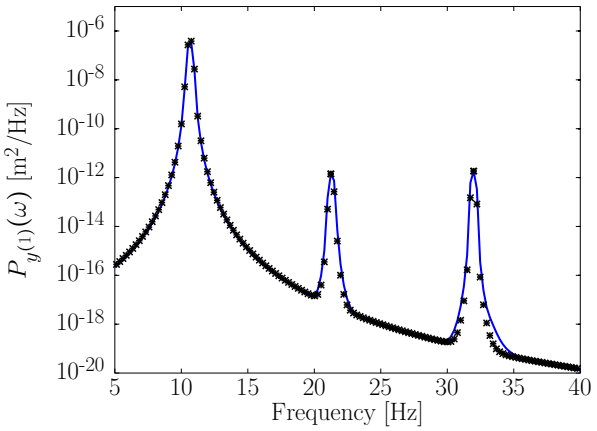

(b) Output spectrum simulated (–) and predicted by extended harmonic probing method (∗).

Source: Prepared by the author.

The results in this chapter have shown the applicability of the extended harmonic probing method to characterize and detect nonlinear behavior in vibrating systems. The conventional harmonic probing method is quite illustrative when the differential equations that describe the problem are known analytically. On the other hand, it has been verified

that the extended harmonic probing method gives the same results, but considering the knowledge of the output-only instead input and output as in the conventional case.

2.6 Conclusions

An extended version of the harmonic probing method was presented in this chapter. Based on the Theorem 1, the extended HOFRFs can be directly related to the conventional ones. Consequently, it is verified that the new approach provides an alternative tool to compute the HOFRFs where only the structural responses are available. The extended HOFRFs can be useful to give information about the nonlinear behavior and output prediction.

The analytical expressions of extended HOFRFs were provided and an alternative procedure based on the conventional harmonic probing method for analysis of weakly nonlinear systems was proposed. Furthermore, theoretical aspects of the model based on output-only signals as well as its significance, benefits and possible limitations were discussed.

The results obtained by using a classical Duffing oscillator with 2DOF characterized by quadratic and cubic stiffnesses have shown the benefits of this new approach for structural dynamics analysis. Furthermore, the method can be applied in nonlinear parameter estimation problems once the new kernels are function of the conventional ones where the dynamical properties appear clearly. Further applications are concerned with new perspectives on the concept of transmissibility for nonlinear systems based on the extended HOFRFs.

3 From Input-Output to Output-Only System Identification Based on Volterra Series

This chapter treats the characterization and identification of nonlinear single-input and multi-output (SIMO) systems through discrete-time Volterra series and Kautz filters expansion. A new methodology to treat applications where the equations of motion and the excitation signal are unknown is proposed. This chapter is basically organized as follows. Initially, the section 3.1 is dedicated to review briefly the state-of-the-art of existing literature and recent major developments of topics covering modelling, identification, parameter estimation and output prediction of nonlinear systems. After that, some remarks on Volterra series models and others existing methods in the literature are addressed. The contributions, advantages and drawbacks of the proposed approach are also carried out. In section 3.2 is presented the approach for system identification based on output-only and the discrete-time Volterra-Kautz filters. The optimization procedure used to identify the Kautz filters parameters is presented in section 3.3. A numerical application using a classical Duffing oscillator system with cubic stiffness is studied in section 3.4. Furthermore, an example based on experimental vibration data measured in a test rig with hardening effect and different levels of nonlinearities is investigated in section 3.5. The results have shown that the modified kernels computed by output-only signals can simulate and predict the linear and nonlinear contributions contained in the responses in a similar way as the conventional Volterra kernels computed with input and output signals. Finally, the conclusions with suggestions for further works are discussed in section 3.6.

3.1 Theoretical background and challenging issues

Modelling, identification and analysis of real-world engineering applications have been important topics of interest for the development of researches involving recent problems of

structural dynamics. Usually, such problems are inherently nonlinear and various methods and interesting applications have been investigated to treat nonlinear phenomena: frequency distortions, sub-harmonic and super-harmonic components, bolts, gaps, backlashes and discontinuities, jumps, chaos and bifurcations, limit-cycles, and so on (CHENG et al., 2017). Among the several methods, the Volterra series expansion have shown to be a very powerful tool with a wide range of industrial applications involving smooth nonlinearities (CARASSALE; KAREEM, 2010; XIA et al., 2016).

The Volterra series allow to compute the output of nonlinear systems by multidimensional kernels which represent the direct generalization of well-known impulse response functions (SCHETZEN, 1980; RUGH, 1981). The Volterra series have already been extensively applied to a wide variety of research areas such as biological systems (KORENBERG; HUNTER, 1996; ZHANG et al., 1998), electrical engineering for modeling of nonlinear circuits (BJÖRSELL et al., 2008; NARAYANAN; POON, 1973), nonlinear model predictive control (NMPC) (GRUBER et al., 2013; GRUBER et al., 2012), prediction of wind farm (LEE, 2011), signal processing involving electrodynamic loudspeaker, power amplifies and audio systems (KAIZER, 1987; NOVÁK, 2007; CUNHA et al., 2010), adaptive filtering (OGUNFUNMI, 2007; VAERENBERGH et al., 2008), aeroelastic systems (SILVA, 2005), modal analysis (TAWFIQ; VINH, 2003) and applications in the frequency-domain through the harmonic probing technique as treated in chapter 2 (CAFFERTY; TOMLINSON, 1997; PENG et al., 2008; CHATTERJEE, 2010a; CHATTERJEE; VYAS, 2003; SCUSSEL; da Silva, 2016a). Recently, a comparative overview of frequency domain methods such as: Volterra-based models, nonlinear frequency response functions (NFRFs) and bode plot, linear approximations and describing functions was presented by Rijlaarsdam et al. (2017). The authors compared four frequency domain techniques based on numerical examples via nonlinear oscillators and an industrial high precision stage used in a transmission electron microscope is also investigated. The results showed the applicability of Volterra based models and great benefits compared to other methodologies and model types.

Additionally, the useful properties of analysing the polynomial contributions of the total output predicted by Volterra models have presented great benefits in, for instance, structural health monitoring applications (CHATTERJEE, 2009; CHATTERJEE, 2011; SHIKI et al., 2017). An interesting method for damage detection and fault diagnosis based on Volterra series for rotating machinery was presented by Tang et al. (2010). In such work, the authors used the generalized frequency response functions to identify faults under different states. Genetic Algorithms was used to compute the Volterra kernels and

the effectiveness of this fault identification approach is verified through numerical and experimental simulations performed in a two-mass rotor system. Recently, Xia et al. (2016) developed a method based on a key kernel-PSO to identify the Volterra models for rotor-bearing test rig in different states. The fault classification is made on the test rig through a neural network. In general, the results showed that the proposed method has a good performance and benefits in the fault diagnosis of rotor-bearing system. Shiki et al. (2017) proposed statistical metrics based on indexes to show the importance of taking into account nonlinear effects of the structure in the model and to estimate whether there is any eventual damage in the structure or not. The main feature of the Volterra models, the possibility of separating linear and nonlinear contributions of the total output predicted, was applied with hypothesis tests in order to detect variations in the statistical properties of the damage features in a magneto-elastic beam. The results revealed that these indexes are extremely sensitive to the appearance of damage and, consequently, they can be used for damage detection.

The models based on Volterra series have been widely applied in problems of nonlinear mechanical system identification (SHIKI et al., 2014b; SCUSSEL et al., 2013a; SCUSSEL et al., 2013b; SCUSSEL; da Silva, 2015). Zhang and Billings (2017) developed a novel method based on orthogonal least squares algorithm regularised by an adjustable prediction error sum of squares criterion in order to truncate and estimate the Volterra kernels of higher-order at one time. Some simulations demonstrated that the approach can correctly truncate the Volterra series (order selection) and estimate Volterra kernels coefficients of nonlinear systems with weak nonlinearities. Prawin and Rao (2017) proposed an approach for nonlinear identification using truncated Volterra series via adaptive filter. The method is based on the concept of finite order and memory and shows to be computationally more efficient than the traditional Volterra series methodologies. Numerical studies using two classical single-degree-of-freedom systems (breathing crack problem and Duffing Holmes oscillator) and multi-degree-of-freedom systems showed the applicability of strategy adopted.

Basically, the Volterra series theory extends the well-known concept of linear impulse response function for the nonlinear case based on polynomial expansion and multidimensional convolutions between the higher-order Volterra kernels and the respective input signal. Consequently, several numerical drawbacks as overparametrization and matrices ill-posed arise due to the large number of parameters to be estimated. Fortunately, an orthonormal expansion can be applied in order to overcome these limitations of conventional methods (WIENER, 1958; BEDROSIAN; RICE, 1971). Several types of functions,

such as Chebyshev, Legendre, Laguerre, Kautz, Wavelet and many others, can be used for building an orthonormal basis to expand the Volterra kernels to reduce the number of parameters to be estimated. However, the choice of an appropriate set of orthogonal functions depends on how this set of functions is related with system of interest and how accurate they do represent and reproduce the dynamical behaviour (HEUBERGER et al., 2005; CHENG et al., 2014). Among them, the Kautz filters compose a convenient orthonormal basis to expand the Volterra series to identify lightly damped vibrating systems due to their useful properties and abilities in describing oscillatory behaviour (KAUTZ, 1954; WAHLBERG, 1994; BJÖRSELL et al., 2010; SHIKI et al., 2012; HANSEN et al., 2014).

It is important noting that models based on the Volterra series expansion compose a powerful tool for identification and output prediction of nonlinear systems. However, this representation presents some limitations such as convergence of the series, the order of the kernels and number of parameters to be estimated. The convergence problems are directly related with the amplitude of excitation, discontinuities and complex nonlinearities (TOMLINSON et al., 1996; THOUVEREZ, 1998; CHATTERJEE; VYAS, 2000; PENG; LANG, 2007). Consequently, the Volterra series representation might not be so adequate to deal with systems characterized by effects such as strong jump phenomena as investigated by Peng et al. (2008). However, the Harmonic Balance method can capture the jump phenomenon, but its implementation has huge computational cost and limits. Similar difficulties arise by using nonlinear parametric methods based on NARX or NARMAX models (CHEN; BILLINGS, 1989; SAKELLARIOU; FASSOIS, 2002; BILLINGS, 2013). Despite these parametric models provide good properties for time-series modelling, its not simple to select the structure of the model efficiently as well as the degree of the nonlinear terms and the lags for the input, output and noise. Additionally, methods based on artificial neural networks have been widely applied in nonlinear systems identification problems due to their useful properties and effectiveness (IBNKAHLA, 2003; JAFARIAN et al., 2015). Furthermore, to design properly an architecture of artificial neural networks by using a learning algorithm for achieving an optimal performance is quite difficult.

Additionally, in some engineering applications involving acoustics, telecommunications and structural dynamics problems, the force excitations are unmeasured and the approaches should consider taking into account only the outputs data measured along the structure of interest (BRINCKER et al., 2001). Several methods have been extensively studied, for instance, modal identification through the frequency domain decomposition (FDD) where the modal parameters are estimated by simple peak picking (CALDWELL;

FEENY, 2014) and functional series time-dependent auto-regressive moving average (FS-TARMA) models (POULIMENOS; FASSOIS, 2009; SPIRIDONAKOS; FASSOIS, 2009). The methods for applications where the excitation signal is not directly available are also known as blind identification methods (RAZ; VEEN, 2000). Tan et al. (2008) proposed a blind technique for SISO systems excited by distributed stationary random sequences. Numerical examples illustrate the effectiveness of the method based on the second-order and third-order moment through the LMS algorithm. However, this method is limited under sufficient conditions, the Volterra kernels are restricted to being zero and only sparse Volterra kernels are blindly identified.

Fernandes et al. (2009) proposed a channel identification technique based on Volterra series and parallel factor (PARAFAC) decomposition of a tensor formed of spatio-temporal covariance matrices where the channel is estimated by using a two-steps alternating least squares (ALS) algorithm. This algorithm is extended in Cherif et al. (2012) to an iterative alternating least squares (IALS) for blind identification of general second-order Wiener-Hammerstein systems. In addition, an algorithm using adaptive kernel canonical correlation analysis for nonparametric identification of Wiener-Hammerstein system was proposed by Vaerenbergh et al. (2008). Recent works have revealed several techniques to deal with the problem of blind identification in signal processing, equalization and telecommunications as stated in different examples (XU et al., 1995; ABED-MERAIN, 1997; KALOUPTSIDIS; KOUKOULAS, 2003; TAN; ABOULNASR, 2006). Consequently, an alternative method for applications involving mechanical systems in structural dynamics problems is very desirable. In this context, the present chapter is driven by the following contributions and advantages:

i) The identification of the model is made in a practical and easier way based on output-only data.

ii) The orthonormal expansion of the Volterra kernels onto Kautz basis is very welcome in order to reduce drastically the number of parameters to be estimated during the identification procedure.

iii) Kautz functions described by complex-conjugated poles allow to insert oscillatory behavior in the model and to capture the dynamic of vibrating systems.

iv) The order selection of the Volterra kernels η is made by the visual inspection of the power spectrum density (PSD) function of the output data. The order is selected based on the number of harmonic components.

On the other hand, the method proposed here can present some drawbacks and limitations when it is used in cases involving strong nonlinearities and complex discontinuities. The procedure for order selection in iv) might fail in applications involving multi-degree-of-freedom systems operating over a range of frequencies with multiple resonances where is difficult to distinguish resonance frequencies and the respective harmonic components. However, the numerical and experimental applications investigated in the present thesis are described by systems operating in a range of frequency containing only the first resonance and the integer harmonics of second and third order. Thus, it is considered in the nonlinear model the Volterra kernels up to third order to represent the dynamics of the system. The contribution presented in this chapter was published in Scussel and da Silva (2016b).

The next section proposes an approach which aims at the extension of the conventional Volterra series procedure for cases where only responses are available in order to treat weak nonlinearities for analysis, identification and design of vibrating structures. The requirements of this technique rely in systems with at least two vibration outputs measured in different locations.

3.2 Nonlinear identification using output-only data and Volterra-Kautz filters

The Volterra series were proposed by Vito Volterra[1] and have been broadly used in several engineering applications (VOLTERRA, 1959). The main idea is to compute the output $y(k)$ of nonlinear systems by multiple convolutions involving the input $u(k)$ as the following expression in the discrete-time domain (SCHETZEN, 1980):

$$y(k) = \sum_{\eta=1}^{\infty} \sum_{n_1=0}^{N_1} \sum_{n_2=0}^{N_2} \dots \sum_{n_\eta=0}^{N_\eta} \mathcal{H}_\eta(n_1, n_2 \dots, n_\eta) \prod_{i=1}^{\eta} u(k-n_i) = y_1(k) + y_2(k) + y_3(k) + \dots \quad (30)$$

with $k = 1, 2, \dots, K$ number of samples and $\mathcal{H}_\eta(n_1, n_2, \dots, n_\eta)$ are the conventional discrete-time Volterra kernels of ηth order considering the truncated values $N_1, N_2, \dots, N_\eta$ for each kernel. The term $y_1(k)$ denotes the linear contribution, $y_2(k)$ is the contribution of second

[1]Vito Volterra (May 3, 1860 - Ancona, Italy/ October 11, 1940 - Rome, Italy) was an Italian mathematician and physicist that contributed significantly with the development of important tools of modern calculus and the theory of functionals involving solution of integral and differential equations.

order and $y_3(k)$ is the contribution of third order as follows:

$$y_1(k) = \sum_{n_1=0}^{N_1} \mathcal{H}_1(n_1)u(k-n_1) \tag{31}$$

$$y_2(k) = \sum_{n_1=0}^{N_1}\sum_{n_2=0}^{N_2} \mathcal{H}_2(n_1,n_2)u(k-n_1)u(k-n_2) \tag{32}$$

$$y_3(k) = \sum_{n_1=0}^{N_1}\sum_{n_2=0}^{N_2}\sum_{n_3=0}^{N_3} \mathcal{H}_3(n_1,n_2,n_3)u(k-n_1)u(k-n_2)u(k-n_3) \tag{33}$$

In general, the polynomial contribution $y_\eta(k)$ is computed separately by the convolution between the Volterra kernel $\mathcal{H}_\eta(n_1,n_2,\ldots,n_\eta)$ and the excitation signal $u(k)$. Basically, the concept of Volterra series, that relies on multidimensional kernel transforms and convolution integrals/sums, is analogous to the concept of Taylor series expansion as stated by Milanese (2009). The Volterra series are described by the integro-differential functional mapping the output signals of nonlinear dynamical systems as a multidimensional convolution of Volterra kernels and past input, i.e., has the concept of memory intrinsic in its definition, as verified in Eq. (30).

Recently, Shiki et al. (2014a) proposed a technique to identify the coefficients of the Volterra kernels until third order ($\eta = 3$). The identification procedure is made in two steps, the linear kernel is estimated by using low level of amplitude excitation and the nonlinear kernels are estimated with high level of amplitude excitation. It has shown to be an alternative and efficient tool for model updating and nonlinear identification of mechanical systems (SHIKI et al., 2012; HANSEN et al., 2014). Unfortunately, in industrial applications under operational conditions the input signals are difficult to obtain or not possible to measure. Under these circumstances, the present work aims to extend this conventional Volterra technique in order to consider cases where at least two output signals are available. The main idea is to relate two responses of the system in a similar way as performed by the conventional Volterra model. Thus, the prediction of $y(k)$ from Eq. (30) is rewritten as:

$$y(k) = \sum_{\eta=1}^{\infty}\sum_{n_1=0}^{N_1}\sum_{n_2=0}^{N_2}\cdots\sum_{n_\eta=0}^{N_\eta} \mathcal{G}_\eta(n_1,n_2,\ldots,n_\eta)\prod_{i=1}^{\eta} y'(k-n_i) = y_1(k)+y_2(k)+y_3(k)+\ldots \tag{34}$$

where the term $y'(k)$ denotes another output of the system measured in a different location of $y(k)$ and $\mathcal{G}_\eta(n_1,n_2,\ldots,n_\eta)$ denotes the extended kernel of ηth order that can be able to describe the output $y(k)$ in linear and nonlinear contributions in a similar way of $\mathcal{H}_\eta(n_1,n_2,\ldots,n_\eta)$.

A proof of the Eq. (34) is presented in Theorem 2 below. Basically, it is an extended version of the Theorem 1, presented in chapter 2, for solutions of weakly discrete-time nonlinear systems that has Volterra series expansion. It is proved that the output can be represented alternatively by a multidimensional convolution between the modified kernels and another output. Thus, the main contribution lies in the fact that the input force is not required and the modified Volterra kernels are computed based on output-only data in an analogous way to the conventional ones.

Before to state the Theorem 2, the following assumptions are considered:

(i) Without loss of generality, consider a discrete-time SIMO nonlinear system excited by single tone harmonic input $u(k) = Ae^{j\omega k}$ with two outputs denoted by $y(k)$ and $y'(k)$, respectively. The frequency excitation ω is close to the first resonance frequency of the system and A is the force amplitude.

(ii) Suppose that the system has a convergent expansion through discrete-time Volterra series in which the outputs are represented by:

$$y(k) = \sum_{\eta=1}^{\infty} \sum_{n_1=-\infty}^{+\infty} \sum_{n_2=-\infty}^{+\infty} \cdots \sum_{n_\eta=-\infty}^{+\infty} \mathcal{H}_\eta(n_1, n_2 \ldots, n_\eta) \prod_{i=1}^{\eta} u(k-n_i) \tag{35}$$

and

$$y'(k) = \sum_{\eta=1}^{\infty} \sum_{n_1=-\infty}^{+\infty} \sum_{n_2=-\infty}^{+\infty} \cdots \sum_{n_\eta=-\infty}^{+\infty} \mathcal{H}'_\eta(n_1, n_2 \ldots, n_\eta) \prod_{i=1}^{\eta} u(k-n_i) \tag{36}$$

The multi-dimensional z transform of the kernels can be calculated as the following power series expansion:

$$\mathscr{H}_\eta(z_1, z_2, \ldots, z_\eta) = \sum_{n_1=-\infty}^{+\infty} \sum_{n_2=-\infty}^{+\infty} \cdots \sum_{n_\eta=-\infty}^{+\infty} \mathcal{H}_\eta(n_1, n_2, \ldots, n_\eta) \prod_{i=1}^{\eta} z_i^{-n_i} \tag{37}$$

By assuming that the kernels are convergent at the unit circle, $|z_\eta| = 1$, then $\mathscr{H}_\eta(z_1, z_2, \ldots, z_\eta)$ can be reduced as the multidimensional Fourier transform $\mathscr{H}_\eta(j\omega_1, \ldots, j\omega_\eta)$ where $z_1 = e^{j\omega_1}, z_2 = e^{j\omega_1}, \ldots, z_\eta = e^{j\omega_\eta}$. For simplicity of notation, it is considered $\mathscr{H}_\eta(j\omega_1, j\omega_2, \ldots, j\omega_\eta) = \mathscr{H}_\eta(\omega, \omega, \ldots, \omega)$ when the system is excited by single tone harmonic input.

Theorem 2. *By considering the conditions (i) and (ii), the output $y(k)$ can be computed as follows*:

$$y(k) = \sum_{\eta=1}^{\infty} \sum_{n_1=-\infty}^{+\infty} \sum_{n_2=-\infty}^{+\infty} \cdots \sum_{n_\eta=-\infty}^{+\infty} \mathcal{G}_\eta(n_1, n_2, \ldots, n_\eta) \prod_{i=1}^{\eta} y'(k-n_i) \tag{38}$$

where $\mathcal{G}_\eta(.)$ denotes the extended kernel of order η and $y'(k)$ is another output measured in a different location of $y(k)$.

Proof. Firstly, consider the linear contribution ($\eta = 1$) of the output $y(k)$ as follows:

$$\begin{aligned} y_1(k) &= \sum_{n_1=-\infty}^{\infty} \mathcal{H}_1(n_1)u(k-n_1) = Ae^{j\omega k}\mathscr{H}_1(\omega) \\ \Leftrightarrow y_1(k) &= Ae^{j\omega k}\mathscr{H}_1(\omega)\mathscr{H}_1'(\omega)\Big[\mathscr{H}_1'(\omega)\Big]^{-1}, \end{aligned}$$

Assuming that $\mathscr{G}_1(\omega) = \mathscr{H}_1(\omega)\Big[\mathscr{H}_1'(\omega)\Big]^{-1}$ generates:

$$\begin{aligned} y_1(k) &= Ae^{j\omega k}\mathscr{H}_1'(\omega)\mathscr{G}_1(\omega) \\ \Leftrightarrow y_1(k) &= Ae^{j\omega k}\mathscr{H}_1'(\omega)\sum_{n_1=-\infty}^{\infty}\mathcal{G}_1(n_1)e^{-j\omega n_1} \\ \Leftrightarrow y_1(k) &= \sum_{n_1=-\infty}^{\infty}\mathcal{G}_1(n_1)Ae^{j\omega(k-n_1)}\mathscr{H}_1'(\omega) \\ \Leftrightarrow y_1(k) &= \sum_{n_1=-\infty}^{\infty}\mathcal{G}_1(n_1)y'(k-n_1). \end{aligned}$$

The quadratic contribution of the output $y(k)$ in Eq. (35) is calculated as:

$$\begin{aligned} y_2(k) &= A^2e^{j2\omega k}\mathscr{H}_2(\omega,\omega) \\ \Leftrightarrow y_2(k) &= A^2e^{j2\omega k}[\mathscr{H}_1'(\omega)]^2\mathscr{H}_2(\omega,\omega)[\mathscr{H}_1'(\omega)]^{-2} \\ \Leftrightarrow y_2(k) &= A^2e^{j2\omega k}[\mathscr{H}_1'(\omega)]^2\mathscr{G}_2(\omega,\omega) \\ \Leftrightarrow y_2(k) &= A^2e^{j2\omega k}[\mathscr{H}_1'(\omega)]^2\sum_{n_1=-\infty}^{\infty}\sum_{n_2=-\infty}^{\infty}\mathcal{G}_2(n_1,n_2)e^{-j\omega n_1}e^{-j\omega n_2} \\ \Leftrightarrow y_2(k) &= \sum_{n_1=-\infty}^{\infty}\sum_{n_2=-\infty}^{\infty}\mathcal{G}_2(n_1,n_2)y'(k-n_1)y'(k-n_2). \end{aligned}$$

The polynomial contribution of order η is calculated as:

$$\begin{aligned} y_\eta(k) &= A^\eta e^{j\eta\omega k}\mathscr{H}_\eta(\underbrace{\omega,\omega,\ldots,\omega}_{\eta \text{ times}}) \\ \Leftrightarrow y_\eta(k) &= A^\eta e^{j\eta\omega k}[\mathscr{H}_\eta'(\omega)]^\eta\mathscr{H}_\eta(\omega,\omega,\ldots,\omega)[\mathscr{H}_\eta'(\omega)]^{-\eta} \\ \Leftrightarrow y_\eta(k) &= A^\eta e^{j\eta\omega k}[\mathscr{H}_\eta'(\omega)]^\eta\mathscr{G}_\eta(\omega,\omega,\ldots,\omega) \\ \Leftrightarrow y_\eta(k) &= A^\eta e^{j\eta\omega k}[\mathscr{H}_\eta'(\omega)]^\eta\sum_{n_1=-\infty}^{\infty}\sum_{n_2=-\infty}^{\infty}\cdots\sum_{n_\eta=-\infty}^{\infty}\mathcal{G}_\eta(n_1,n_2,\ldots,n_\eta)e^{-j\omega n_1}e^{-j\omega n_2}\ldots e^{-j\omega n_\eta} \\ \Leftrightarrow y_\eta(k) &= \sum_{n_1=-\infty}^{\infty}\sum_{n_2=-\infty}^{\infty}\cdots\sum_{n_\eta=-\infty}^{\infty}\mathcal{G}_\eta(n_1,n_2,\ldots,n_\eta)y'(k-n_1)y'(k-n_2)\ldots y'(k-n_\eta). \end{aligned}$$

By following the procedure above and by considering the fact that $y(k) = y_1(k) + y_2(k) + y_3(k) + \ldots$, thus

$$y(k) = \sum_{\eta=1}^{\infty} \sum_{n_1=-\infty}^{+\infty} \sum_{n_2=-\infty}^{+\infty} \ldots \sum_{n_\eta=-\infty}^{+\infty} \mathcal{G}_\eta(n_1, n_2, \ldots, n_\eta) \prod_{i=1}^{\eta} y'(k - n_i) \qquad \square$$

The excessive computational requirements necessary to identify these kernels points out the main drawbacks and limitations due to the large number of terms $N_1, N_2, \ldots, N_\eta$ to be estimated that grow exponentially by increasing the nonlinearity order (KORENBERG; HUNTER, 1996; BJÖRSELL et al., 2008). Furthermore, convergence and ill-posed problems are also found. In order to overcome these drawbacks an orthonormal expansion can be used and the conventional Volterra kernel in Eq. (30) is approximated as follows (HANSEN et al., 2014; SHIKI et al., 2014):

$$\mathcal{H}_\eta(n_1, n_2, \ldots, n_\eta) \approx \sum_{i_1=1}^{J_1} \sum_{i_2=1}^{J_2} \ldots \sum_{i_\eta=1}^{J_\eta} \mathscr{B}_\eta(i_1, i_2, \ldots, i_\eta) \prod_{j=1}^{\eta} \psi_{i_j}(n_j; \theta_j) \tag{39}$$

where $\mathscr{B}_\eta(i_1, i_2, \ldots, i_\eta)$ are the coefficients of the orthonormal basis and ψ_{i_j} are the Kautz functions. These functions are very effective and useful due to their structure allowing to insert oscillatory behavior in the nonlinear model (KAUTZ, 1954; DA SILVA, 2011a). The term J_η denotes the number of Kautz functions adopted and $\theta_\eta = \begin{bmatrix} z_\eta & \bar{z}_\eta \end{bmatrix}$ in which z_η and $\bar{z}_\eta$ are the complex conjugate parameters of the Kautz filters describing the conventional kernel of η-th order. The number of parameters is considerably reduced in the identification problem since $J_\eta \ll N_\eta$. The kernel based on output-only data can be expanded into orthonormal basis in a similar way of the conventional kernel given by:

$$\mathcal{G}_\eta(n_1, n_2, \ldots, n_\eta) \approx \sum_{i_1=1}^{J_1} \sum_{i_2=1}^{J_2} \ldots \sum_{i_\eta=1}^{J_\eta} \mathscr{V}_\eta(i_1, i_2, \ldots, i_\eta) \prod_{j=1}^{\eta} \psi_{i_j}(n_j; \theta'_j) \tag{40}$$

Its worth to note that the kernels $\mathcal{H}_\eta$ and $\mathcal{G}_\eta$ present similar behaviour due to the orthonormal expansion. However, these kernels are computed using different Kautz filters parameters ($\theta_\eta \neq \theta'_\eta$). In the next section, the Kautz filters are detailed as well as the procedure to obtain their parameters. Thus, through the orthonormal expansion in Eq. (40), the response $y(k)$ in Eq. (34) can be predicted as:

$$y(k; \boldsymbol{\Theta}') = \sum_{\eta=1}^{+\infty} y_\eta(k; \theta'_\eta) = \sum_{\eta=1}^{+\infty} \sum_{i_1=1}^{J_1} \sum_{i_2=1}^{J_2} \ldots \sum_{i_\eta=1}^{J_\eta} \mathscr{V}_\eta(i_1, i_2, \ldots, i_\eta) \prod_{j=1}^{\eta} l_{i_j}(k; \theta'_j) \tag{41}$$

where $\boldsymbol{\Theta}' = \begin{bmatrix} \theta'_1 & \theta'_2 & \ldots & \theta'_\eta \end{bmatrix}$. In practice, the problem can be solved by using the least

squares approach:

$$\mathbf{y} = \mathbf{\Lambda}\mathbf{\Phi} \tag{42}$$

where $\mathbf{y} = \begin{bmatrix} y(1) & y(2) & \dots & y(K) \end{bmatrix}^T$ is the experimental output. The matrix $\mathbf{\Lambda}$ contains the combinations of $l_{i_j}(k)$ given by:

$$\mathbf{\Lambda} = \begin{bmatrix} l_1(k;\theta'_1) & \dots & l_{J_1}(k;\theta'_1) & l_1^2(k;\theta'_1) & \dots & l_{J_2}^2(k;\theta'_2) & l_1^3(k;\theta'_1) \\ l_1(k;\theta'_1)l_2(k;\theta'_2)l_3(k;\theta'_3) & \dots & l_{J_3}^3(k;\theta'_3) & \dots & & & \end{bmatrix} \tag{43}$$

The term $l_{i_j}(k;\theta'_j)$ represents the convolution between the Kautz filters with the output signal $y'(k)$ given by:

$$l_{i_j}(k;\theta'_j) = \sum_{n_i=0}^{V-1} \psi_{i_j}(n_i;\theta'_j)y'(k-n_i) \tag{44}$$

with $V = \max\{J_1,\dots,J_\eta\}$ and $\mathbf{\Phi}$ is a vector containing the unknown coefficients of the orthonormal expansion:

$$\mathbf{\Phi} = \begin{Bmatrix} \mathscr{V}_1(1) & \dots & \mathscr{V}_1(J_1) & \mathscr{V}_2(1,1) & \mathscr{V}_2(1,2) & \dots \\ \mathscr{V}_2(J_1,J_2) & \mathscr{V}_3(1,1,1) & \mathscr{V}_3(1,1,2) & \dots & \mathscr{V}_3(J_1,J_2,J_3) & \dots \end{Bmatrix}^T \tag{45}$$

The coefficients of the vector $\mathbf{\Phi}$ can be obtained by solving Eq. (42) as follows:

$$\mathbf{\Phi} = (\mathbf{\Lambda}^T\mathbf{\Lambda})^{-1}\mathbf{\Lambda}^T\mathbf{y} \tag{46}$$

Section 3.3 shows the structure of Kautz filters and the procedure to select their parameters by using an iterative process via sequential quadratic programming (SQP) algorithm.

3.3 Optimal selection of the Kautz parameters

The Kautz filters are very effective due to their properties and have been broadly used in modelling and identification of oscillatory systems (BJÖRSELL et al., 2010; DA SILVA et al., 2009b; DA SILVA, 2011b). These filters are composed by complex conjugate parameters and are given in the z-domain by (HEUBERGER et al., 2005):

$$\Psi_{2j-1}(z) = \frac{z(z-b_\eta)\sqrt{(1-c_\eta^2)}}{z^2+b_\eta(c_\eta-1)z-c_\eta}\left[\frac{-c_\eta z^2+b_\eta(c_\eta-1)+1}{z^2+b_\eta(c_\eta-1)z-c_\eta}\right]^{j-1} \tag{47}$$

$$\Psi_{2j}(z) = \frac{z\sqrt{(1-c_\eta^2)(1-b_\eta^2)}}{z^2+b_\eta(c_\eta-1)z-c_\eta}\left[\frac{-c_\eta z^2+b_\eta(c_\eta-1)+1}{z^2+b_\eta(c_\eta-1)z-c_\eta}\right]^{j-1} \tag{48}$$

in which the index j denotes the number of Kautz functions adopted where b_η and c_η are given by:

$$b_\eta = \frac{z_\eta + \bar{z}_\eta}{1 + z_\eta \bar{z}_\eta} \tag{49}$$

$$c_\eta = -z_\eta \bar{z}_\eta \tag{50}$$

where the stability condition is satisfied since $\| z_\eta \|$, $\| \bar{z}_\eta \| < 1$. These parameters can be obtained from the transformation $z_\eta = e^{s_\eta . \Delta t}$ where Δt denotes the sampling rate and $s_\eta = -\xi_\eta \varpi_\eta + j\varpi_\eta \sqrt{1 - \xi_\eta^2}$ are the parameters in the s-domain. The set of variables $\boldsymbol{\Theta}' = \begin{bmatrix} \theta'_1 & \theta'_2 & \dots & \theta'_\eta \end{bmatrix}$ with $\theta'_\eta = \begin{bmatrix} z_\eta & \bar{z}_\eta \end{bmatrix}$ is given by minimizing the normalized mean square error function (NMSE):

$$\min F(\boldsymbol{\Theta}') = \frac{\| y(k) - y(k; \boldsymbol{\Theta}') \|}{\| y(k) \|} \tag{51}$$

subject to

$$\varpi_{(low)\eta} \leq \varpi_\eta \leq \varpi_{(up)\eta} \tag{52}$$

$$\xi_{(low)\eta} \leq \xi_\eta \leq \xi_{(up)\eta} \tag{53}$$

and ϖ_η, ξ_η are positive real numbers where the indices *up* and *low* represent the upper and lower bounds, respectively. Furthermore, $y(k)$ is the experimental output and $y(k; \boldsymbol{\Theta}')$ is the output estimated by the nonlinear model. The symbol $\|.\|$ denote the Euclidean norm. Several methods can be used to solve the optimization problem. This work considers the SQP algorithm and the steps of the iterative process to select the Kautz filters are described in Fig. 9. The algorithm starts with the initial condition of the Kautz filters parameters and stops when the stopping criteria is met, $F(\boldsymbol{\Theta}') < \epsilon$. Figure 10 shows the flow chart with the steps of the method based on Volterra series and output-only.

In summary, the first step of the method is the acquisition and pre-processing of the output signals collected in different locations of the structure. The second step consists in to apply the optimization procedure to identify the optimal vector of Kautz filters parameters via SQP algorithm. Simultaneously, the coefficients of the kernels are obtained by using the least squares approach and the estimative is used to predict the output of the nonlinear model identified. After that, in the third step is evaluated the objective function and the stop criteria of convergence. In the fourth step, the kernels using optimal Kautz filters parameters are computed and these kernels are used to predicted the output of the model through validation data. The method is applied in two examples and the results

are compared with the conventional Volterra models as described in the next section.

Figure 9 – Steps of the algorithm for nonlinear system identification based on Volterra series and output-only data.

Input: Vibration data $y'(k)$ and $y(k)$ measured directly in the structure.
Initialize: Build the Kautz filters by using the vector $\boldsymbol{\Theta}'^{(0)}$ with the start point $\varpi_{\eta}^{(0)}$ and $\xi_{\eta}^{(0)}$,
Repeat: For $\iota \geq 1$
Calculate the convolution between the Kautz filters and the experimental data $y'(k)$ as in Eq. (44),
Compute the matrix $\boldsymbol{\Lambda}^{(\iota)}$ by using Eq. (43) with the regressors $l_{i_j}(k;\theta_j'^{(\iota)})$,
Estimate the vector $\boldsymbol{\Phi}^{(\iota)}$ by using least squares approach as in Eq. (46),
With given $\boldsymbol{\Lambda}^{(\iota)}$ and $\boldsymbol{\Phi}^{(\iota)}$ calculate the total prediction $y(k;\boldsymbol{\Theta}'^{(\iota)})$ as in Eq. (41),
Minimize the NMSE cost function $F(\boldsymbol{\Theta}')^{(\iota)}$ as in Eq. (51),
Until Stopping criteria of convergence, $F(\boldsymbol{\Theta}')^{(\iota)} < \epsilon$.
Output Optimal vector of Kautz filters parameters.

Source: Prepared by the author.

Figure 10 – Computational flow chart illustrating the method.

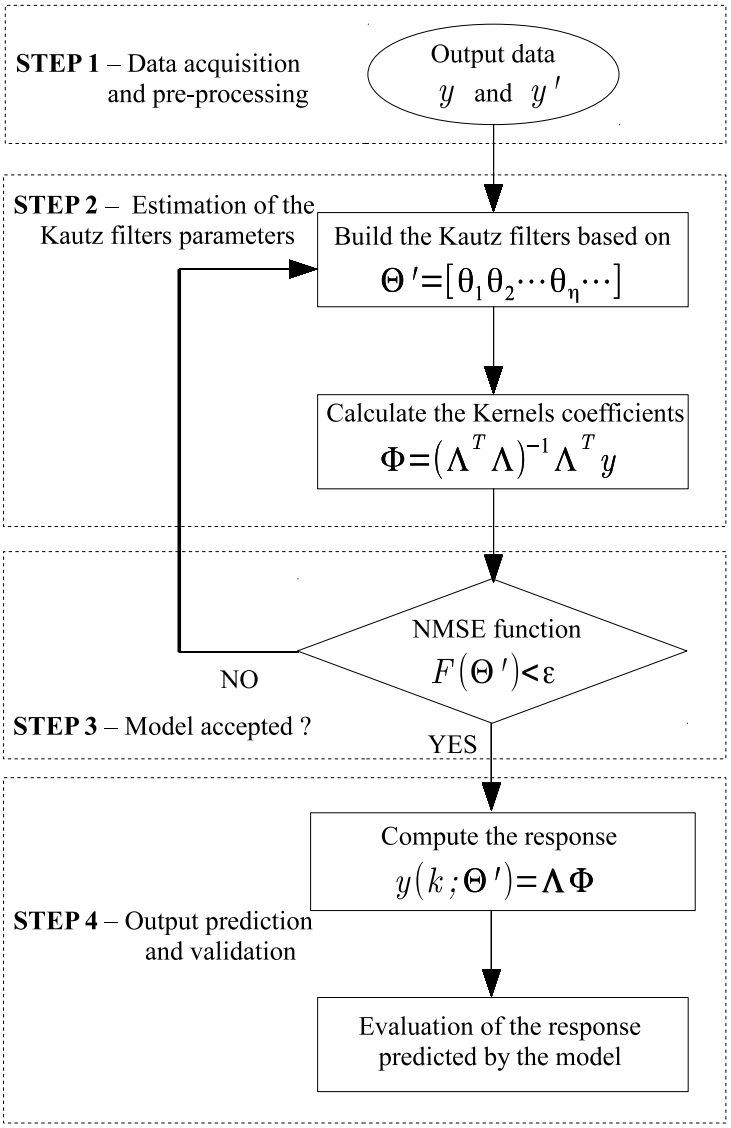

Source: Prepared by the author.

3.4 Application in a Duffing oscillator with 2 DOF

This section is aimed at illustrating the new method based on Volterra series expansion and output-only through a nonlinear two degree-of-freedom system characterized by cubic stiffness. Additionally, comparisons with the conventional Volterra model based on input and output data are also made. The mechanical system showed in Fig. 11 is described in the continuous domain by the equations of motion as follows:

$$\begin{aligned} m_1\ddot{y}_1(t) + (k_1+k_2)y_1(t) - k_2y_2(t) + c_1\dot{y}_1(t) &= u(t) \\ m_2\ddot{y}_2(t) - k_2y_1(t) + k_2y_2(t) + c_3\dot{y}_2(t) + \beta_2y_2^3(t) &= 0 \end{aligned} \tag{54}$$

where $u(t)$ is the force applied to the first mass. Additionally, $\ddot{y}(t)$, $\dot{y}(t)$ and $y(t)$ represent the acceleration [m/s^2], velocity [m/s] and displacement [m], respectively. The parameters of mass and stiffness were chosen based on the example investigated by Sakellariou and Fassois (2002) where m_1 = 10 kg, m_2 = 55 kg, k_1 = 10 kN/m, k_2 = 90 kN/m,β_1 = 0 and β_2 = 900 kN/m^3. Is considered c_1 = 60 Ns/m and c_3 = 15 Ns/m in order to deal with the damping factors 4.30% and 2.45% for the first and second mode, respectively. It is worth noting that the resonance frequencies of the linear part of the system are close to 1.89 Hz and 17.06 Hz.

Figure 11 – Duffing oscillator with 2 DOFs and cubic stiffness.

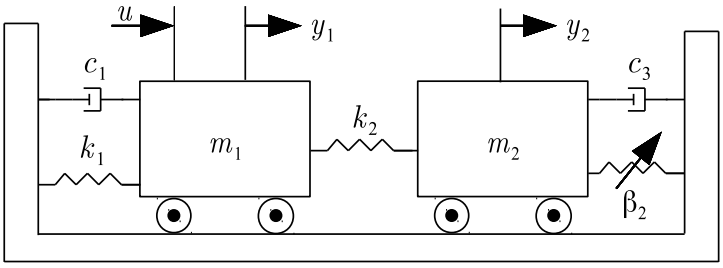

Source: Prepared by the author.

The system simulation was based on the numerical integration of Eq. (54) using the Newmark method combined with Newton-Raphson procedure. The signals of displacement, velocity and acceleration were obtained by applying a chirp excitation sweeping up the frequency range from 0 until 6 Hz with time duration of 32 seconds and 55 N of amplitude. The signals were acquired by considering 4096 samples and sampling frequency of 128 Hz.

The displacement of the first mass was used to compute the restoring force curve in order to verify the presence of nonlinear effects (MASRI; CAUGHEY, 1979). Figure 12 shows the graphic displacement × restoring force where it is possible to note clearly the distortion of the curve described by the cubic stiffness, known as hardening effect once $\beta_2 > 0$.

The algorithm illustrated in Fig. 9 is applied to obtain the optimal vector of Kautz filters parameters. The upper and the lower bounds were chosen as $\varpi_{(low)\eta} = 1 \times 2\pi$ rad/s, $\varpi_{(up)\eta} = 5 \times 2\pi$ rad/s, $\xi_{(low)\eta} = 0.0010$ and $\xi_{(up)\eta} = 0.0900$ and order $\eta = 1, 3$. The initial conditions were chosen as the average of the upper and lower bounds. The tolerances of the objective function, step and optimality were chosen as 10^{-15}. The parameters found by the optimization problems are showed in Tab. 2 and were obtained by solving Eq. (51) via SQP algorithm through the *fmincon* function from optimization toolbox of MATLAB.

Figure 12 – Evidences of nonlinearities through the restoring force curve.

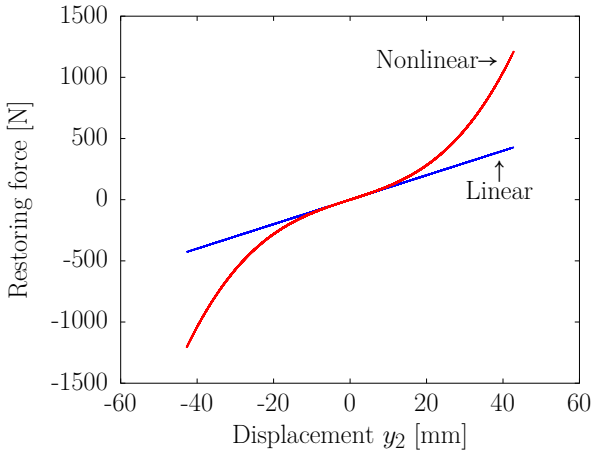

Source: Prepared by the author.

It was considered $J_1 = J_3 = 2$ in order to get a minimum number of parameters to be estimated and avoid problems of convergence of the series and oscillations that arise with a large number of functions. Recently, Shiki et al. (2017) investigated the convergence analysis to select the orders of the higher-order Volterra kernels based on the normalised root mean square error (NRMSE) between the experimental output measured and the respective output predicted by the Volterra models.

The extended kernels $\mathcal{G}_1(n_1)$ and $\mathcal{G}_3(n_1, n_2, n_3)$ were identified based on the optimized Kautz parameters and based on the signals $y'(k)$ and $y(k)$ that correspond to the velocity of the first and the second mass, respectively. Additionally, the Volterra kernels $\mathcal{H}_1(n_1)$ and $\mathcal{H}_3(n_1, n_2, n_3)$ were identified in a similar way by using the chirp excitation $u(k)$ and the velocity of the second mass $y(k)$ through the conventional method as made in Shiki et al. (2012), Shiki et al. (2014a), Shiki (2016) and Hansen et al. (2014). Figure 13 shows the computed kernels of first and third order of each model. It is worth noting that the kernel of second order was neglected once the system is characterized by only cubic stiffness and the response of the system is symmetric. In this case, the quadratic term did not present contribution in the total output predicted by the model.

Table 2 – Kautz parameters obtained by the optimization procedure.

	1^{st} kernel	3^{rd} kernel
Output-only	$0.9428 + j0.3090$	$0.9553 + j0.2581$
Conventional	$0.9909 + j0.1061$	$0.9852 + j0.1199$

Source: Prepared by the author.

Figure 13 – Extended kernels and conventional ones of first and third order.

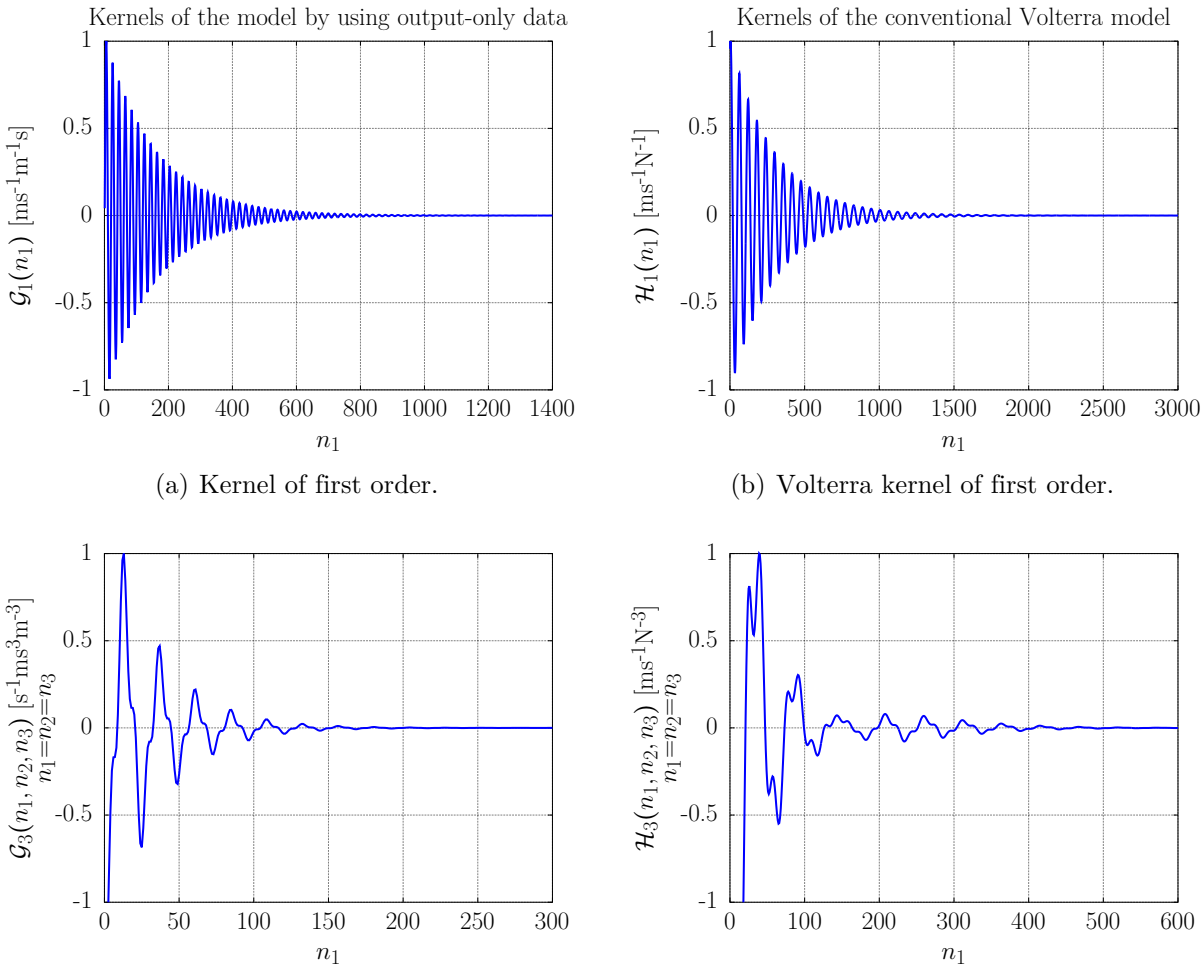

(a) Kernel of first order.

(b) Volterra kernel of first order.

(c) Kernel of third order (main diagonal).

(d) Volterra kernel of third order (main diagonal).

Source: Prepared by the author.

The kernels $\mathcal{G}_1(n_1)$ and $\mathcal{G}_3(n_1, n_2, n_3)$ and the output signal $y'(k)$ (velocity of the first mass) were used to predict the output $y(k; \boldsymbol{\Theta}')$ as described in Eq. (41). In addition, the kernels of the conventional Volterra model $\mathcal{H}_1(n_1)$ and $\mathcal{H}_3(n_1, n_2, n_3)$ and the chirp input signal $u(k)$ were considered to predict the output $y(k; \boldsymbol{\Theta})$.

Figure 14 shows the outputs $y(k; \boldsymbol{\Theta}')$ and $y(k; \boldsymbol{\Theta})$ predicted by each model in comparison with the output $y(k)$ (velocity of the second mass) simulated by numerical integration of the Eq. (54) via Newmark method.

By observing the Fig. 14 it is possible to note an agreement between the output computed by each model and the output simulated. However, a metric of fit is welcome in order to quantify the predictions. Thus, the metric value of fit (VOF) was applied in

order to assess the fit percent of the output predicted that can be calculated as:

$$\text{VOF} = 100 \times \left(1 - \frac{\|y(k) - y(k;\boldsymbol{\Theta})\|_2}{\|y(k)\|_2}\right)\% \tag{55}$$

Figures 14(a) and 14(b) show the responses computed by output-only method and the conventional one with VOF $\approx 98\%$ and VOF $\approx 86\%$, respectively.

The models identified were validated with sinusoidal input with 55 N of amplitude and excitation frequency close to 1.89 Hz in order to detect nonlinear effects through power spectrum density (PSD) of the output predicted. The PSD funtions were calculated through Welch's method using Hanning window with 4 averages (1024 samples) and 50% of overlap.

Figure 14 – Outputs predicted by the nonlinear models (+) in comparison with the response simulated by using Newmark method (–) that corresponds to the velocity of the second mass.

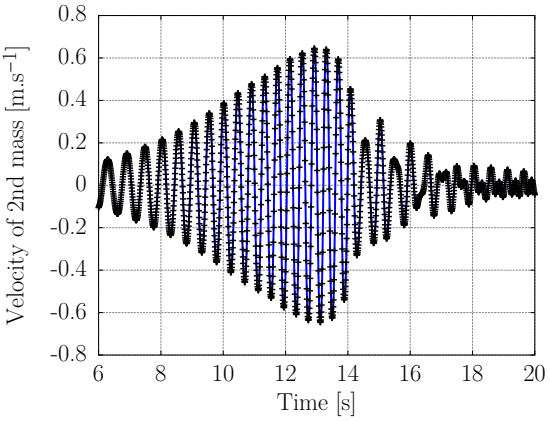

(a) Predicted by using the output-only method ($y(k;\Theta')$ with 98% of fit).

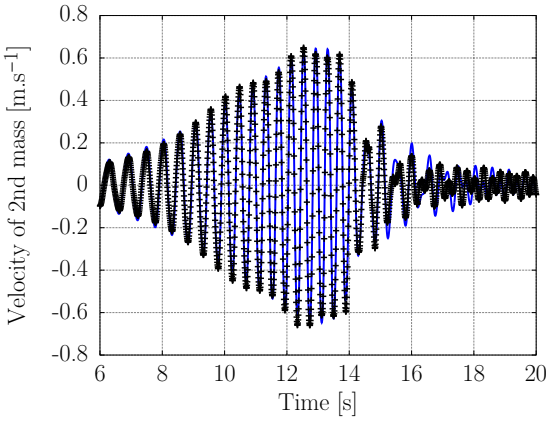

(b) Predicted by the conventional method ($y(k;\Theta)$ with 86% of fit).

Source: Prepared by the author.

Figure 15 shows the PSDs of the outputs estimated by each model in comparison with the PSD of the response simulated. In each case, it is possible to see a good agreement between the curves illustrating that both nonlinear models can detect the presence of the fundamental resonance in 1.89 Hz and the respective harmonic with value around 5.7 Hz (3× 1.89).

Figure 15 – PSD of the predictions (dotted line □) in comparison with the PSD of the response simulated (–).

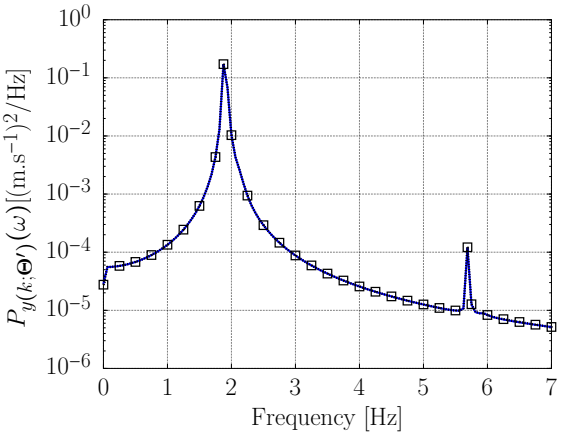

(a) PSD of the output predicted by the output-only method.

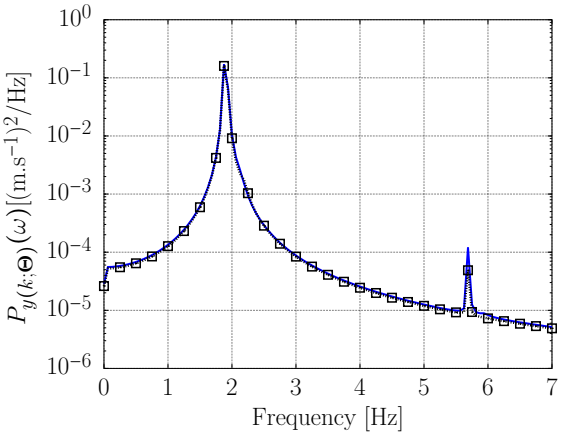

(b) PSD of the output predicted by the conventional Volterra model.

Source: Prepared by the author.

3.5 Experimental application in a buckled beam

The test rig performed by Hansen et al. (2014) is used here in order to illustrate the potential of the approach based on output-only data. The experimental application is composed by an aluminium beam in a clamped-free configuration characterized by geometrical nonlinearity due to the compressive axial force applied on the beam by using a screw at the top. The vibration data were used to identify a model based on output-only. In addition, the conventional Volterra model which requires the knowledge of the excitation signal was also identified. The results have illustrated that the novel output-only identification method is able to detect nonlinear behaviour and to predict responses as good as the conventional method used in Hansen et al. (2014).

An aluminium beam with 460×20×1.8 mm of length, width and thickness, respectively, in a clamped-free configuration and with an axial load applied in the top. A TIRA shaker is attached 65 mm from the clamped end of the beam in order to excite the beam and two DYTRAN accelerometers were used to measure the vibration along the beam. Figures 16(a) and 16(b) show the test rig and the experimental setup used. This structure was also investigated in similar conditions in Tang et al. (2015a).

A strain gauge was also used to monitor the strain in the top of the beam when an axial load of compression using a screw is applied. This compression force caused

Figure 16 – Experimental setup and the schematic diagram illustrating the test rig.

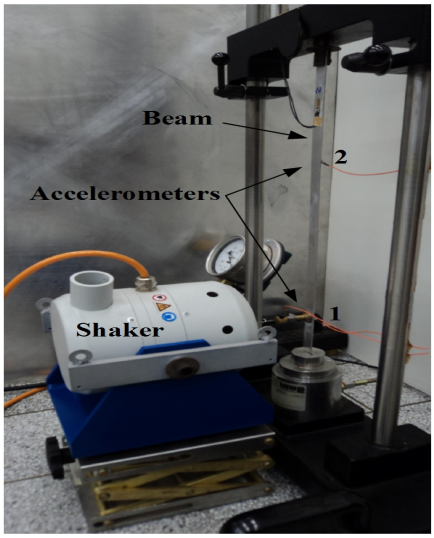

(a) View of the experimental setup.

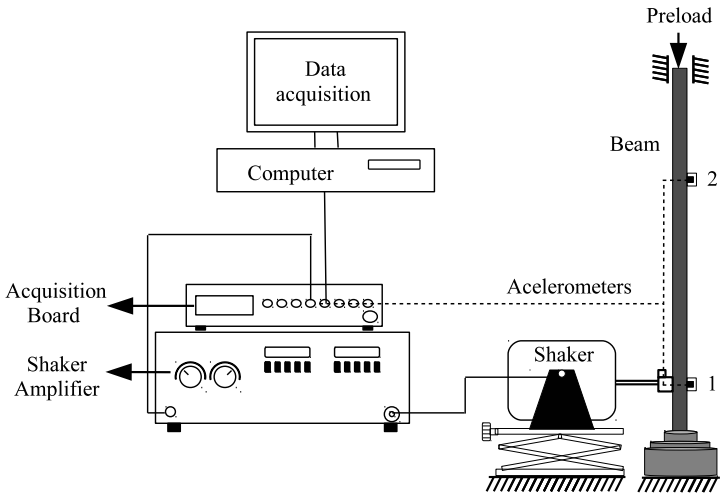

(b) Sketch of the test rig.

Source: Prepared by the author.

a curvature in the beam and it allowed to create a geometrical nonlinearity. All tests were performed using 1024 Hz as sample frequency and 4096 samples with time duration of 4 seconds. In order to verify the presence of nonlinear effects, it was made several tests using sinusoidal input with excitation frequency in 37 Hz and growing excitation levels of controlled voltage amplitude applied in the signal generator, 0.01 V (low), 0.05 V (medium) and 0.10 V (high). Figure 17(a) shows the input with high amplitude applied in the structure and it is power spectral density (PSD) is showed in Fig. 17(b). All PSD functions were calculated through Welch's method using Hanning window with 4

averages (1024 samples) and 50% of overlap.

Figure 17 – Analysis of the nonlinear effects present in the outputs when is applied a sinusoidal input with excitation frequency close to 37 Hz and high level of amplitude (0.10 V).

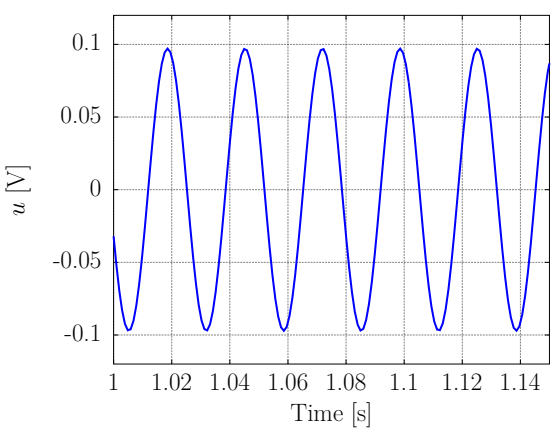

(a) Harmonic input with 0.10 V of amplitude.

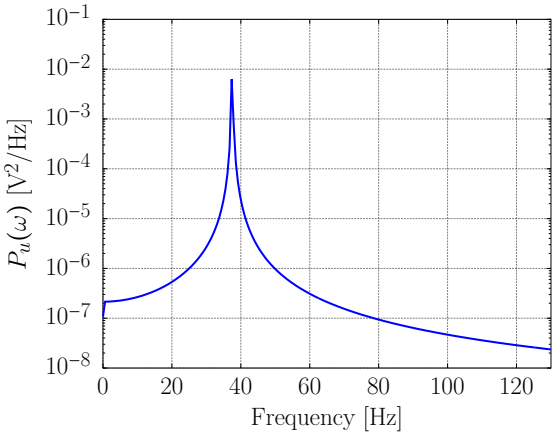

(b) PSD of harmonic input.

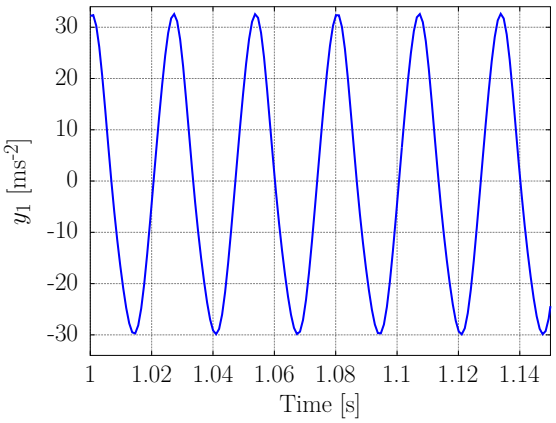

(c) Experimental output at the sensor 1.

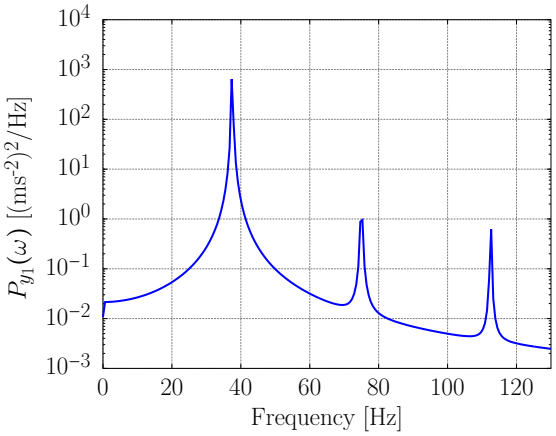

(d) PSD of output y_1.

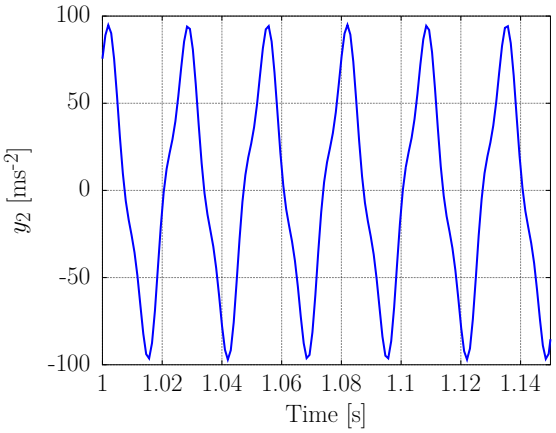

(e) Experimental output at the sensor 2.

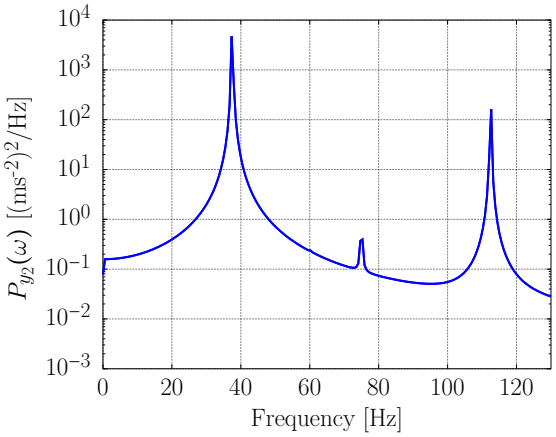

(f) PSD of output y_2.

Source: Prepared by the author.

By analysing Figs. 17(c) and 17(e) one can observe that for high amplitude of harmonic excitation, the distortions of the response at the sensor 2 are stronger than the response recorded by the sensor 1. Furthermore, the nonlinear effects of the test rig can be observed through the spectrum of the outputs. As showed in Figs. 17(d) and 17(f), the response spectrum of the system contains peaks related to the excitation frequency close to 37 Hz and the respective harmonics of second and third order in 74 Hz and 111 Hz, respectively. More details about the test-rig and evidences of nonlinearities can be found in Hansen et al. (2014) and in Tang et al. (2015a).

It is important to emphasize that in this work it is assumed the combination beam-shaker acting as a SDOF oscillator as performed by (TANG et al., 2015a). Thus, it is considered the voltage signal to the amplifier as input instead of the force signal collected by the load cell that might be contaminated by the nonlinear responses. Moreover, the structure presents hardening nonlinearity and has characteristics of systems with cubic stiffness. Due to these facts are considered kernels until third order ($\eta = 1, 2, 3$) to identify the nonlinear models operating over the frequency range that contains only the first resonance frequency.

Firstly, the acceleration in the opposite side of the load cell (sensor 1 as $y'(k)$) and the acceleration on top of the beam (sensor 2 as $y(k)$) were taken. The vibration responses were obtained by applying a chirp input sweeping up the frequency range from 20 to 50 Hz containing the first mode of the system in 37 Hz with time duration of 4 seconds (50% of burst) and 0.10 V of amplitude.

After select the experimental data set, the kernels $\mathcal{G}_1(n_1), \mathcal{G}_2(n_1, n_2)$ and $\mathcal{G}_3(n_1, n_2, n_3)$ in Eq. (40) were identified with minimal number of Kautz filters ($J_1 = J_2 = J_3 = 2$) in order to get a minimum number of parameters to be estimated. Additionally, the kernels $\mathcal{H}_1(n_1), \mathcal{H}_2(n_1, n_2)$ and $\mathcal{H}_3(n_1, n_2, n_3)$ were identified through the conventional method assuming the chirp input $u(k)$ known. The Kautz filters parameters were obtained through the optimization problem in Eq. (51) via SQP algorithm through the *fmincon* function from optimization toolbox of MATLAB. After several tests, the upper and lower bounds as $\varpi_{(low)\eta} = 30 \times 2\pi$, $\varpi_{(up)\eta} = 65 \times 2\pi$, $\xi_{(low)\eta} = 0.0010$ and $\xi_{(up)\eta} = 0.0900$ for $\eta = 1, 2, 3$ were selected. The initial conditions were chosen as the average of upper and lower bounds. Figure 18 shows the performance of the objective functions in both methods. As showed in Fig. 18(a), the function $F(\boldsymbol{\Theta}')$ converged to the value 0.065 after 15 iterations. The function based on the conventional Volterra model $F(\boldsymbol{\Theta})$ converged to 0.1685 after 45 iterations as illustrated in Fig. 18(b). The tolerances of the objective function, step and optimality were chosen as 10^{-15}.

The parameters found by the optimization problems are showed in Tab. 3 and they were used to compute the kernels from Eqs. (39) and (40).

Figure 18 – Evolution of the objective function in the identification procedure using SQP algorithm.

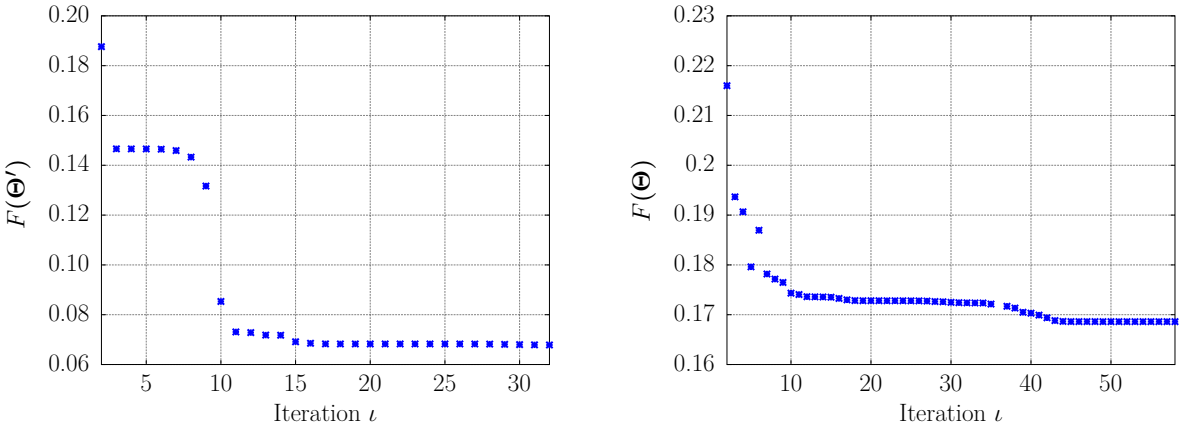

(a) Objective function using the model based on output-only data.

(b) Objective function using the conventional Volterra model.

Source: Prepared by the author.

From the identification procedure, it is worth noting that the Kautz filters allowed to reduce the large amount of parameters to be estimated. The parameters of the model without orthonormal expansion were related with the number of samples recorded, $N_1 = N_2 = N_3 = 4096$. On the other hand, the parameters of the model with orthonormal expansion are related with the number of Kautz filters, $J_1 = J_2 = J_3 = 2$.

The identified kernels up to third order for the conventional and output-only models are shown in Fig. 19. The definition of these kernels based on Volterra series represents a generalization of the Taylor series expansion. These kernels allow to describe the mapping between the input and the output of the nonlinear model by using a polynomial structure with memory. In such cases, the output predicted also depends on past inputs (SCHETZEN, 1980).

Table 3 – Optimized Kautz parameters of each model.

	1^{st} kernel	2^{nd} kernel	3^{rd} kernel
Output-only	$0.9238 + j0.3371$	$0.9212 + j0.3690$	$0.9472 + j0.2918$
Conventional	$0.9602 + j0.2256$	$0.9712 + j0.2215$	$0.9688 + j0.2193$

Source: Prepared by the author.

Figure 19 – Kernels of first, second and third order.

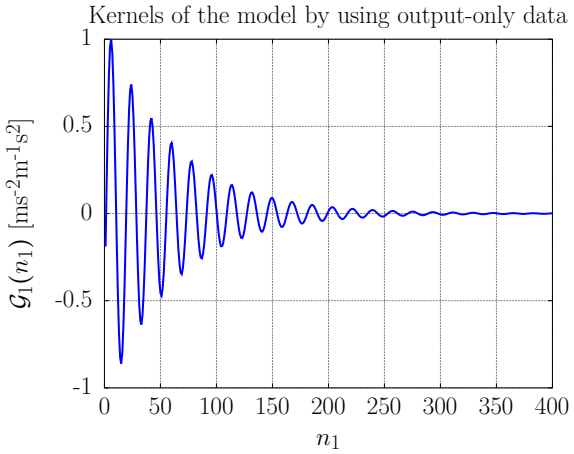

(a) Kernel of first order.

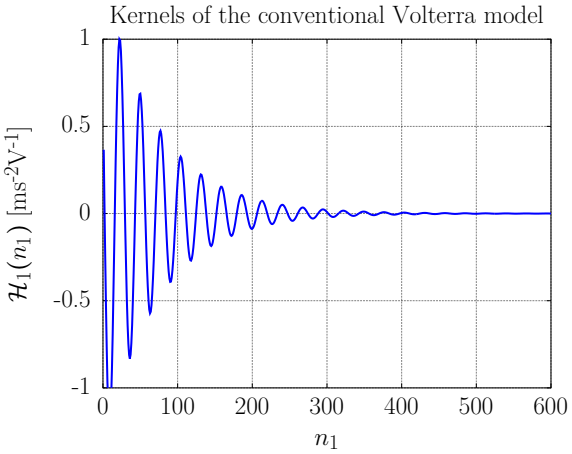

(b) Volterra kernel of first order.

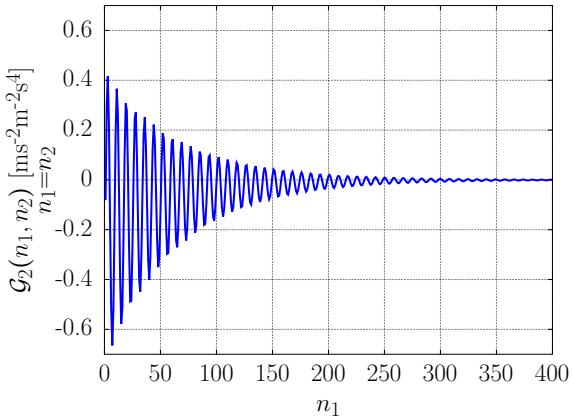

(c) Kernel of second order (main diagonal).

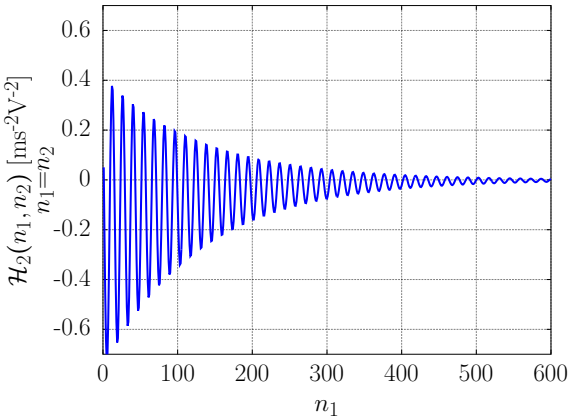

(d) Volterra kernel of second order (main diagonal).

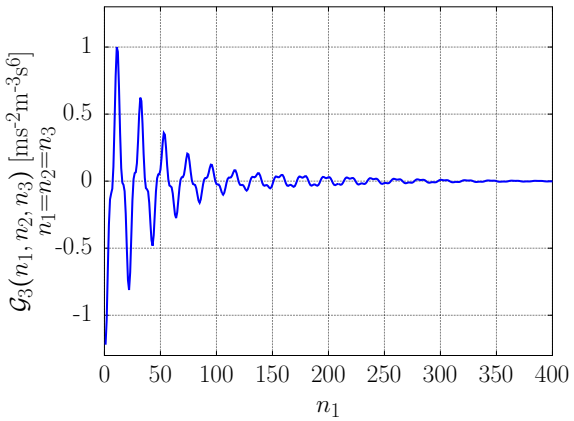

(e) Kernel of third order (main diagonal).

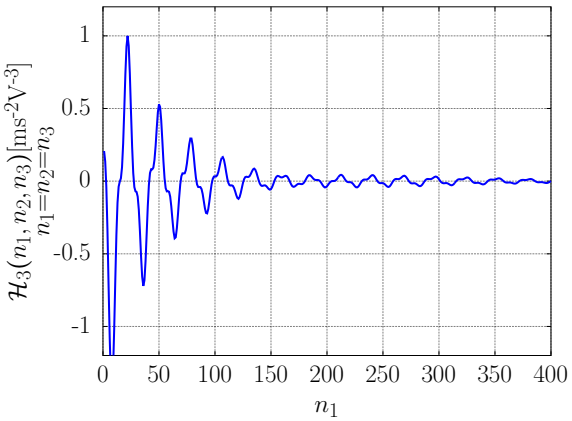

(f) Volterra kernel of third order (main diagonal).

Source: Prepared by the author.

Moreover, the kernels of first order showed in Figs. 19(a) and 19(b) are vectors representing the standard impulse response function (IRF) and are used to predict the linear contribution of the response. The kernel of second order is a matrix that contains the regressors related with the quadratic contribution of the model. Figures 19(c) and 19(d) show the main diagonal of the second order kernels where it is possible to note the asymmetric behaviour. The kernel of third order is a three-dimensional array that describes the cubic contribution and the main diagonal of the cubic kernels identified are showed in Figs. 19(e) and 19(f).

The models identified were used to estimate the outputs $y(k;\boldsymbol{\Theta}')$ and $y(k;\boldsymbol{\Theta})$ where $\boldsymbol{\Theta}'$ and $\boldsymbol{\Theta}$ are the vectors with the Kautz filters parameters of the output-only model and the conventional model, respectively. In Table 3 it can be seen that the parameters are slightly different. This fact is due to the nature of the input signals utilized in each model identified. The conventional model used the voltage signal and the model with output-only used the acceleration in the sensor 1.

Figure 20(a) shows the output predicted by the model with output-only data and VOF $\approx 94\%$ from eq. (55). Figure 20(b) shows the output predicted by the conventional Volterra model with VOF $\approx 84\%$. Both models were able to predict considerably the output desired (acceleration in the sensor 2).

Figure 20 – Output estimated by the output-only method and by the conventional Volterra method (+) in comparison with the acceleration (sensor 2) measured (–).

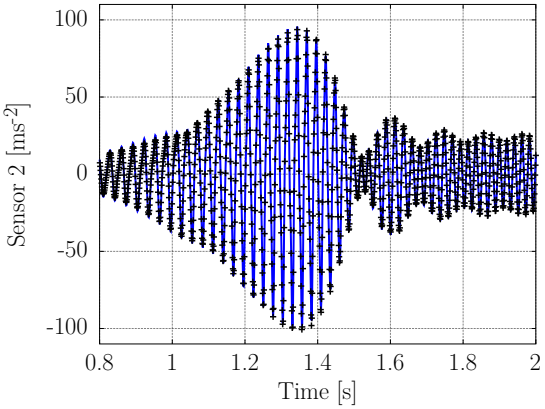

(a) Predicted by using the output-only method ($y(k;\Theta')$ with 94% of fit).

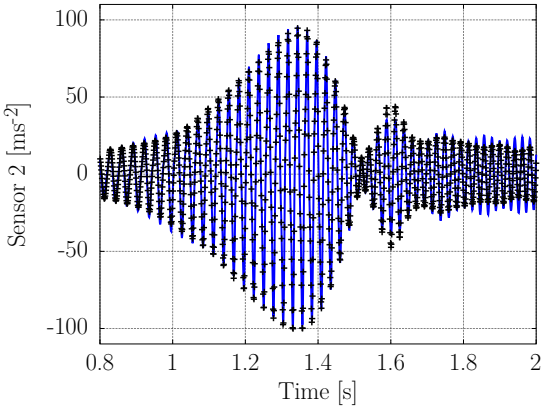

(b) Predicted by the conventional method ($y(k;\Theta)$ with 84% of fit).

Source: Prepared by the author.

The nonlinear models were validated by using a sinusoidal input with excitation

frequency close to 37 Hz and amplitude of 0.10 V applied in power amplifier in order to detect the presence of harmonics in the PSD of the outputs predicted. In Figure 21 is showed the PSD of the output predicted by each model where its possible to note a considerable agreement with the PSD of the experimental output in the Fig. 17(f). These facts showed the accuracy of the models identified and their benefits in to predict adequately nonlinearities present in the responses.

Figure 21 – Nonlinearity detection through PSD of the output predicted when is applied a sinusoidal input with high level of amplitude (0.10 V) and excitation frequency in 37 Hz.

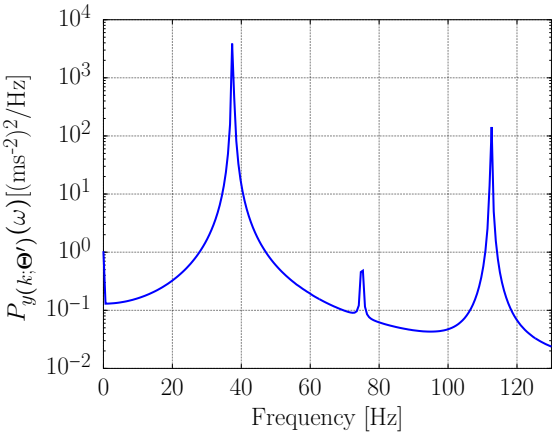

(a) PSD of the output predicted by the output-only model.

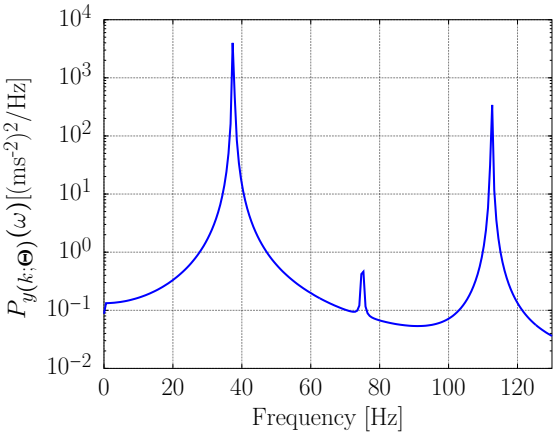

(b) PSD of the output predicted by the Volterra model.

Source: Prepared by the author.

Figure 22 shows the spectral contribution of the output components separately. As can be seen, the PSD function for $\eta = 1$ is the component with a single peak in 37 Hz that represents the linear contribution. The PSD for $\eta = 2$ represents the spectral contribution of second order with a single peak close to 74 Hz (even harmonic). This component has nonsymmetric effects possibly due to shaker-beam interaction. Further, the curve of the PSD for $\eta = 3$ is the spectrum of the cubic order where its possible to observe the peaks in 37 Hz and 111 Hz (odd harmonic). These facts illustrated that the system is essentially characterized by dominant symmetric nonlinear stiffness and weak nonsymmetric nonlinearities as verified also in Hansen et al. (2014).

Figure 22 – Frequency contribution of the components for $\eta = 1$ (–), $\eta = 2$ (line ▲) and $\eta = 3$ (dotted line □).

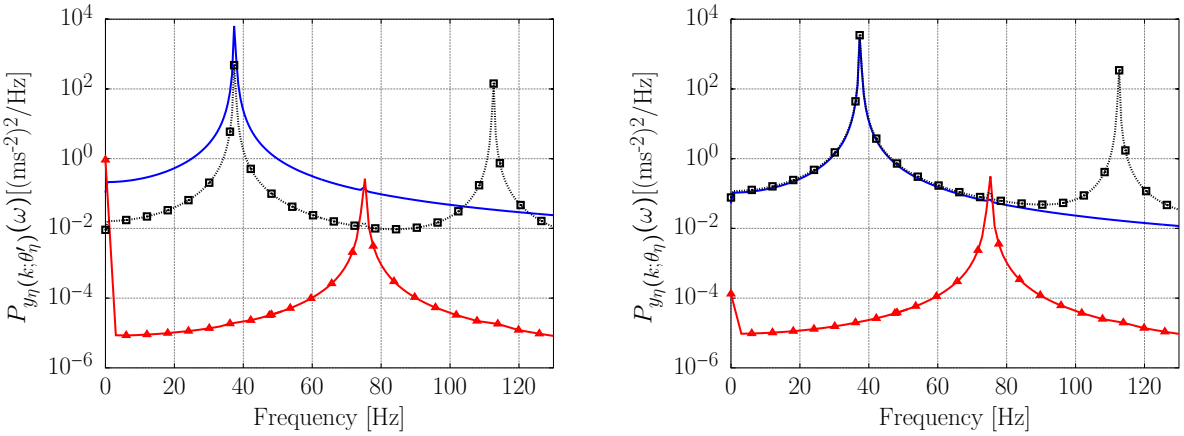

(a) Output-only method.

(b) Conventional Volterra method.

Source: Prepared by the author.

3.6 Conclusions

This chapter presented an alternative approach for nonlinear system identification based on output-only measurements. The Theorem 2 shows that the discrete-time extended Volterra kernels have analytical expressions based on the conventional ones and can be useful for analysis, identification and output prediction of nonlinear systems.

The contribution lies in the fact the force excitation is not required as in conventional case. The possibility in to analyse separately the linear and nonlinear components of the response demonstrated a powerful advantage of Volterra series expansion. Furthermore, the use of orthonormal expansion of the Volterra kernels from the physical basis to Kautz filters basis allows to reduce the large amount of parameters associated to the higher-order kernels. Additionally, such kind of orthonormal basis representation insert vibratory behaviour in the model allowing to deal with oscillatory lightly-damped systems.

The examples based on the Duffing oscillator with 2 DOFs and the buckled beam showed the benefits of the models based on Volterra series and output-only data to detect nonlinear effects and characterize nonlinear behaviour of weakly nonlinear systems. A simple comparison with the conventional Volterra model showed similar results and conclusions about the nonlinear behaviour. However, the model cannot represent adequately nonlinear systems operating in regime with strong nonlinearities and discontinuities. Moreover, the method proposed was evaluated for cases in laboratory conditions involving controlled excitation with harmonic nature. Further works are concerned with

application involving structures in their operating environment under random excitations and multi-input and multi-output (MIMO) systems.

4 Applications of Volterra Series in Modal Analysis and Structural Dynamics

The algebraic analysis and physical interpretation of the Higher-Order Frequency Response Functions (HOFRFs) based on Volterra series expressed in terms of parameters obtained through a simple transformation of coordinates is presented in this chapter. This transformation leads the problem from the spatial space to the modal space. Thus, the analytical expressions of the HOFRFs and their powerful applicability in vibrating problems of structural dynamics are presented. This new representation in modal space allows to analyse the inherent properties and natural characteristics of systems with mild nonlinearities in terms of natural (modal or resonant) frequencies, damping factors as well as the modes shape. Initially, some remarks on existing methods of modal analysis and challenging issues are carried out in section 4.1. In section 4.2 are reviewed the expressions of the conventional HOFRFs for single-degree-of-freedom (SDOF) system case. Afterwards, such expressions are generalized for the multi-degree-of-freedom (MDOF) system case and an algorithm to identify the HOFRFs in modal space is proposed in section 4.3. Section 4.4 presents an application in a benchmark with nonlinear features. Finally, the conclusions are summarized in section 4.5.

4.1 A brief review on modal analysis and nonlinear systems

The development of methods for modal analysis has grown significantly during the last decades due to the increasing number of industrial applications in aerospace, mechanical and civil engineering (PLATTEN et al., 2009; ZWOLSKI; BIEŃ, 2011; NOËL et al., 2014b; BROWNJOHN et al., 2015; OZBEK; RIXEN, 2016). The main goal of modal analysis lies in to characterize the dynamic behaviour of a testing structure in terms of its natural characteristics: natural frequencies, damping ratio and mode shapes

(CAUGHEY; O'KELLY, 1965; MAYBEE, 1966; MAIA; SILVA, 1997; EWINS, 2000). The representation in terms of modal space brings several benefits in testing, project, design and maintenance of engineering structures. It can be done, either numerically or experimentally, based on the testing physical system under study (CUNHA; CAETANO, 2006; GROSEL et al., 2014; XUE et al., 2015).

Several studies on vibrating tests have been conducted aiming structural modal identification of bridges and dams (CUNHA; CAETANO, 2006; CABBOI et al., 2017), automotive structures (ZOU et al., 2016), aerospace structures (KERSCHEN et al., 2013), towers (DIAFERIO et al., 2011; CHEN et al., 2011), wind turbines (ALLEN et al., 2011; YANG; ALLEN, 2012), high rise structures (XU et al., 1997; BRINCKER; ANDERSEN, 2000), huge offshore platforms based on non-stationary response data (TANG et al., 2015b), time-variant vibration systems via wavelet-based frequency response function (FRF) (DZIEDZIECH et al., 2015), analysis of uncertainties that affect the estimation of the modal parameters (BANFI; CARASSALE, 2016) and many other applications.

Nevertheless, it is notable the increasing demand for extensions of linear experimental modal analysis techniques to study dynamical behaviour of nonlinear structures based on experimental vibration data associated to several applications in electrical engineering, mechanical engineering, mathematics, and many others (VIRGIN, 2000; TAWFIQ; VINH, 2003; KERSCHEN et al., 2006; NOËL; KERSCHEN, 2017).

Frachebourg et al. (1988) proposed the use of Volterra models and a modal analysis procedure on each kernel allowing to get the respective mode shapes for higher-order kernels as well as their physical interpretation. The authors investigated numerical simulations subjected to impulse excitation only and was verified that they are convergent to a bounded solution when the order of the model is increased. Additionally, the localisation of the nonlinear spring becomes possible in the case of weakly coupled modes. The method present some negative aspects due to the weakness of Volterra series expansion in representing nonlinear phenomena of applications with strong nonlinearities.

A few years later, Tawfiq and Vinh (2003) extended a conventional modal analysis technique based on Volterra functional series for mechanical structures viewed as a multi-input multi-output (MIMO) system. The authors have found that the basis of nonlinear modal analysis of weakly nonlinear systems is constituted by the generalised superposition principle present in the definition of the Volterra series expansion. The expressions for higher-order transfer functions are proposed and remarks concerning their applicability in practical cases are addressed.

Recently, Worden and Green (2017) have proposed an interesting machine learning approach to nonlinear modal analysis based on the nonlinear normal modes (NNMs) theory (ROSENBERG, 1962; SHAW; PIERRE, 1993; SHAW; PIERRE, 1994; VAKAKIS, 1997). As stated by the authors, the paper proposes an approach that extends the principal orthogonal decomposition (POD) and the concept of invariant manifold approach, which exploits the idea of statistical independence to optimise a parametric form of the mapping, aiming nonlinear modal analysis. Some case of studies through numerical and experimental data are investigated and the approach have shown to be an efficient technique to deal with practical applications of nonlinear systems.

However, an alternative approach able to provide a better understanding of these phenomenon based on its modal properties is very desirable. In this sense, the contributions of the present chapter are:

(i) To provide a brief algebraic analysis and physical interpretation of the higher-order frequency response functions (HOFRFs) expressed in terms of parameters obtained through of a simple transformation of coordinates.

(ii) To show how to use orthonormal Kautz basis to identify the HOFRFs based on experimental vibration data.

(iii) To combine both approaches, HOFRFs via harmonic probing (white box) with the multidimensional Fourier transform of Volterra-Kautz kernels (grey box) developing a methodology to analyse and treat weak nonlinearities of mechanical vibrating systems in a more practical way.

The main idea behind the methodology is simply to construct easily a nonlinear model based on modal parameters identified by using any conventional method via input-output vibration data. Thus, the HOFRFs that represent the nonlinear part of the model can be estimated by discrete-time Volterra based methods, as reviewed in chapter 3, and a fit approach using the harmonic probing can be performed in a similar way as it is made in the linear case.

4.2 Single-degree-of-freedom nonlinear system theory

The equation of motion of a SDOF Duffing oscillator with quadratic and cubic stiffnesses under harmonic input $u(t) = A\cos(\omega t)$ is given as follows:

$$m\ddot{y}(t) + c\dot{y}(t) + ky(t) + \alpha y^2(t) + \beta y^3(t) = A\cos(\omega t) \tag{56}$$

where the physical parameter m is the mass in [kg], c is the damping in [N.s/m], k is the stiffness in [N/m]. The terms α in [N/m^2] and β in [N/m^3] correspond to the quadratic and cubic stiffnesses, respectively. Equation (56) can be alternatively rewritten in the following form:

$$\ddot{y}(t) + 2\zeta\omega_n\dot{y}(t) + \omega_n^2 y(t) + \varrho y^2(t) + \varsigma y^3(t) = \frac{A}{2m}(e^{j\omega t} + e^{-j\omega t}) \tag{57}$$

where $\zeta = \frac{c}{2m\omega_n}$ is the damping ratio, $\varpi = \sqrt{\frac{k}{m}}$ is the natural frequency, $\varrho = \frac{\alpha}{m}$ and $\varsigma = \frac{\beta}{m}$ are the nonlinear stiffnesses.

By using the Volterra series expansion the output $y(t)$ is calculated as:

$$y(t) = \sum_{\eta=1}^{+\infty} \int_{\mathbb{R}^\eta} h_\eta(\tau_1, \tau_2, \ldots, \tau_\eta) \prod_{i=1}^{\eta} u(t-\tau_i) d\tau_i = y_1(t) + y_2(t) + y_3(t) + \ldots \tag{58}$$

where $h_\eta(\tau_1, \tau_2, \ldots, \tau_\eta)$ is the Volterra kernel of ηth order that represents direct generalization of the impulse response function and $u(t)$ is the input signal. Furthermore, it is important to point out that is assumed:

$$\int_{\mathbb{R}^\eta} = \int_{\mathbb{R}\times\mathbb{R}\times\ldots\times\mathbb{R}} = \underbrace{\int_{-\infty}^{+\infty} \int_{-\infty}^{+\infty} \cdots \int_{-\infty}^{+\infty}}_{\eta \text{ times}}$$

in order to simplify the notation. The term $y_1(t)$ is the linear contribution of the total response predicted and it is calculated through the convolution between the Volterra kernel of first order $h_1(\tau_1)$ (the well known IRF) and the input signal as follows:

$$y_1(t) = \int_{\mathbb{R}^1} h_1(\tau_1) u(t-\tau_1) d\tau_1 \tag{59}$$

Additionally, the terms $y_2(t)$ and $y_3(t)$ are the quadratic and cubic polynomial contributions given by:

$$y_2(t) = \int_{\mathbb{R}^2} h_2(\tau_1, \tau_2) u(t-\tau_1) u(t-\tau_2) d\tau_1 d\tau_2 \tag{60}$$

and

$$y_3(t) = \int_{\mathbb{R}^3} h_3(\tau_1,\tau_2,\tau_3)u(t-\tau_1)u(t-\tau_2)u(t-\tau_3)d\tau_1 d\tau_2 d\tau_3 \tag{61}$$

The possibility of analysing separately the polynomial contributions of the total output predicted points out one of the main benefits of the Volterra series expansion. Physically, the higher-order Volterra kernels $h_\eta(\tau_1,\tau_2,\ldots,\tau_\eta)$ are the hyper-surfaces that are used to describe the respective ηth order polynomial contribution of the total output predicted via the nonlinear convolution with the past input terms. Furthermore, by calculating the multidimensional Fourier transform of the higher-order Volterra kernels generates the higher-order frequency response functions (HOFRFs) as follows:

$$\mathcal{H}_\eta(\omega_1,\omega_2,\ldots,\omega_\eta) = \int_{\mathbb{R}^\eta} h_\eta(\tau_1,\tau_2,\ldots,\tau_\eta)\prod_{i=1}^{\eta} e^{-j\omega_i\tau_i}d\tau_1 d\tau_2\ldots d\tau_\eta \tag{62}$$

Thus, for a harmonic input $u(t) = A\cos(\omega t) = \frac{A}{2}e^{j\omega t} + \frac{A}{2}e^{-j\omega t}$, the polynomials contributions up to third order of the output $y(t)$ are defined by Tomlinson et al. (1996):

$$\begin{aligned}
y_1(t) &= \int_{\mathbb{R}^1} h_1(\tau_1)u(t-\tau_1)d\tau_1 = \int_{\mathbb{R}^1} h_1(\tau_1)\left\{\frac{A}{2}e^{j\omega(t-\tau_1)} + \frac{A}{2}e^{-j\omega(t-\tau_1)}\right\}d\tau_1 \\
&= \frac{A}{2}\int_{\mathbb{R}^1} h_1(\tau_1)e^{-j\omega\tau_1}d\tau_1 e^{j\omega t} + \frac{A}{2}\int_{\mathbb{R}^1} h_1(\tau_1)e^{j\omega\tau_1}d\tau_1 e^{-j\omega t} \\
&= \frac{A}{2}\mathcal{H}_1(\omega)e^{j\omega t} + \frac{A}{2}\mathcal{H}_1(-\omega)e^{-j\omega t}, \\
y_2(t) &= \int_{\mathbb{R}^2} h_2(\tau_1\tau_2)u(t-\tau_1)u(t-\tau_2)d\tau_1 d\tau_2 \\
&= \int_{\mathbb{R}^2} h_2(\tau_1,\tau_2)\left\{\frac{A}{2}e^{j\omega(t-\tau_1)} + \frac{A}{2}e^{-j\omega(t-\tau_1)}\right\}\left\{\frac{A}{2}e^{j\omega(t-\tau_2)} + \frac{A}{2}e^{-j\omega(t-\tau_2)}\right\}d\tau_1 d\tau_2 \\
&= \frac{A^2}{4}\mathcal{H}_2(\omega,\omega)e^{j2\omega t} + \frac{A^2}{4}\mathcal{H}_2(-\omega,\omega) + \frac{A^2}{4}\mathcal{H}_2(\omega,-\omega) + \frac{A^2}{4}\mathcal{H}_2(-\omega,-\omega)e^{-j2\omega t}, \\
y_3(t) &= \int_{\mathbb{R}^3} h_3(\tau_1,\tau_2,\tau_3)u(t-\tau_1)u(t-\tau_2)u(t-\tau_3)d\tau_1 d\tau_2 d\tau_3 \\
&= \frac{A^3}{8}\mathcal{H}_3(\omega,\omega,\omega)e^{j3\omega t} + \frac{A^3}{8}\mathcal{H}_3(-\omega,\omega,\omega)e^{j\omega t} + \frac{A^3}{8}\mathcal{H}_3(\omega,-\omega,\omega)e^{j\omega t} \\
&+ \frac{A^3}{8}\mathcal{H}_3(\omega,\omega,-\omega)e^{j\omega t} + \frac{A^3}{8}\mathcal{H}_3(-\omega,-\omega,\omega)e^{-j\omega t} + \frac{A^3}{8}\mathcal{H}_3(-\omega,\omega,-\omega)e^{-j\omega t} \\
&+ \frac{A^3}{8}\mathcal{H}_3(\omega,-\omega,-\omega)e^{-j\omega t} + \frac{A^3}{8}\mathcal{H}_3(-\omega,-\omega,-\omega)e^{-j3\omega t}.
\end{aligned}$$

the expression for the response in Eq. (58) can be rewritten as:

$$\begin{aligned} y(t) &= \frac{A}{2}\mathcal{H}_1(\omega)e^{j\omega t} + \frac{A}{2}\mathcal{H}_1(-\omega)e^{-j\omega t} \\ &+ \frac{A^2}{4}\mathcal{H}_2(\omega,\omega)e^{j2\omega t} + \frac{A^2}{2}\mathcal{H}_2(-\omega,\omega) + \frac{A^2}{4}\mathcal{H}_2(-\omega,-\omega)e^{-j2\omega t} \\ &+ \frac{A^3}{8}\mathcal{H}_3(\omega,\omega,\omega)e^{j3\omega t} + \frac{3A^3}{8}\mathcal{H}_3(-\omega,\omega,\omega)e^{j\omega t} \\ &+ \frac{3A^3}{8}\mathcal{H}_3(-\omega,-\omega,\omega)e^{-j\omega t} + \frac{A^3}{8}\mathcal{H}_3(-\omega,-\omega,-\omega)e^{-j3\omega t} + \dots \end{aligned} \tag{63}$$

that provides an alternative way to represent the output of a nonlinear system described by polynomial nonlinearities subject to a single-tone harmonic input through the HOFRFs. Now, by differentiating $y(t)$ in Eq. (63) for the velocity and the acceleration yields

$$\begin{aligned} \dot{y}(t) &= j\omega\frac{A}{2}\mathcal{H}_1(\omega)e^{j\omega t} - j\omega\frac{A}{2}\mathcal{H}_1(-\omega)e^{-j\omega t} \\ &+ j2\omega\frac{A^2}{4}\mathcal{H}_2(\omega,\omega)e^{j2\omega t} - j2\omega\frac{A^2}{4}\mathcal{H}_2(-\omega,-\omega)e^{-j2\omega t} \\ &+ j3\omega\frac{A^3}{8}\mathcal{H}_3(\omega,\omega,\omega)e^{j3\omega t} + j\omega\frac{3A^3}{8}\mathcal{H}_3(-\omega,\omega,\omega)e^{j\omega t} \\ &- j\omega\frac{3A^3}{8}\mathcal{H}_3(-\omega,-\omega,\omega)e^{-j\omega t} + \dots \end{aligned} \tag{64}$$

and

$$\begin{aligned} \ddot{y}(t) &= -\omega^2\frac{A}{2}\mathcal{H}_1(\omega)e^{j\omega t} - \omega^2\frac{A}{2}\mathcal{H}_1(-\omega)e^{-j\omega t} \\ &- (2\omega)^2\frac{A^2}{4}\mathcal{H}_2(\omega,\omega)e^{j2\omega t} - (2\omega)^2\frac{A^2}{4}\mathcal{H}_2(-\omega,-\omega)e^{-j2\omega t} \\ &- (3\omega)^2\frac{A^3}{8}\mathcal{H}_3(\omega,\omega,\omega)e^{j3\omega t} - \omega^2\frac{3A^3}{8}\mathcal{H}_3(-\omega,\omega,\omega)e^{j\omega t} \\ &- \omega^2\frac{3A^3}{8}\mathcal{H}_3(-\omega,-\omega,\omega)e^{-j\omega t} + \dots \end{aligned} \tag{65}$$

Thus, substituting the expressions of the terms $y(t)$, $\dot{y}(t)$ and $\ddot{y}(t)$ in Eq. (57) gives:

$$\begin{aligned}
&\Bigg[-\omega^2\frac{A}{2}\mathcal{H}_1(\omega)e^{j\omega t}-\omega^2\frac{A}{2}\mathcal{H}_1(-\omega)e^{-j\omega t}-(2\omega)^2\frac{A^2}{4}\mathcal{H}_2(\omega,\omega)e^{j2\omega t}-(2\omega)^2\frac{A^2}{4}\mathcal{H}_2(-\omega,-\omega)e^{-j2\omega t}\\
&-(3\omega)^2\frac{A^3}{8}\mathcal{H}_3(\omega,\omega,\omega)e^{j3\omega t}-\omega^2\frac{3A^3}{8}\mathcal{H}_3(-\omega,\omega,\omega)e^{j\omega t}-\omega^2\frac{3A^3}{8}\mathcal{H}_3(-\omega,-\omega,\omega)e^{-j\omega t}\\
&-(3\omega)^2\frac{A^3}{8}\mathcal{H}_3(-\omega,-\omega,-\omega)e^{-j3\omega t}+\ldots\Bigg]+2\zeta\varpi\Bigg[j\omega\frac{A}{2}\mathcal{H}_1(\omega)e^{j\omega t}-j\omega\frac{A}{2}\mathcal{H}_1(-\omega)e^{-j\omega t}\\
&+j2\omega\frac{A^2}{4}\mathcal{H}_2(\omega,\omega)e^{j2\omega t}-j2\omega\frac{A^2}{4}\mathcal{H}_2(-\omega,-\omega)e^{-j2\omega t}+j3\omega\frac{A^3}{8}\mathcal{H}_3(\omega,\omega,\omega)e^{j3\omega t}+j\omega\frac{3A^3}{8}\mathcal{H}_3(-\omega,\omega,\omega)e^{j\omega t}\\
&-j\omega\frac{3A^3}{8}\mathcal{H}_3(-\omega,-\omega,\omega)e^{-j\omega t}-j3\omega\frac{A^3}{8}\mathcal{H}_3(-\omega,-\omega,-\omega)e^{-j3\omega t}+\ldots\Bigg]+\varpi^2\Bigg[\frac{A}{2}\mathcal{H}_1(\omega)e^{j\omega t}\\
&+\frac{A}{2}\mathcal{H}_1(-\omega)e^{-j\omega t}+\frac{A^2}{4}\mathcal{H}_2(\omega,\omega)e^{j2\omega t}+\frac{A^2}{2}\mathcal{H}_2(-\omega,\omega)+\frac{A^2}{4}\mathcal{H}_2(-\omega,-\omega)e^{-j2\omega t}+\frac{A^3}{8}\mathcal{H}_3(\omega,\omega,\omega)e^{j3\omega t}\\
&+\frac{3A^3}{8}\mathcal{H}_3(-\omega,\omega,\omega)e^{j\omega t}+\frac{3A^3}{8}\mathcal{H}_3(-\omega,-\omega,\omega)e^{-j\omega t}+\frac{A^3}{8}\mathcal{H}_3(-\omega,-\omega,-\omega)e^{-j3\omega t}+\ldots\Bigg]\\
&+\varrho\Bigg[\frac{A}{2}\mathcal{H}_1(\omega)e^{j\omega t}+\frac{A}{2}\mathcal{H}_1(-\omega)e^{-j\omega t}+\frac{A^2}{4}\mathcal{H}_2(\omega,\omega)e^{j2\omega t}+\frac{A^2}{2}\mathcal{H}_2(-\omega,\omega)+\frac{A^2}{4}\mathcal{H}_2(-\omega,-\omega)e^{-j2\omega t}\\
&+\frac{A^3}{8}\mathcal{H}_3(\omega,\omega,\omega)e^{j3\omega t}+\frac{3A^3}{8}\mathcal{H}_3(-\omega,\omega,\omega)e^{j\omega t}+\frac{3A^3}{8}\mathcal{H}_3(-\omega,-\omega,\omega)e^{-j\omega t}\\
&+\frac{A^3}{8}\mathcal{H}_3(-\omega,-\omega,-\omega)e^{-j3\omega t}+\ldots\Bigg]^2+\varsigma\Bigg[\frac{A}{2}\mathcal{H}_1(\omega)e^{j\omega t}+\frac{A}{2}\mathcal{H}_1(-\omega)e^{-j\omega t}+\frac{A^2}{4}H_2(\omega,\omega)e^{j2\omega t}\\
&+\frac{A^2}{2}\mathcal{H}_2(-\omega,\omega)+\frac{A^2}{4}\mathcal{H}_2(-\omega,-\omega)e^{-j2\omega t}+\frac{A^3}{8}\mathcal{H}_3(\omega,\omega,\omega)e^{j3\omega t}+\frac{3A^3}{8}\mathcal{H}_3(-\omega,\omega,\omega)e^{j\omega t}\\
&+\frac{3A^3}{8}\mathcal{H}_3(-\omega,-\omega,\omega)e^{-j\omega t}+\frac{A^3}{8}\mathcal{H}_3(-\omega,-\omega,-\omega)e^{-j3\omega t}+\ldots\Bigg]^3=\frac{A}{2m}e^{j\omega t}+\frac{A}{2m}e^{-j\omega t},
\end{aligned}$$

Now, by equating the terms with $e^{j\omega t}$ yields the FRF of first order:

$$\mathcal{H}_1(\omega)=\frac{\frac{1}{m}}{\varpi^2-\omega^2+2\zeta\varpi j\omega} \tag{66}$$

The FRF of second order $\mathcal{H}_2(\omega,\omega)$ is obtained equating the terms with $e^{j2\omega t}$

$$[-(2\omega)^2+j2\omega 2\zeta\varpi+\varpi^2]\mathcal{H}_2(\omega,\omega)+\mathcal{H}_1^2(\omega)=0\Leftrightarrow\mathcal{H}_2(\omega,\omega)=-\varrho\mathcal{H}_1^2(\omega)\mathcal{H}_1(2\omega) \tag{67}$$

To determine an algebraic expression for $\mathcal{H}_3(\omega,\omega,\omega)$ the coefficients with $e^{j3\omega t}$ are equated

$$\mathcal{H}_3(\omega,\omega,\omega)=2\varrho^2\mathcal{H}_1^3(\omega)\mathcal{H}_1(2\omega)\mathcal{H}_1(3\omega)-\varsigma\mathcal{H}_1^3(\omega)\mathcal{H}_1(3\omega) \tag{68}$$

The FRFs $\mathcal{H}_1(\omega)$ describe the linear dynamic part of the nonlinear oscillator in Eq. (56). The terms $\mathcal{H}_2(\omega,\omega)$ and $H_3(\omega,\omega,\omega)$ are the higher-order frequency response functions (HOFRFs) and they characterize the polynomial nonlinear restoring forces of quadratic and cubic order, respectively.

For the case where the nonlinearity is symmetric ($\varrho = 0$), the HOFRF of fifth order can be computed as the following analytical expression (WORDEN; MANSON, 2005):

$$\mathcal{H}_5(\omega,\omega,\omega,\omega,\omega) = 3\varsigma^2\mathcal{H}_1(5\omega)[\mathcal{H}_1(\omega)]^5\mathcal{H}_1(3\omega) \tag{69}$$

that represents the nonlinear dynamic of fifth order. For such case, the total response of can be directly calculated as a summation of the polynomial contributions of odd order:

$$y(t) = y_1(t) + y_3(t) + y_5(t) \tag{70}$$

where the polynomial contributions are calculated as

$$y_1(t) = \frac{A}{2}\mathcal{H}_1(\omega)e^{j\omega t} + \frac{A}{2}\mathcal{H}_1(-\omega)e^{-j\omega t} = A\mathscr{R}\mathrm{e}\{\mathcal{H}_1(\omega)e^{j\omega t}\} \tag{71}$$

$$y_3(t) = \frac{A^3}{4}\mathscr{R}\mathrm{e}\{\mathcal{H}_3(\omega,\omega,\omega)e^{j3\omega t}\} + \frac{3A^3}{4}\mathscr{R}\mathrm{e}\{\mathcal{H}_3(\omega,\omega,-\omega)e^{j\omega t}\} \tag{72}$$

and

$$\begin{aligned} y_5(t) &= \frac{A^5}{16}\mathscr{R}\mathrm{e}\{\mathcal{H}_5(\omega,\omega,\omega,\omega,\omega)e^{j5\omega t}\} + \frac{5A^5}{16}\mathscr{R}\mathrm{e}\{\mathcal{H}_5(\omega,\omega,\omega,\omega,-\omega)e^{j3\omega t}\} \\ &+ \frac{10A^5}{16}\mathscr{R}\mathrm{e}\{\mathcal{H}_5(\omega,\omega,\omega,-\omega,-\omega)e^{j\omega t}\} \end{aligned} \tag{73}$$

in which $\mathscr{R}\mathrm{e}\{.\}$ denotes the real part. In order to show the framework of the HOFRFs and their applicability, consider a symmetric nonlinear oscillator with the following physical parameters m = 1 kg, c = 2 N.s/m, $k_1 = 10^3$ k/m. The modal parameters are ϖ = 5.03 Hz as the first resonance frequency and ζ = 3.1% as damping ratio. Figure 23 shows the magnitude and phase of the FRFs characterising the linear dynamic of the system. The parameters of nonlinear part of Eq. (56) are ϱ = 0 N/m^2 and $\varsigma = 10^6$ N/m^3. Figure 24 shows the main diagonal of $\mathcal{H}_3(\omega,\omega,\omega)$, in magnitude and phase, computed through using the analytical expression in Eq. (68) where it is possible to see two resonance peaks, the first one refers to the first resonance frequency at 5.03 Hz and the other one is the respective tertiary resonance at $\frac{5.03}{3} \approx 1.67$ Hz. Furthermore, the main diagonal of $\mathcal{H}_5(\omega,\omega,\omega,\omega,\omega)$ is showed in the Fig. 25 with resonance peaks at 5.03, $\frac{5.03}{3}$ and $\frac{5.03}{5}$ Hz.

The equation of motion in Eq. (56) was integrated through the Newmark method (NEWMARK, 1959) combined with Newton-Raphson procedure subjected to a single-tone harmonic input $u(t) = A\cos(2\pi\omega t)$ and $\Delta dt = (50\varpi)^{-1}$ of integration step along 20 seconds and 5033 samples. It was chosen the excitation frequency ω close to 5 Hz (first resonance frequency) and different forcing levels of amplitude by increasing from $A = 0.05$ N up to $A = 0.4$ N to compute the response of the system. For all cases, it was considered $y^{(0)} = 0$ for the displacement and $\dot{y}^{(0)} = 0.07$ for the velocity as initial conditions because they lead the transient-state response be similar to the steady-state response in amplitude.

Moreover, the responses were predicted through the Eq. (70) for the all cases of forcing levels and the metric value of fit (VOF) in percentage:

$$\text{VOF} = \left(1 - \frac{||y(t) - (y_1(t) + y_3(t) + y_5(t))||}{||y(t)||}\right) \times 100\ \% \tag{74}$$

was applied to verify the accuracy and convergence analysis of the model with HOFRFs up until fifth order. Figure 26 shows the curves and the significant contribution of higher-order kernels by increasing the amplitude level of excitation. As can be seen, for low level of excitation ($A = 0.05$ N) the linear model that predicted the contribution y_1 is enough to predict the total output $y(t)$ with fit above 98 %. However, as far as the forcing level increases, it can be noted that the linear contribution decreases pointing out the need of HOFRFs of third and fifth order for high level of amplitude ($A = 0.40$ N).

Figure 23 – FRF of first order (linear FRF) with cubic stiffness modal parameters are given as $\omega = 5.03$ Hz as the first resonance frequency and $\zeta = 3.1\%$ as damping ratio.

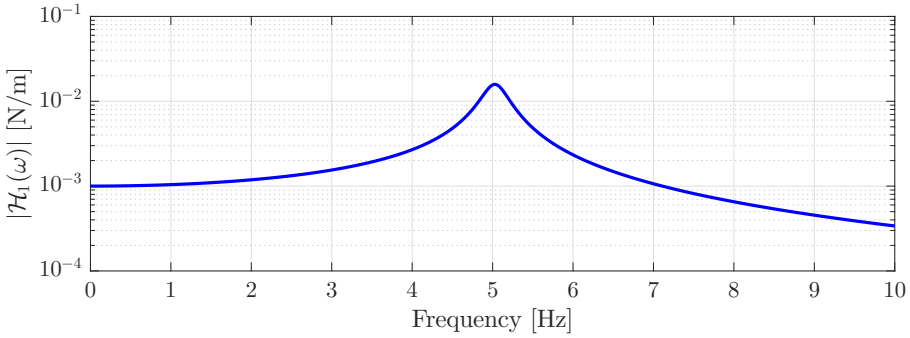

(a) Magnitude of $\mathcal{H}_1(\omega)$.

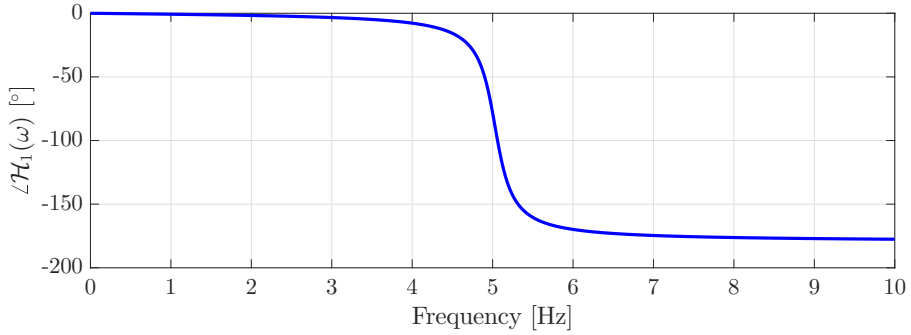

(b) Phase of $\mathcal{H}_1(\omega)$.

Source: Prepared by the author.

Figure 24 – Main diagonal of FRF of cubic order where is showed the first fundamental resonance at 5.03 Hz and the respective tertiary resonance at 1.67 Hz .

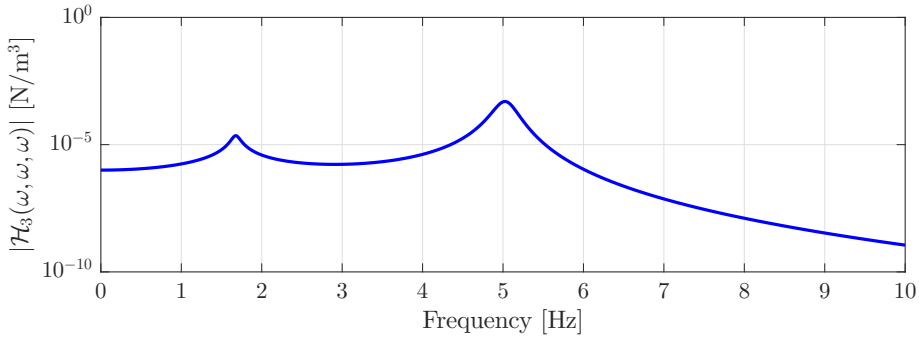

(a) Magnitude of $\mathcal{H}_3(\omega,\omega,\omega)$.

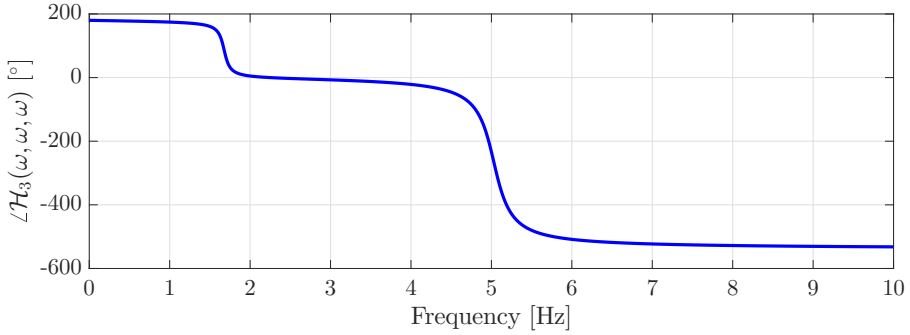

(b) Phase of $\mathcal{H}_3(\omega,\omega,\omega)$.

Source: Prepared by the author.

Figure 25 – Main diagonal of FRF of fifth order with the first fundamental resonance in 5.03 Hz and the subharmonic resonances at 1.67 Hz and 1 Hz, approximately.

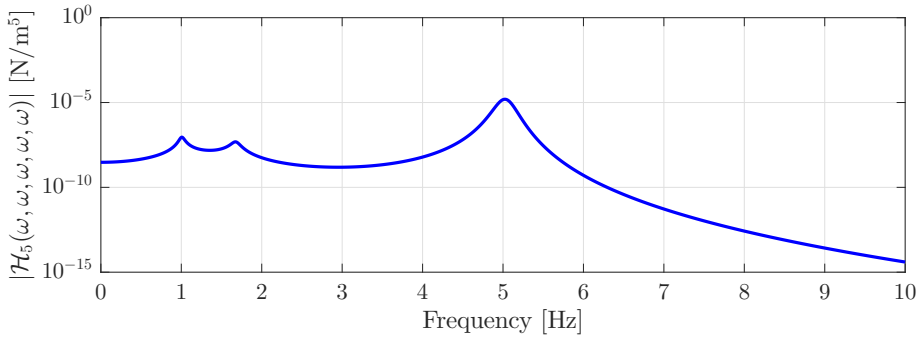

(a) Magnitude of $\mathcal{H}_5(\omega,\omega,\omega,\omega,\omega)$.

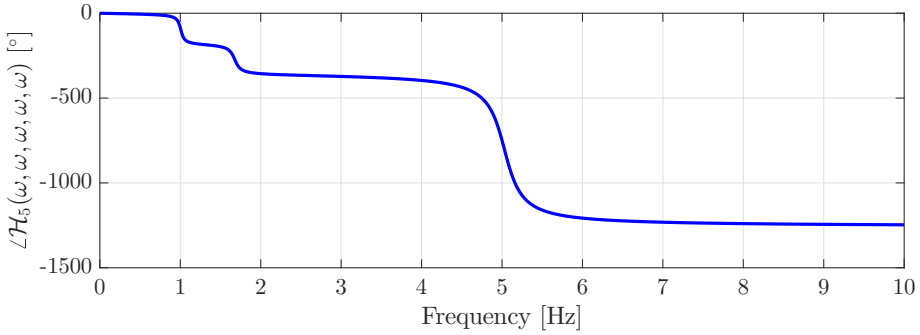

(b) Phase of $\mathcal{H}_5(\omega,\omega,\omega,\omega,\omega)$.

Source: Prepared by the author.

Figure 26 – Analysis of the polynomial contribution by using the HOFRFs up to fifth order for different values of forcing levels.

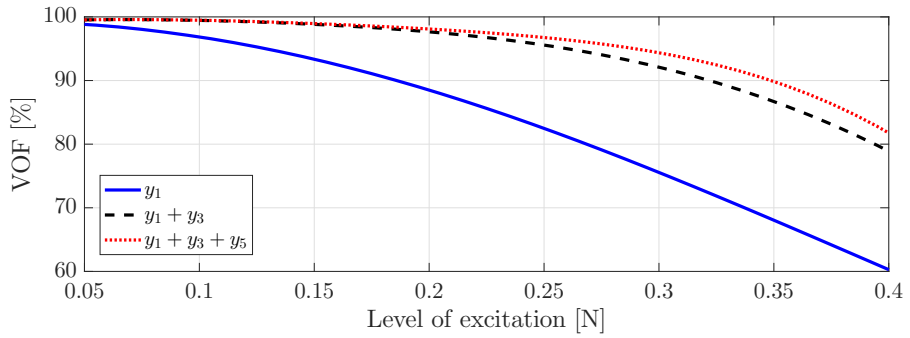

Source: Prepared by the author.

4.3 Multi-degree-of-freedom nonlinear system theory

Figure 27 shows a multi-degree-of-freedom oscillator where the nonlinear component is located at the block of mass m_n.

Figure 27 – Duffing oscillator with MDOF and polynomial nonlinear restoring forces.

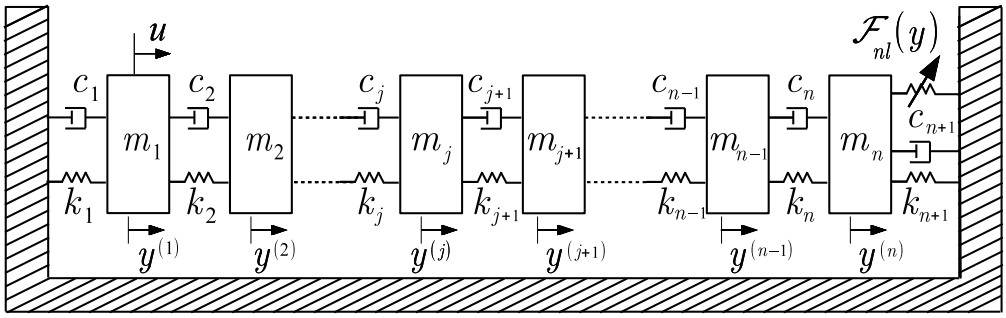

Source: Prepared by the author.

The structural system in Fig. 27 is described by the set of n equations of motion in matrix form as follows:

$$\mathbf{M}\ddot{\mathbf{y}} + \mathbf{C}\dot{\mathbf{y}} + \mathbf{K}\mathbf{y} + \boldsymbol{\mathcal{F}}_{nl}(\mathbf{y}) = \boldsymbol{\mathcal{F}}(\mathbf{u}) \tag{75}$$

where $\mathbf{M}, \mathbf{C}$ and $\mathbf{K}$ are mass, damping and stiffness matrices, respectively, described as:

$$\mathbf{M} = \begin{bmatrix} m_1 & 0 & 0 & \dots & 0 \\ 0 & m_2 & 0 & \dots & 0 \\ 0 & 0 & m_3 & \dots & 0 \\ \vdots & \vdots & \vdots & \ddots & \vdots \\ 0 & 0 & 0 & \dots & m_n \end{bmatrix},$$

$$\mathbf{C} = \begin{bmatrix} c_1 + c_2 & -c_2 & 0 & \dots & 0 \\ -c_2 & c_2 + c_3 & -c_3 & \dots & 0 \\ 0 & \ddots & \ddots & \ddots & 0 \\ \vdots & \ddots & -c_{n-1} & c_{n-1} + c_n & -c_n \\ 0 & \dots & 0 & -c_n & c_n + c_{n+1} \end{bmatrix},$$

and

$$\mathbf{K} = \begin{bmatrix} k_1 + k_2 & -k_2 & 0 & \dots & 0 \\ -k_2 & k_2 + k_3 & -k_3 & \dots & 0 \\ 0 & \ddots & \ddots & \ddots & 0 \\ \vdots & \ddots & -k_{n-1} & k_{n-1} + k_n & -k_n \\ 0 & \dots & 0 & -k_n & k_n + k_{n+1} \end{bmatrix}.$$

The set of vectors $\mathbf{y} = \{y^{(1)}(t)\ y^{(2)}(t)\ \dots\ y^{(n\text{-}1)}(t)\ y^{(n)}(t)\}^T$ contains n outputs of the

system where $\mathbf{y}$, $\dot{\mathbf{y}}$ and $\ddot{\mathbf{y}}$ denote displacement, velocity and acceleration, respectively. In addition, the term $\boldsymbol{\mathcal{F}}(\mathbf{u})$ represents a set of force vectors. In the present paper, it is assumed that an excitation force is applied at the first mass:

$$\boldsymbol{\mathcal{F}}(\mathbf{u}) = \{u(t)\ \underbrace{0\ \ldots\ 0\ 0}_{n-1}\}^T \tag{76}$$

Furthermore, the term $\boldsymbol{\mathcal{F}}_{nl}(\mathbf{y})$ is a set of vectors with the nonlinear components of restoring forces $\boldsymbol{f}_{nl}(\Delta^{(j)}(t))$ given as:

$$\boldsymbol{\mathcal{F}}_{nl}(\mathbf{y}) = \{\underbrace{0\ldots}_{j-2}, \boldsymbol{f}_{nl}(\Delta^{(j)}(t)), \text{-}\boldsymbol{f}_{nl}(\Delta^{(j)}(t)), \underbrace{\ldots 0}_{n-j}\}^T$$

where $\Delta^{(j)}(t) = (y^{(j)}(t) - y^{(j\text{-}1)}(t))$ is the operator of difference between jth and $(j$-1)th masses and is associated with the nonlinear stiffness. Figure 27 shows the particular case where nonlinear restoring force is given as:

$$\boldsymbol{\mathcal{F}}_{nl}(\mathbf{y}) = \{\underbrace{0\ldots}_{n-1}, \boldsymbol{f}_{nl}(\Delta^{(n)}(t))\}^T$$

where the component of restoring force is related to nonlinearities connected at the nth mass. The transformation of physical coordinates to modal coordinates is made up by taking the matrices $\mathbf{K}$ and $\mathbf{M}$ to solve the classical eigenvalue problem:

$$\left(\mathbf{K} - \varpi_n^2 \mathbf{M}\right) \boldsymbol{\phi}^{(n)} = 0 \tag{77}$$

where ϖ_n^2 is the natural frequencies of the nth mode shape of the system and $\boldsymbol{\phi}^{(n)}$ is the respective eigenvector. The eigenvectors are grouped in the matrix $\boldsymbol{\Phi} = [\boldsymbol{\phi}^{(1)}\ \boldsymbol{\phi}^{(2)}\ \ldots\ \boldsymbol{\phi}^{(n)}]$ that is used in the following transformation of coordinates:

$$\mathbf{y} = \boldsymbol{\Phi}\mathbf{q}, \quad \dot{\mathbf{y}} = \boldsymbol{\Phi}\dot{\mathbf{q}} \quad \text{and} \quad \ddot{\mathbf{y}} = \boldsymbol{\Phi}\ddot{\mathbf{q}}.$$

where $\mathbf{q} = \{q^{(1)}(t)\ q^{(2)}(t)\ \ldots\ q^{(n\text{-}1)}(t)\ q^{(n)}(t)\}^T$ is the set of modal coordinates. Thus, the Eq. (75) can be rewritten alternatively in terms of modal coordinates:

$$\mathbf{M}\boldsymbol{\Phi}\ddot{\mathbf{q}} + \mathbf{C}\boldsymbol{\Phi}\dot{\mathbf{q}} + \mathbf{K}\boldsymbol{\Phi}\mathbf{q} + \boldsymbol{\mathcal{F}}_{nl}(\boldsymbol{\Phi}\mathbf{q}) = \boldsymbol{\mathcal{F}}(\boldsymbol{u}) \tag{78}$$

multiplying by $\boldsymbol{\Phi}^T$ provides:

$$\underbrace{\boldsymbol{\Phi}^T\mathbf{M}\boldsymbol{\Phi}}_{diag(\bar{m}_n)}\ddot{\mathbf{q}} + \underbrace{\boldsymbol{\Phi}^T\mathbf{C}\boldsymbol{\Phi}}_{diag(2\zeta_n\bar{m}_n\varpi_n)}\dot{\mathbf{q}} + \underbrace{\boldsymbol{\Phi}^T\mathbf{K}\boldsymbol{\Phi}}_{diag(\bar{m}_n\varpi_n^2)}\mathbf{q} + \boldsymbol{\Phi}^T\boldsymbol{\mathcal{F}}_{nl}(\boldsymbol{\Phi}\mathbf{q}) = \boldsymbol{\Phi}^T\boldsymbol{\mathcal{F}}(\boldsymbol{u}) \tag{79}$$

that can be rewritten as follows:

$$\ddot{\mathbf{q}} + 2\boldsymbol{Z}\boldsymbol{\Omega}\dot{\mathbf{q}} + \boldsymbol{\Omega}^2\mathbf{q} + \bar{\mathbf{M}}^{-1}\boldsymbol{\Phi}^T\boldsymbol{\mathcal{F}}_{nl}(\boldsymbol{\Phi}\mathbf{q}) = \bar{\mathbf{M}}^{-1}\boldsymbol{\Phi}^T\boldsymbol{\mathcal{F}}(\boldsymbol{u}) \tag{80}$$

where $\boldsymbol{Z} = diag(\zeta_n)$ is the damping factor matrix and $\boldsymbol{\Omega} = diag(\varpi_n)$ is the spectral matrix and $\bar{\mathbf{M}} = diag(\bar{m}_n)$ is the matrix of modal mass. Equation (80) can be rewritten as:

$$\ddot{\mathbf{q}} + 2\boldsymbol{Z}\boldsymbol{\Omega}\dot{\mathbf{q}} + \boldsymbol{\Omega}^2\mathbf{q} = \bar{\boldsymbol{\mathcal{F}}}(\boldsymbol{u}) - \bar{\boldsymbol{\mathcal{F}}}_{nl}(\boldsymbol{\Phi}\mathbf{q}) \tag{81}$$

where $\bar{\boldsymbol{\mathcal{F}}}(\boldsymbol{u}) = \bar{\mathbf{M}}^{-1}\boldsymbol{\Phi}^T\boldsymbol{\mathcal{F}}(\boldsymbol{u})$ and $\bar{\boldsymbol{\mathcal{F}}}_{nl}(\boldsymbol{\Phi}\mathbf{q}) = \bar{\mathbf{M}}^{-1}\boldsymbol{\Phi}^T\boldsymbol{\mathcal{F}}_{nl}(\boldsymbol{\Phi}\mathbf{q})$. Basically, the external modal force $\bar{\boldsymbol{\mathcal{F}}}(\boldsymbol{u})$ act together with the internal nonlinear feedback modal forces $\bar{\boldsymbol{\mathcal{F}}}_{nl}(\boldsymbol{\Phi}\mathbf{q})$ on the underlying linear system generating the set of modal responses $\mathbf{q}$ (WORDEN et al., 2009).

Without loss of generality, it is assumed the simple case, $n = 1, 2$ masses, described by the physical parameters $m = m_1 = m_2$, $c = c_1 = c_2$ and $k = k_1 = k_2$. Additionally, the modal parameters related to the linear part of Eq. (80) are calculated from the problem in (i) and from the proportional damping relationship (ii) as follows:

$$(i)\ \det\left[\mathbf{K} - \varpi_n^2\mathbf{M}\right] = \det\begin{bmatrix} 2k - \varpi_n^2 m & -k \\ -k & 2k - \varpi_n^2 m \end{bmatrix} = 0$$

$$\Leftrightarrow (2k - \varpi_n^2 m)^2 - k^2 = 0 \Leftrightarrow \pm 2k - \varpi_n^2 m = \pm k^2 \Longrightarrow \varpi_1 = \sqrt{\frac{k}{m}} \text{ and } \varpi_2 = \sqrt{\frac{3k}{m}}.$$

$$(ii)\ \mathbf{C} = \alpha_M\mathbf{M} + \alpha_K\mathbf{K} \Longrightarrow \zeta_1 = \frac{\alpha_M}{2\varpi_1} + \frac{\alpha_K\varpi_1}{2} \text{ and } \zeta_2 = \frac{\alpha_M}{2\varpi_2} + \frac{\alpha_K\varpi_2}{2}.$$

Thus, the modal parameters are given as:

$$\varpi_1 = \sqrt{\frac{k}{m}},\ \zeta_1 = \frac{c}{2m\varpi_1},\ \varpi_2 = \sqrt{\frac{3k}{m}} \ \text{ and } \ \zeta_2 = \frac{3c}{2m\varpi_2}.$$

Since the values of ϖ_n are known, is possible then to calculate the matrix of eigenvectors by solving the eigenvalue value problem through Eq. (77):

$$\boldsymbol{\Phi} = \begin{bmatrix} \boldsymbol{\phi}^{(1)} & \boldsymbol{\phi}^{(2)} \end{bmatrix} = \begin{bmatrix} \frac{1}{\sqrt{2}} & \frac{1}{\sqrt{2}} \\ \frac{1}{\sqrt{2}} & -\frac{1}{\sqrt{2}} \end{bmatrix} \tag{82}$$

The transformation of coordinates $\mathbf{y} = \boldsymbol{\Phi}\mathbf{q}$ leads to

$$\begin{Bmatrix} y^{(1)}(t) \\ y^{(2)}(t) \end{Bmatrix} = \frac{1}{\sqrt{2}} \begin{Bmatrix} q^{(1)}(t) + q^{(2)}(t) \\ q^{(1)}(t) - q^{(2)}(t) \end{Bmatrix} \tag{83}$$

allowing to rewrite the linear part of Eq. (75) as:

$$\begin{aligned}\ddot{q}^{(1)}(t) + 2\zeta_1\varpi_1\dot{q}^{(1)}(t) + \varpi_1^2 q^{(1)}(t) &= \frac{1}{m\sqrt{2}}u^{(1)}(t)\\ \ddot{q}^{(2)}(t) + 2\zeta_2\varpi_2\dot{q}^{(2)}(t) + \varpi_2^2 q^{(2)}(t) &= \frac{1}{m\sqrt{2}}u^{(1)}(t)\end{aligned} \tag{84}$$

It is worthing to emphasize that Eq. (84) is composed by the modal coordinates, a compact version of the equations of motion in Eq. (75). This alternative way represents the dynamic characteristics, known as the modal model. It describes the modal properties (natural frequencies, damping ratios and mode shapes) as opposed way to the spatial model (physical parameters) described by its spatial properties (masses, viscous dampings, stiffnesses). Furthermore, it can be noted in Eq. (84) that the modes are sufficiently expressed in an uncoupled way in order to be estimated independently (MAIA; SILVA, 1997; EWINS, 2000).

Now, by assuming a single-tone harmonic input, $u^{(1)}(t) = \frac{A}{m\sqrt{2}}e^{j\omega t}$, the outputs of the modal model in Eq. (84) can be rewritten as a function of the modal FRFs as follows:

$$q^{(1)}(t) = \frac{A}{m\sqrt{2}}\mathcal{Q}_1^{(1)}(\omega)e^{j\omega t},\ q^{(2)}(t) = \frac{A}{m\sqrt{2}}\mathcal{Q}_1^{(2)}(\omega)e^{j\omega t} \tag{85}$$

Hence, by differentiating $q^{(1)}(t)$ and $q^{(2)}(t)$ for the velocity and the acceleration yields:

$$\dot{q}^{(1)}(t) = \frac{j\omega A}{m\sqrt{2}}\mathcal{Q}_1^{(1)}(\omega)e^{j\omega t},\ \dot{q}^{(2)}(t) = \frac{j\omega A}{m\sqrt{2}}\mathcal{Q}_1^{(2)}(\omega)e^{j\omega t},$$

$$\ddot{q}^{(1)}(t) = -\frac{\omega^2 A}{m\sqrt{2}}\mathcal{Q}_1^{(1)}(\omega)e^{j\omega t},\ \ddot{q}^{(2)}(t) = -\frac{\omega^2 A}{m\sqrt{2}}\mathcal{Q}_1^{(2)}(\omega)e^{j\omega t},$$

Substituting the modal responses $q^{(1)}(t)$, $\dot{q}^{(1)}(t)$ and $\ddot{q}^{(1)}(t)$ into the first equation in (84) generates:

$$-\frac{\omega^2 A}{m\sqrt{2}}\mathcal{Q}_1^{(1)}(\omega)e^{j\omega t} + 2\zeta_1\varpi_1\frac{j\omega A}{m\sqrt{2}}\mathcal{Q}_1^{(1)}(\omega)e^{j\omega t} + \varpi_1^2\frac{A}{m\sqrt{2}}\mathcal{Q}_1^{(1)}(\omega)e^{j\omega t} = \frac{Ae^{j\omega t}}{m\sqrt{2}},$$

that yields the analytical expression of the first modal FRF:

$$\mathcal{Q}_1^{(1)}(\omega) = \frac{1}{\varpi_1^2 - \omega^2 + 2\zeta_1\varpi_1 j\omega} \tag{86}$$

The same procedure can be used with the modal responses $q^{(2)}(t)$, $\dot{q}^{(2)}(t)$ and $\ddot{q}^{(2)}(t)$ in order to provide the expression of the second modal FRF:

$$\mathcal{Q}_1^{(2)}(\omega) = \frac{1}{\varpi_2^2 - \omega^2 + 2\zeta_2\varpi_2 j\omega} \tag{87}$$

The transformation of coordinates:

$$\begin{Bmatrix} y^{(1)}(t) \\ y^{(2)}(t) \end{Bmatrix} = \begin{bmatrix} \frac{1}{\sqrt{2}} & \frac{1}{\sqrt{2}} \\ \frac{1}{\sqrt{2}} & -\frac{1}{\sqrt{2}} \end{bmatrix} \begin{Bmatrix} q^{(1)}(t) \\ q^{(2)}(t) \end{Bmatrix}$$

leads to

$$\begin{Bmatrix} y^{(1)}(t) \\ y^{(2)}(t) \end{Bmatrix} = \begin{Bmatrix} \frac{1}{\sqrt{2}} \\ \frac{1}{\sqrt{2}} \end{Bmatrix} \frac{A}{m\sqrt{2}} \mathcal{Q}_1^{(1)}(\omega) e^{j\omega t} + \begin{Bmatrix} \frac{1}{\sqrt{2}} \\ -\frac{1}{\sqrt{2}} \end{Bmatrix} \frac{A}{m\sqrt{2}} \mathcal{Q}_1^{(2)}(\omega) e^{j\omega t} \tag{88}$$

Equation (88) shows an alternative way to predict the outputs $y^{(1)}(t)$ and $y^{(2)}(t)$, known as modal coordinates or natural coordinates. It means that the outputs can be calculated in terms of the mode shape vectors $\boldsymbol{\phi}^{(1)}$ and $\boldsymbol{\phi}^{(2)}$ and the modal parameters ϖ_i and ζ_i with $i = 1, 2$. Furthermore, note that Eq. (88) can be rewritten in a more compact way as follows:

$$\begin{Bmatrix} y^{(1)}(t) \\ y^{(2)}(t) \end{Bmatrix} = \begin{bmatrix} \frac{1}{\sqrt{2}} & \frac{1}{\sqrt{2}} \\ \frac{1}{\sqrt{2}} & -\frac{1}{\sqrt{2}} \end{bmatrix} \begin{Bmatrix} \frac{A}{m\sqrt{2}} e^{j\omega t} \mathcal{Q}_1^{(1)}(\omega) \\ \frac{A}{m\sqrt{2}} e^{j\omega t} \mathcal{Q}_1^{(2)}(\omega) \end{Bmatrix} \tag{89}$$

On the other hand, the vector of outputs can be calculated by the conventional FRFs, spatial model, as follows:

$$\begin{Bmatrix} y^{(1)}(t) \\ y^{(2)}(t) \end{Bmatrix} = \begin{Bmatrix} A e^{j\omega t} \mathcal{H}_1^{(1)}(\omega) \\ A^3 e^{j3\omega t} \mathcal{H}_1^{(2)}(\omega) \end{Bmatrix} \tag{90}$$

Now, from the Eqs. (89) and (90) it is possible to express the modal FRFs $\mathcal{Q}_1^{(i)}(\omega)$ in therms of the spatial FRFs $\mathcal{H}_1^{(i)}(\omega)$ with $i = 1, 2$, and vice-versa, as follows:

$$\begin{bmatrix} \frac{1}{\sqrt{2}} & \frac{1}{\sqrt{2}} \\ \frac{1}{\sqrt{2}} & -\frac{1}{\sqrt{2}} \end{bmatrix} \begin{Bmatrix} \frac{A}{m\sqrt{2}} e^{j\omega t} \mathcal{Q}_1^{(1)}(\omega) \\ \frac{A}{m\sqrt{2}} e^{j\omega t} \mathcal{Q}_1^{(2)}(\omega) \end{Bmatrix} = \begin{Bmatrix} A e^{j\omega t} \mathcal{H}_1^{(1)}(\omega) \\ A^3 e^{j3\omega t} \mathcal{H}_1^{(2)}(\omega) \end{Bmatrix}$$

Thus, the spatial FRFs can be alternatively rewritten as a combination of the modal FRFs:

$$\mathcal{H}_1^{(1)}(\omega) = \frac{\frac{1}{2m}}{\varpi_1^2 - \omega^2 + 2\zeta_1 \varpi_1 j\omega} + \frac{\frac{1}{2m}}{\varpi_2^2 - \omega^2 + 2\zeta_2 \varpi_2 j\omega} \tag{91}$$

$$\mathcal{H}_1^{(2)}(\omega) = \frac{\frac{1}{2m}}{\varpi_1^2 - \omega^2 + 2\zeta_1 \varpi_1 j\omega} - \frac{\frac{1}{2m}}{\varpi_2^2 - \omega^2 + 2\zeta_2 \varpi_2 j\omega} \tag{92}$$

It is important to note that Eqs. (91) and (92) can be rewritten in a more general

way for systems with N mode shapes as:

$$\mathcal{H}_1^{(n)}(\omega) = \frac{U(\omega)}{Y^{(n)}(\omega)} = \sum_{r=1}^{N}\left(\frac{\phi_{1r}\phi_{nr}}{j\omega - s_r} + \frac{\phi_{1r}^{*}\phi_{nr}^{*}}{j\omega - s_r^{*}}\right) \tag{93}$$

where $s_r = -\varpi_r\zeta_r + j\varpi_r\sqrt{1-\zeta_r^2}$ is the modal complex parameter with $r = 1,\ldots,N$ mode shapes and the symbol $*$ denotes the complex conjugated. The FRFs of second and third order can be computed consequently computed as:

$$\mathcal{H}_2^{(n)}(\omega,\omega) = -\alpha[\mathcal{H}_1^{(n)}(\omega)]^2\mathcal{H}_1^{(n)}(2\omega) \tag{94}$$

and

$$\mathcal{H}_3^{(n)}(\omega,\omega,\omega) = [\mathcal{H}_1^{(n)}(\omega)]^3\mathcal{H}_1^{(n)}(3\omega)\Big[2\alpha^2\mathcal{H}_1^{(n)}(2\omega) - \beta\Big] \tag{95}$$

The FRFs $\mathcal{H}_1^{(1)}(\omega)$ and $\mathcal{H}_1^{(2)}(\omega)$ describe the linear part of the nonlinear oscillator in Eq. (75) when $n = 1, 2$. Additionally, the HOFRFs $\mathcal{H}_2^{(n)}(\omega,\omega)$ and $\mathcal{H}_3^{(n)}(\omega,\omega,\omega)$ describe the nonlinear part of the model characterized by quadratic and cubic stiffnesses, respectively. In the Appendix A, is showed the algebraic expressions and the respective location nonlinearities by considering a 2DOF Duffing oscillator with eighteen cases.

Without loss of generality, consider the nonlinear system investigated in chapter 2 with physical parameters showed in Tab. 1. In such case, the analytical modal parameters are given as $\varpi_1 = 11.0 \times 2\pi$ rad/s and $\varpi_2 = 68.5 \times 2\pi$ rad/s as resonance frequencies, and $\zeta_1 = 0.41\%$ and $\zeta_2 = 0.79\%$ as damping ratios. It is worthing to note that the simulation is performed under the same conditions as stated in chapter 2. The main goal here is to use this nonlinear oscillator to apply the methodology based on modal space in order to reach the same results as the nonlinear model in spatial space as showed in chapter 2.

Initially, a random input with Gaussian distribution and amplitude level of 0.15 N over the frequency range of (0-120) Hz is applied at the first block as illustrated in system described by Eq. (15) and depicted in Fig. 1. The respective displacements are obtained by numerical integration (Newmark method with Newton-Raphson procedure) with sampling frequency of 500 Hz, time duration of 10 seconds and 5001 samples collected. Those dataset are used to compute the first order FRFs, showed in Fig. 28, via $\mathscr{H}1$ estimator through Welch periodogram and boxcar window, 10 averages and 50% of overlap.

The modal properties are extracted by using a conventional curve-fit procedure from experimental modal analysis method (MAIA; SILVA, 1997; EWINS, 2000). In such case, the modal parameters estimated are given as $\varpi_1 = 10.91 \times 2\pi$ rad/s and $\varpi_2 = 68.16 \times 2\pi$

rad/s as resonance frequencies, and $\zeta_1 = 0.34\%$ and $\zeta_2 = 0.82\%$ as damping ratios. The respective modal vectors estimated are grouped in the matrix mode shape vector as follows:

$$\mathbf{\Phi} = \begin{bmatrix} 0.5148 & 0.0195 \\ 0.5444 & -0.0189 \end{bmatrix} \tag{96}$$

An statistical indicator known as modal assurance criterion (MAC) is used to verify the consistency of the modal vectors estimated. Basically, it measures through a correlation coefficient the degree of proportion/consistency between one modal vector and another modal vector (ALLEMANG, 2003). Basically, this scalar constant is calculated by:

$$\text{MAC}(\phi_r, \phi_s) = \frac{|\phi_r^* \phi_s|}{(\phi_r^* \phi_r)(\phi_s^* \phi_s)} \tag{97}$$

where ψ_r, ψ_s are the modal vectors of $\mathbf{\Phi}$. Figure 29 shows the 3D bar plot of MAC values calculated through the modal vectors (eigenvectors) matrix from Eq. (96).

The restoring force method is used to identify the polynomial structure of fitting associated to the functional of nonlinear restoring forces $\mathcal{F}_{nl}(\mathbf{y})$:

$$\mathcal{F}_{nl}(\mathbf{y}) = \left\{ \alpha_1 [y^{(1)}(t)]^2 + \beta_1 [y^{(1)}(t)]^3 \quad \alpha_2 [y^{(2)}(t)]^2 + \beta_2 [y^{(2)}(t)]^3 \right\}^T.$$

where the nonlinear parameter identified are $\alpha_1 = 7.934{\times}10^4$, $\beta_1 = 8.60{\times}10^8$, $\alpha_2 = 7.931{\times}10^4$ and $\beta_2 = 8.11 \times 10^8$. Figure 30 shows the restoring force curves computed based on the polynomial curve fitting procedure applied in the restoring forces as follows (MASRI; CAUGHEY, 1979):

$$\mathcal{F}_{re}(y^{(1)}(t)) = u(t) - m_1 \ddot{y}^{(1)}(t) \tag{98}$$

$$\mathcal{F}_{re}(y^{(2)}(t)) = u(t) - m_2 \ddot{y}^{(2)}(t) \tag{99}$$

where $m_1 = m_2 = 1$ kg as showed in Tab. 1 of chapter 2. The restoring force curves are showed in Fig. 30 based on input harmonic signal $u(t)$ with $A = 0.15$ N low level of excitation, Fig. 30(a), and $A = 1.59$ N as high level of excitation, Fig. 30(b), with excitation frequency close to the first resonance 11 Hz.

The modal parameters estimated by the conventional experimental modal analysis technique and the coefficients α_n, β_n estimated through polynomial curve fitting procedure (RFS method) are used to compute the respective HOFRFs through the analytical

expressions in Eqs. (93), (94) and (95). Figure 31 shows the comparison of the HOFRFs computed by the exact (by assuming the knowledge of equations of motion) and identified parameters. Although, the values of real and estimated parameters are slightly different, it is possible to see a good agreement between the curves pointing out the efficiency of the methodology proposed.

The methodology to compute the HOFRFs based on input and output dataset collected is then summarized in Fig. 32. As illustrated in the flowchart, the technique is basically divided in two steps by considering inputs with low and higher level of amplitude excitation.

Firstly, the input signal with low level of amplitude excitation and the respective outputs data are used and a conventional experimental modal analysis method, such as line-fit, circle-fit and many others (EWINS, 2000; MAIA et al., 2001), can be used to extract the modal parameters ϖ_n and ζ_n and the matrix of eigenvectors $\mathbf{\Phi}$ (mode shapes). After that, the first order FRFs are computed as showed in Eq. (93).

Secondly, the dataset with higher level of amplitude is used to estimate the nonlinear parameters via a simple curve fitting of the nonlinear restoring force surface (RFS). The nonlinear parameters related to the nature of RFS and the respective first order FRFs estimated in step 1 are used to compute the higher-order FRFs to compose the nonlinear model. After that, the nonlinear model is evaluated and validated. Next section presents another application based on vibration data of an experimental system composed by a nonlinear beam.

Figure 28 – Magnitude and imaginary components of frequency response functions calculated by $\mathscr{H}1$ spectral estimator based on acceleration signals measured at low forcing level (0.15 N) over the frequency range 0-120 Hz with resonance frequencies close to 11.0 and 68.5 Hz and damping factors 0.41 % and 0.79%.

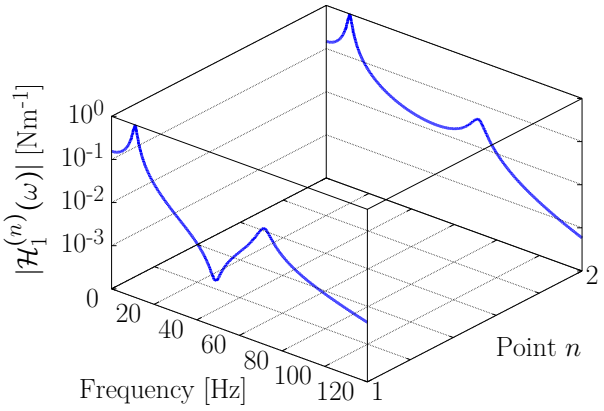

(a) Magnitude of $\mathcal{H}_1^{(n)}(\omega)$.

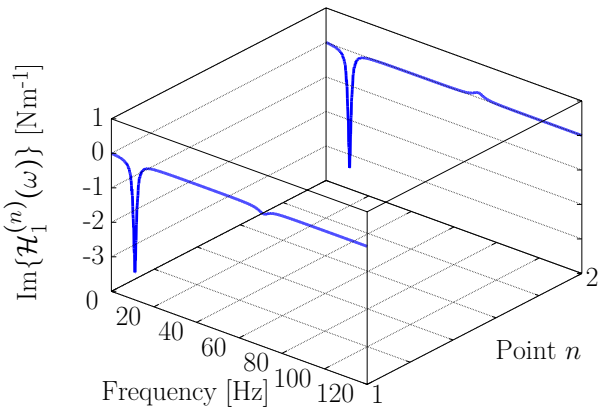

(b) Imaginary part of $\mathcal{H}_1^{(n)}(\omega)$.

Source: Prepared by the author.

Figure 29 – Modal assurance criterion (MAC) values.

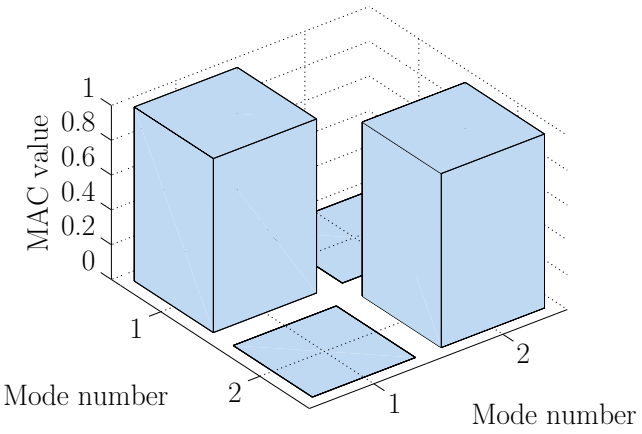

Source: Prepared by the author.

Figure 30 – Restoring force curves estimated via input and output (first mass), red squares □, compared to the one reconstructed through polynomial curve fitting based on $\mathcal{F}_{re}(y^{(1)}(t))$, continuous line -.

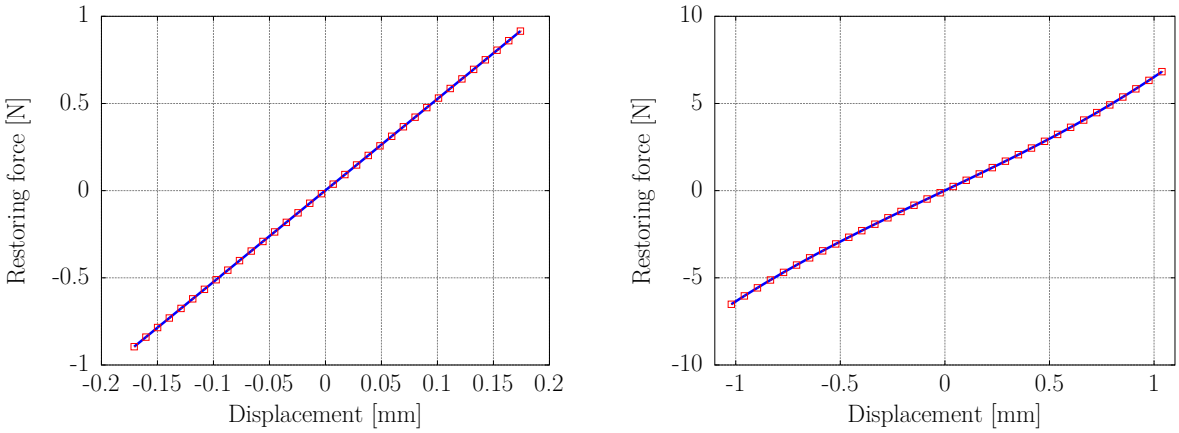

(a) Low level of amplitude.

(b) Higher level of amplitude.

Source: Prepared by the author.

Figure 31 – HOFRFs computed via modal parameters and nonlinear coefficients, exact values (-) compared to the identified ones (--△--).

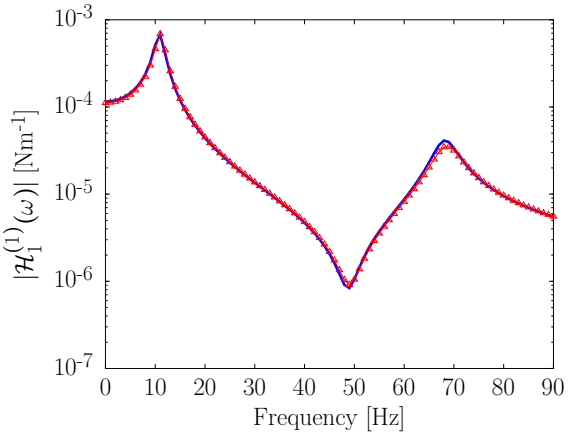

(a) First order FRF.

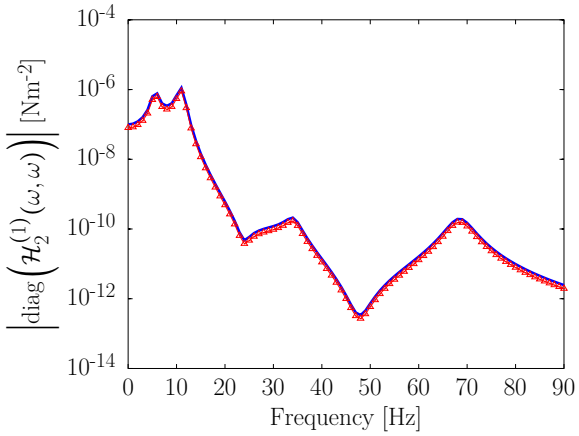

(b) Second order FRF (main diagonal).

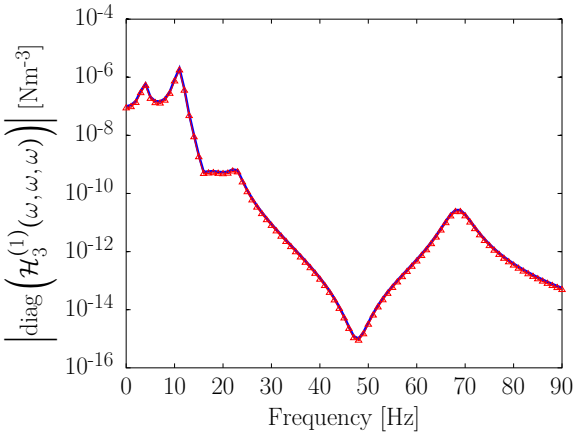

(c) Third order FRF (main diagonal).

Source: Prepared by the author.

Figure 32 – Overall of the technique based on HOFRFs with parameters obtained through conventional experimental modal analysis and line-fit procedure.

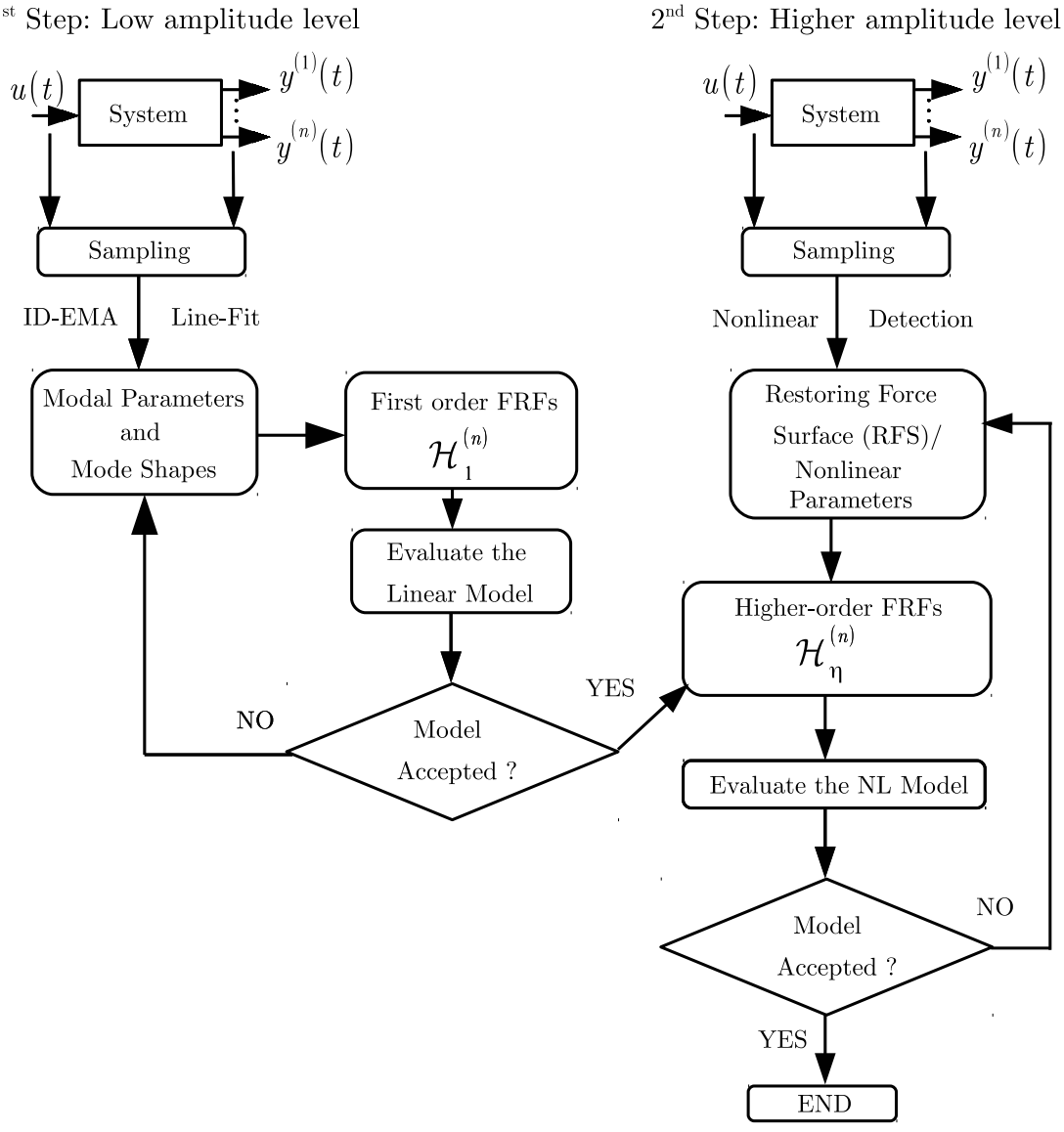

Source: Prepared by the author.

4.4 Application in a benchmark with nonlinear features

The method presented in the previous section is used here to analyse the nonlinear behavior of an experimental system, investigated by Shiki et al. (2017), composed by a cantilever aluminum beam and a neodymium magnet positioned closed to the steel mass attached to the free end of the beam as can be seen in Fig. 33. The nonlinear behavior arises from interaction between the permanent magnet and the small mass as depicted in Fig. 33(a). The test rig is composed by a cantilever aluminum beam with dimensions of 300 × 19 × 3.2 mm with a small steel mass attached to the free end and a neodymium magnet with a gap of 2 mm from the mass as can be seen through the sketch of the test rig in Fig. 33(b). A shaker, Modal Shop Shaker K2004E01, is connected 50 mm away from the clamped end instrumented with a load cell, Dytran load cell model 1022V - IEPE force sensor. One laser vibrometer, Polytec OFV-525/-5000-S modular laser vibrometer, is used to measure the velocity at the free end of the beam and three PCB accelerometers are used to collect the respective acceleration signals through m+p VibPilot data acquisition system.

Figure 33 – Experimental setup and the schematic representation illustrating the magneto-elastic nonlinear system.

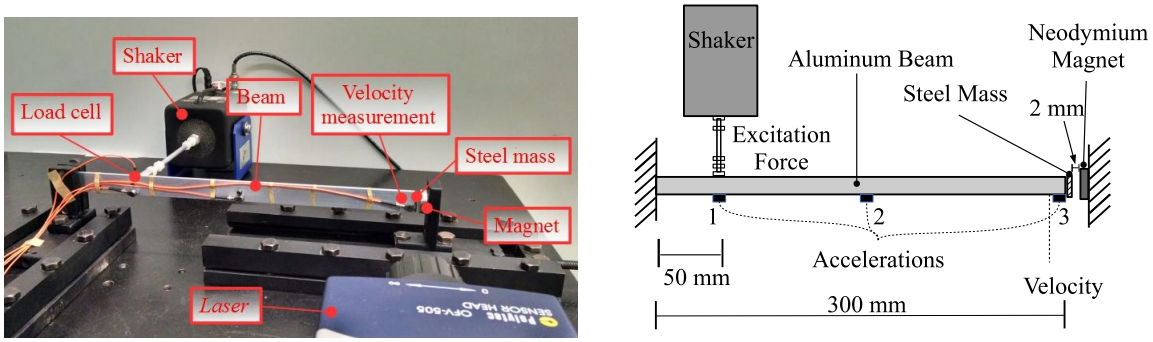

(a) Experimental setup investigated by Shiki et al. (2017).

(b) Sketch of the test rig (view from the top).

Source: Prepared by the author.

A random input with Gaussian distribution and amplitude level of 0.01 V applied in the shaker (linear regime of motion) across the frequency range of interest (from 10 to 400 Hz) is applied at point 1 in the beam and the respective accelerations are measured at the points 1, 2 and 3 by using 1024 Hz as sampling frequency, 4096 samples and total time duration of 4 s. The random input signal $u(t)$ and the respective outputs, accelerations $y^{(1)}(t)$, $y^{(2)}(t)$ and $y^{(3)}(t)$, are used to compute the linear FRFs based on

$\mathscr{H}1$ spectral estimator. In order to attend this purpose, a Welch periodogram with boxcar (rectangular) window, 10 averages and 50% of overlap is used. Figure 34(a) shows the magnitude of the FRFs $\mathcal{H}_1^{(P)}(\omega)$ with $P = 1, 2, 3$ outputs measured by the accelerometers. Figure 34(b) shows the waterfall plot of the imaginary components of each FRF denoted by $\mathrm{Im}\{\mathcal{H}_1^{(P)}(\omega)\}$.

Figure 34 – Magnitude and imaginary components of frequency response functions calculated by $\mathcal{H}1$ spectral estimator based on acceleration signals measured at low amplitude level (0.01 V) over the frequency range 10-400 Hz with resonance frequencies close to 23.3, 132.0 and 291.4 Hz.

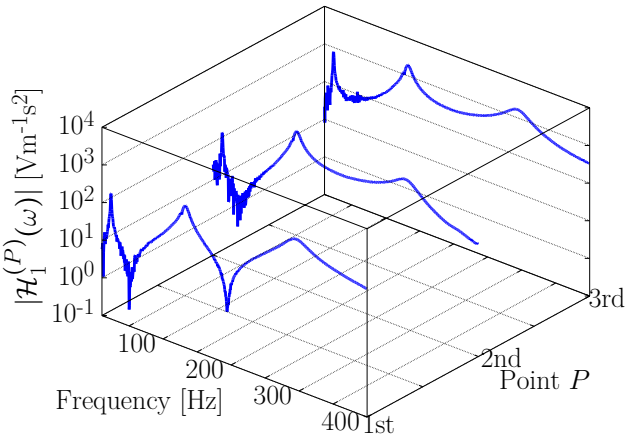

(a) Magnitude of $\mathcal{H}_1^{(P)}(\omega)$.

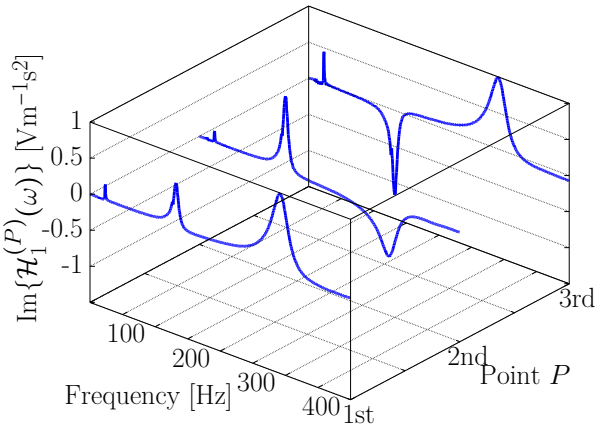

(b) Imaginary part of $\mathcal{H}_1^{(P)}(\omega)$.

Source: Prepared by the author.

Additionally, the modal properties are extracted by using a conventional curve-fit procedure from experimental modal analysis method. In such case, the system presents resonance frequencies close to $\varpi_1 = 23.3$, $\varpi_2 = 132.0$ and $\varpi_3 = 291.4$ Hz and the damping factors estimated are close to $\zeta_1 = 1.60$ %, $\zeta_2 = 2.80$ % and $\zeta_3 = 5.25$ % and the respective

modal vectors are grouped in the matrix mode shape vector $\mathbf{\Phi}$. Figure 35 shows the 3D plot modal assurance criterion (MAC) based on modal vectors values extracted by a conventional curve-fit procedure using dataset when the magneto-elastic system operates in linear regime of motion.

$$\mathbf{\Phi} = \begin{bmatrix} 0.05 - j0,02 & -0.03 - j0.01 & -0.01 - j0.01 \\ -0.10 + j0.15 & -0.53 - j0.68 & -1.12 - j0.29 \\ -2.31 + j2.10 & -1.15 - j0.29 & -2.49 - j1.16 \end{bmatrix} \tag{100}$$

It is important to emphasize that this geometric representation of each mode shape

Figure 35 – Modal assurance criterion (MAC) values based on modal vectors.

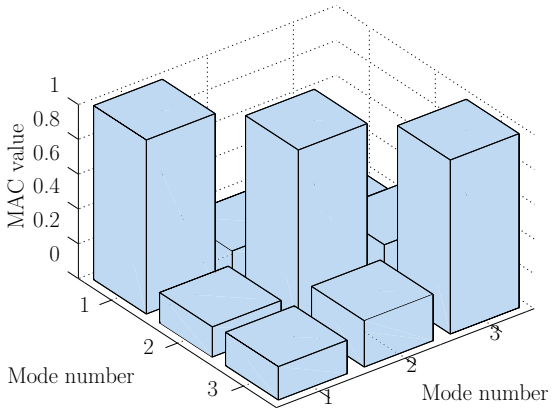

Source: Prepared by the author.

can be improved by adding more input-output location to measure (AVITABILE, 2001). Nevertheless, the linear FRFs estimated are to compute the second and third order FRFs when the system operates in nonlinear regime of motion. Initially, the detection and characterization of the nonlinear behavior is done. Afterwards, the results obtained by the HOFRFs computed through the multidimensional Fourier transform of the Volterra kernels estimated via orthonormal Kautz basis functions are analysed and compared with the proposed analytical model. This model is used to predict the outputs when the system is subject to chirp (swept-sine) and random input signals under low and high amplitude levels applied in the shaker.

Now, the FRFs of first order estimated before are used to compute the higher-order frequency response functions (HOFRFs) in order to characterize and predict the dynamical behavior of the magneto-elastic beam operating in nonlinear regime (higher amplitude

levels). In this test rig, the nonlinear effects arise when large displacements are induced in the system and it is because the magnetic interactions between the neodymium magnet and the steel mass attached at the free end of the beam. More details about the experimental setup and nonlinear characterization can be found in Shiki et al. (2017). A stepped-sine up test is performed with two different amplitude levels, $A = 0.01$ V (low) and $A = 0.15$ V (higher).

The test is performed based on the velocity measured at point 3 subjected to the input $u(t) = A\sin(\omega t)$ with excitation frequency ω over the frequency range from 10 up to 400 Hz with steps of 0.5 Hz and 4 s for each block to reach the steady-state response.

The results of the frequency response curve of the experimental setup to a stepped sine input are showed in Fig. 36. In Figure 36(b) is possible to observe a hardening effect (jump-down phenomenon) with frequency values around the first mode of vibration. It can be seen that the first resonance peak moves to the right with a sudden drop in the response amplitude as far as the frequency of excitation is increased.

Figure 36 – Nonlinearity detection through frequency response function of the stepped sine testing. The test is performed based on the velocity measured at point 3 subjected to the input $u(t) = A\sin(\omega t)$ with excitation frequency ω from 10 up to 400 Hz (steps of 0.5 Hz) in two different input amplitude levels, low $A = 0.01$ V (-) and higher $A = 0.15$ V (--▲--).

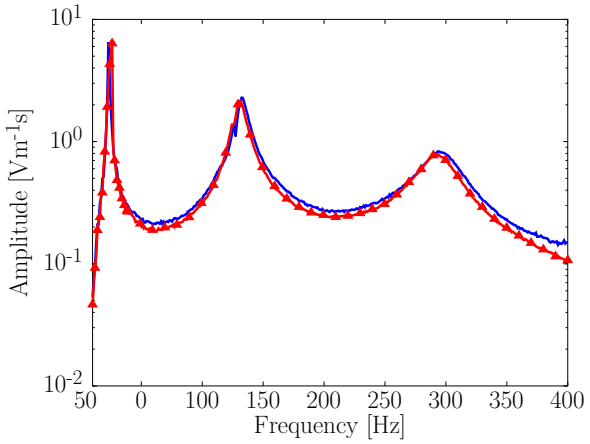

(a) Stepped-up test based on the velocity $\dot{y}^{(3)}(t)$.

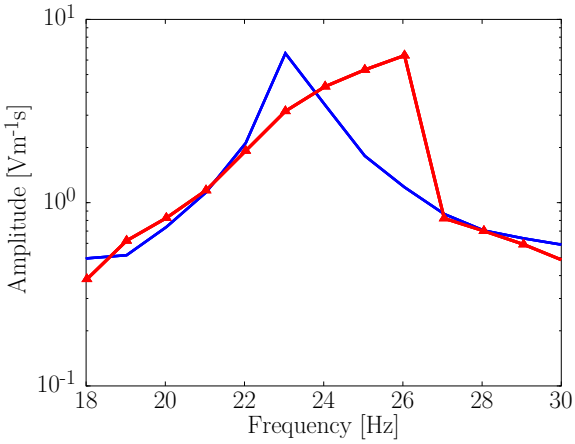

(b) Zoom at the first resonance frequency range (jump phenomenon).

Source: Prepared by the author.

The results based on controlled stepped-sine up show clearly that the structure presents nonlinear regime of motion associated with hardening stiffness. Moreover, the experimental results have shown that the nonlinearity location is close to the magnet's position. Another important issue is the fact that the nonlinear effect acts more significantly on

the first mode frequency range than the second and third ones. Thus, it is considered the responses over a frequency range around the first vibration mode and the respective second and third resonance frequencies can be neglected due to their less significant contribution. Consequently, a single mode can be enough to predict the nonlinear regime of motion.

In order to represent the behaviour of the magneto-elastic beam around the first resonance frequency, the coefficients $\alpha = -2.31 \times 10^4$ Nm^{-2} and $\beta = 2.91 \times 10^7$ Nm^{-3} are estimated parametrically based on a simple fit to reconstruct the restoring force $\mathcal{F}_{re}(y^{(3)}(t))$ depicted in Fig. 37. Basically, the restoring force is defined as:

$$\mathcal{F}_{re}(y^{(3)}(t)) = u(t) - 0.21\ddot{y}^{(3)}(t) \tag{101}$$

in which the polynomial to reconstruct the restoring force is calculated through $\mathcal{F}_{nl}(y^{(3)}(t)) = \alpha[y^{(3)}(t)]^2 + \beta[y^{(3)}(t)]^3$. As shown in Fig. 37(a), the restoring force presents linear behavior for dataset for low level of amplitude (0.01 V) applied in the shaker. On the other hand, it is possible to see in Fig. 37(b) that for higher level of excitation amplitude, the magneto-elastic beam presents nonlinear behavior.

Figure 37 – Restoring force surface (RFS) based on experimental dataset, cloud of green dots ($*$), and RFS reconstructed through an adjusting polynomial curve fit, blue continuous line ($--$).

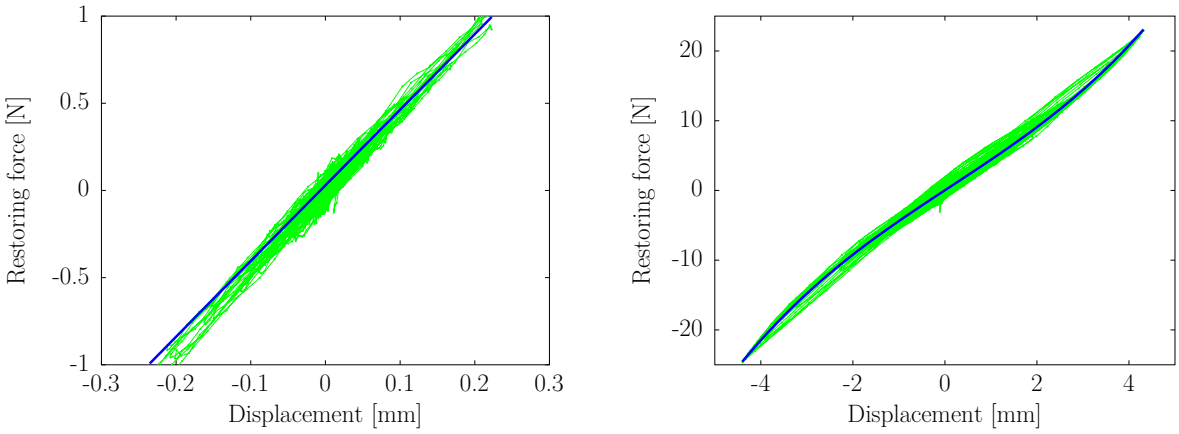

(a) Low level of amplitude (0.01 V).

(b) Higher level of amplitude (0.15 V).

Source: Prepared by the author.

The coefficients α and β estimated are used to compute the respective HOFRFs through the analytical expressions in Eqs. (93), (94) and (95).

As reviewed in Chapter 3, the extraction of the Volterra kernels can be performed directly in the discrete-time domain. In such case, the n-th output in Eq. (11) can be

rewritten in terms of discrete-time Volterra series expansion:

$$y^{(n)}(k) = \sum_{\eta=1}^{\infty} \sum_{n_1=1}^{N_1} \sum_{n_2=1}^{N_2} \dots \sum_{n_\eta=1}^{N_\eta} h_\eta^{(n)}(n_1, n_2 \dots, n_\eta) \prod_{i=1}^{\eta} u(k-n_i) = y_1^{(n)}(k) + y_2^{(n)}(k) + y_3^{(n)}(k) + \dots \tag{102}$$

where $h_\eta^{(n)}(n_1, n_2 \dots, n_\eta)$ are Volterra kernels related to the nth output. Unfortunately, the large number of parameters $N_1, N_2, \dots, N_\eta$ implies in excessive computational requirements and overparametrization effects to identify these kernels (DA SILVA et al., 2010; SHIKI et al., 2014a; SCUSSEL; da Silva, 2017). In order to overcome these drawbacks, an orthonormal expansion is used and the kernels are computed as follows:

$$h_\eta^{(n)}(n_1, n_2, \dots, n_\eta) \approx \sum_{i_1=1}^{J_1} \sum_{i_2=1}^{J_2} \dots \sum_{i_\eta=1}^{J_\eta} \mathscr{B}_\eta^{(n)}(i_1, i_2, \dots, i_\eta) \prod_{j=1}^{\eta} \psi_{i_j}(n_j; z_r) \tag{103}$$

where $\mathscr{B}_\eta^{(n)}(i_1, i_2, \dots, i_\eta)$ are the coefficients of the orthonormal basis expansion of the transfer functions corresponding to the nth output and $\psi_{i_\eta}(n_\eta; z_r)$ are the Kautz filters. It is adopted the Kautz filters basis due to its ability in representing properly the oscillatory behaviour of vibrating systems (KAUTZ, 1954; SCUSSEL; da Silva, 2015). Furthermore, the Kautz filters depend on the modal parameters that can be related to the modal complex parameter s_r pointing out another benefit of this method for structural dynamic problems. Nevertheless, is it necessary to apply a discretization method on the continuous-time Volterra series representation. In order to attend this purpose, Tustin method (or bilinear approximation) is used to convert from s-domain to z-domain as the following approximation:

$$z = e^{s\Delta t} \approx \left. \frac{1 + \frac{s\Delta t}{2}}{1 - \frac{s\Delta t}{2}} \right|_{s=j\omega} \tag{104}$$

where Δt denotes the sampling rate. In this context, the discretization of the nth continuous transfer function $\mathcal{H}_1^{(n)}(\omega)$ in the Kautz-filters orthonormal basis is given by:

$$\mathcal{H}_1^{(n)}(\omega) \approx \sum_{i_1=1}^{J_1} \mathscr{B}_1^{(n)}(i_1)\, \psi_{i_1}(n_1; z_r) \tag{105}$$

and

$$\mathcal{H}_2^{(n)}(\omega, \omega) \approx \sum_{i_1=1}^{J_1} \sum_{i_2=1}^{J_2} \mathscr{B}_2^{(n)}(i_1, i_2)\, \psi_{i_1}(n_1; z_r) \psi_{i_2}(n_2; z_r) \tag{106}$$

$$\mathcal{H}_3^{(n)}(\omega, \omega, \omega) \approx \sum_{i_1=1}^{J_1} \sum_{i_2=1}^{J_2} \sum_{i_3=1}^{J_3} \mathscr{B}_3^{(n)}(i_1, i_2, i_3)\, \psi_{i_1}(n_1; z_r) \psi_{i_2}(n_2; z_r) \psi_{i_3}(n_3; z_r) \tag{107}$$

are the second order and third order FRFs, respectively. This alternative way of representing the framework of HOFRFs brings benefits in practical cases. The conventional harmonic probing is very illustrative, but is a white box modelling and depends on the knowledge of the system (either modal or physical parameters). On the other hand, if the differential equations are unknown and are available only input and output measurements, the Volterra models based on Kautz functions expansion can be quite useful.

In order to compare the estimative, the HOFRFs via Volterra series and orthonormal Kautz filters basis from Eqs. (105), (106) and (107) are also computed. Figure 38 shows the comparison of harmonic probing and Volterra-Kautz series where an agreement is verified. As can be seen in Fig. 38(a), the linear FRF $\mathcal{H}_1^{(1)}(\omega)$ presents the resonance peak around 23 Hz and characterize the linear dynamic part of the model. On the other hand, the second order FRF $\mathcal{H}_2^{(1)}(\omega,\omega)$ represents the dynamic of quadratic polynomial nonlinearities and is used to compute the quadratic contribution of the total output predicted by the model. Furthermore, it presents the first resonance close to 23 Hz and the secondary resonance 23/2 Hz as showed in Fig. 38(b). The third order FRF $\mathcal{H}_3^{(1)}(\omega,\omega,\omega)$ is used to describe the dynamic of cubic nonlinearities and is used to predict the cubic contribution of the total output estimated. Figure 38(c) shows the principal diagonal of the third FRF with resonance peaks close to 23, 23/2 and 23/3 Hz representing the fundamental, secondary and tertiary resonances, respectively.

In this work, the Volterra kernels $h_1^{(1)}(n_1)$, $h_2^{(1)}(n_1,n_2)$ and $h_3^{(1)}(n_1,n_2,n_3)$, showed in Fig. 39, from Eq. (103) are estimated through orthonormal Kautz basis expansion based on the chirp input dataset (around the first resonance frequency) and based on modal parameters of the linear part identified with low amplitude excitation level.

The model obtained is used to predict outputs subject to low (0.01 V) and higher (0.15 V) chirp input amplitude with range of excitation frequency around the first resonance frequency. In such case, the Volterra kernels are used to calculate the multiple convolutions with the excitation signals considered in order to estimate the linear, quadratic and cubic contributions where the total output is predicted as a sum of all contributions computed by Volterra series as stated in Eq. (11).

Figure 40 shows the comparison of the output measured (acceleration signal measured at point 3 in the free of the beam) with the one computed by Volterra models where it is possible to see a good agreement for low (in Fig. 40(a)) and higher level of excitation (in Fig. 40(b)). Moreover, it is possible to see clearly that the contribution of the nonlinear components increases significantly by increasing the input amplitude level as

Figure 38 – HOFRFs computed by harmonic probing (–) and discrete-time Volterra-Kautz filters (--▲--).

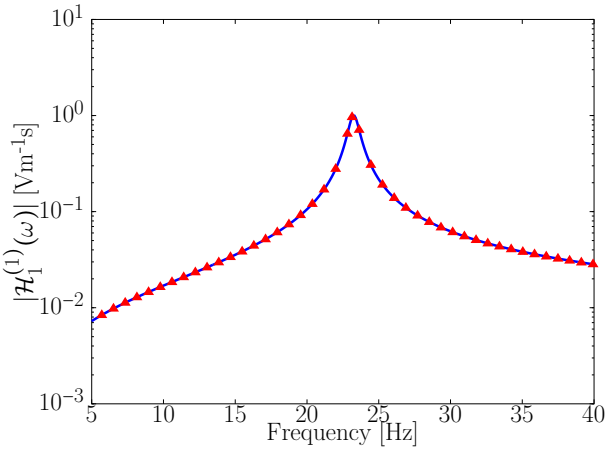

(a) First order FRF.

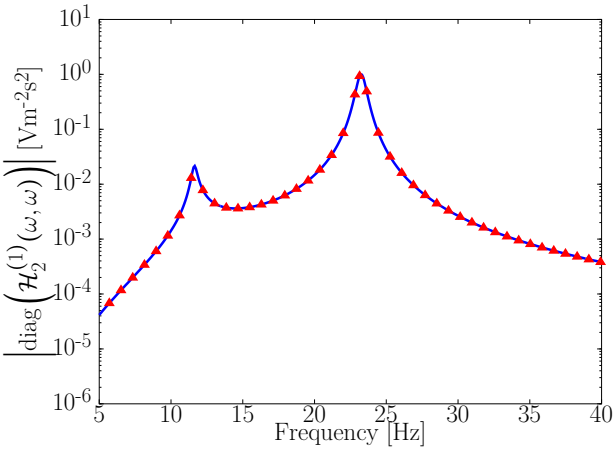

(b) Second order FRF (main diagonal).

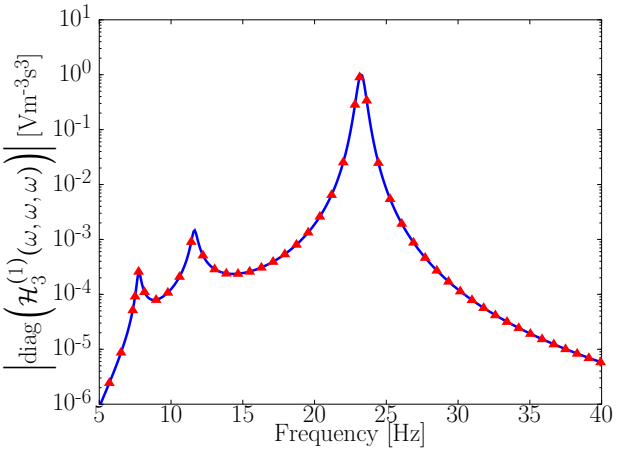

(c) Third order FRF (main diagonal).

Source: Prepared by the author.

showed in Figs 40(c) and 40(d). However, the quadratic prediction presents a very small contribution compared to the cubic one. It is due to the fact that the magneto-elastic system investigated presents characteristics and dominant nonlinearities related to the cubic stiffness. Furthermore, the nonlinear behavior associated to quadratic contributions comes from shaker-stinger-structure interactions than the inherent nonliearities. In order to verify the accuracy of the model, the responses subject to random inputs with low (0.01 V) and higher level (0.15 V) of amplitude are also used. Figures 40(e) and 40(f) show the total responses predicted and is possible to see the response components to the low and high level inputs in Figs. 40(g) and 40(h). In both levels it is observed that the second order component has a small contribution as checked previously by taking into account signals with harmonic nature. Furthermore, it is possible to note that the third order component increases by increasing the amplitude level input pointing out their im-

Figure 39 – Representation of Volterra kernels of first, second and third order in the physical basis.

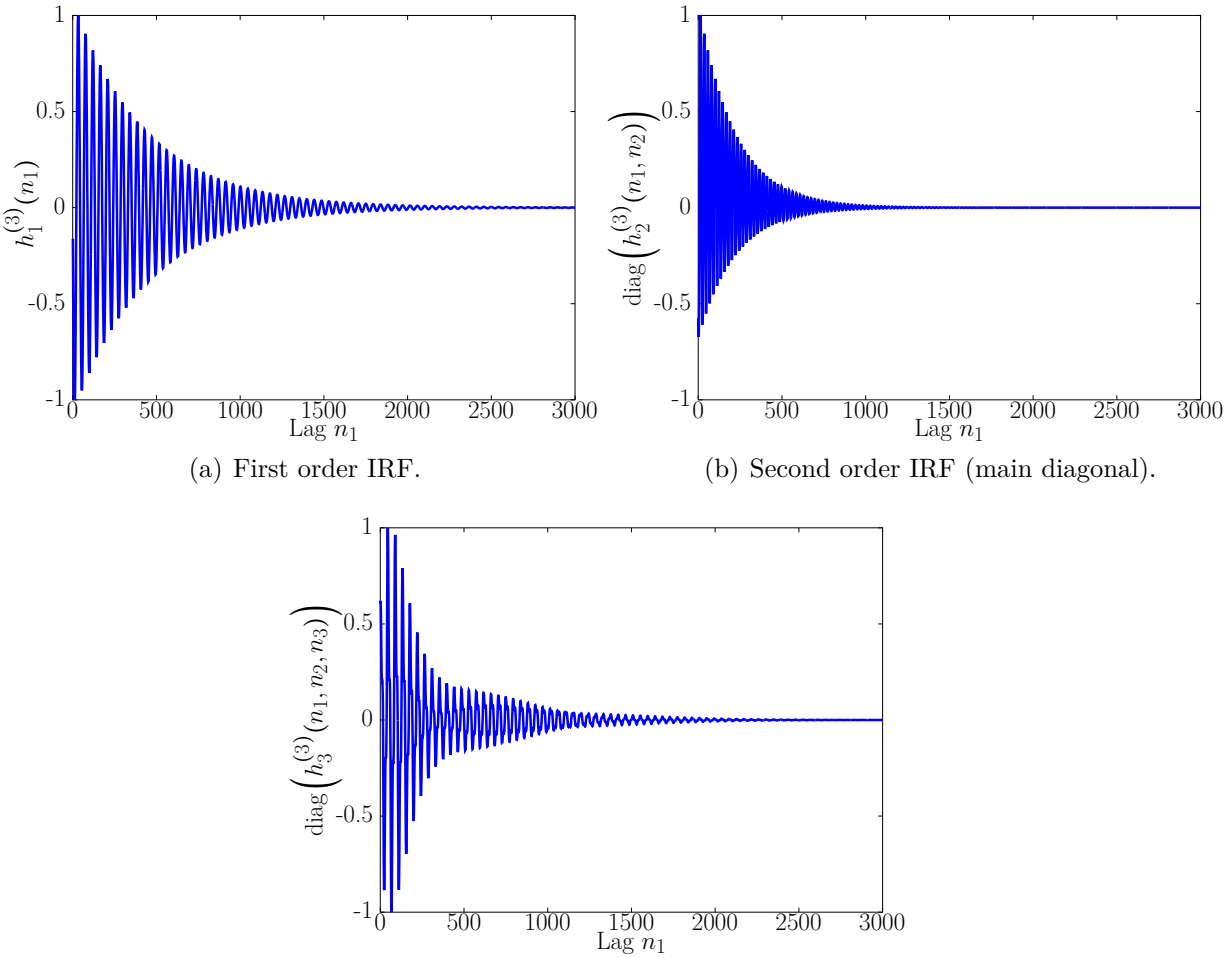

(a) First order IRF.

(b) Second order IRF (main diagonal).

(c) Third order IRF (main diagonal).

Source: Prepared by the author.

portance of being considered in the model when the magneto-elastic beam operates under higher displacements. However, the limitation of the present method lies in the fact that is assumed HOFRFs up to third order only and they might not be adequate/enough to model strong nonlinear effects characterized by restoring forces with more complex effects such as discontinuities. Some limitations related to problem of convergence of Volterra series, strongly nonlinear systems, and errors arise due to measurement noise as expected in some experimental applications. The methodology presented in this chapter has shown to be an alternative tool for modal analysis of weakly nonlinear systems. When the system operates in linear regime of motion, low level of input amplitude, a classical experimental modal analysis technique (curve-fit) can be used to extract the modal parameters to build the linear FRFs. The HOFRFs, multi-dimensional Fourier transform of Volterra kernels, are computed to predict the dynamic behaviour when the system operates in nonlinear

regime of motion. The results based on magneto-elastic beam under low and higher forcing level involving restoring forces characterized by quadratic and cubic stiffness have showed the capabilities of the method proposed to describe and predict inherent weak nonlinearities. Despite having used the vibration data around the first resonance frequency and the respective multiple harmonics of second and third order, the results demonstrated effectiveness of the Volterra series to detect and characterize nonlinear behavior of dynamic structures with effects caused by different levels of excitation.

Figure 40 – Direct comparison between the measured response at point 3 with the response predicted by Volterra model and the respective linear and nonlinear contributions for low 0.01 V (figures on the left) and high amplitude levels 0.15 V (figures on the right) subject to chirp and random input.

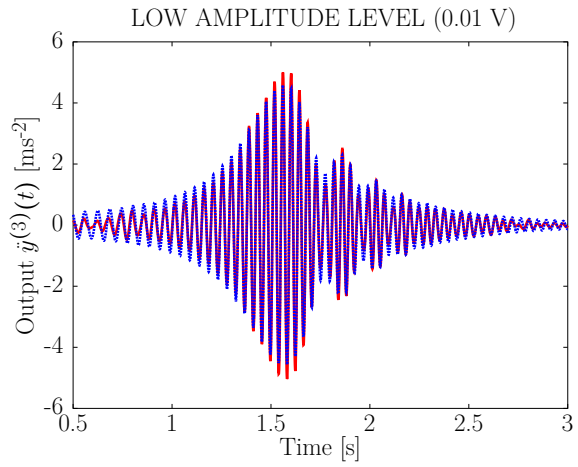

(a) Measured (--) × Predicted (···) response at low level.

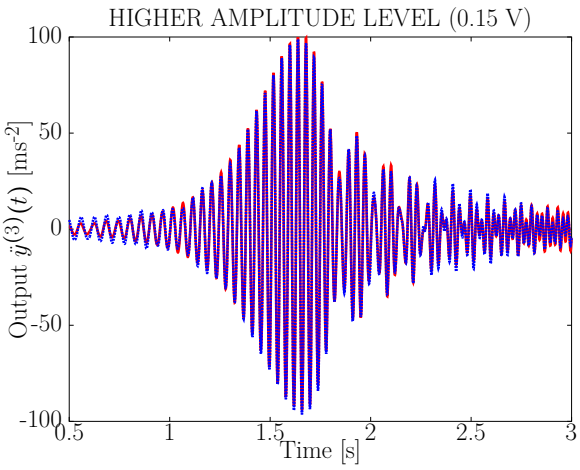

(b) Measured (--) × Predicted (···) response at higher level.

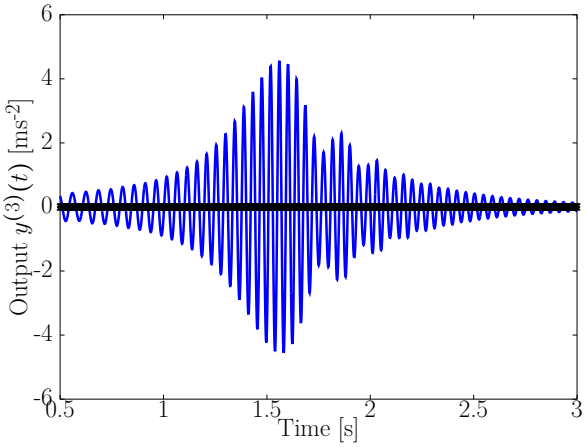

(c) Linear (--), quadratic (*) and cubic (···) contributions.

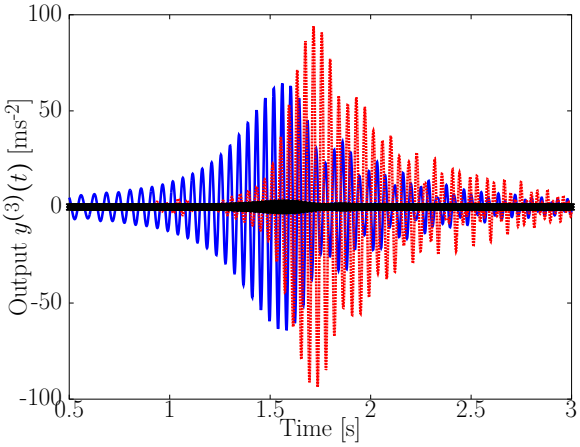

(d) Linear (--), quadratic (*) and cubic (···) contributions.

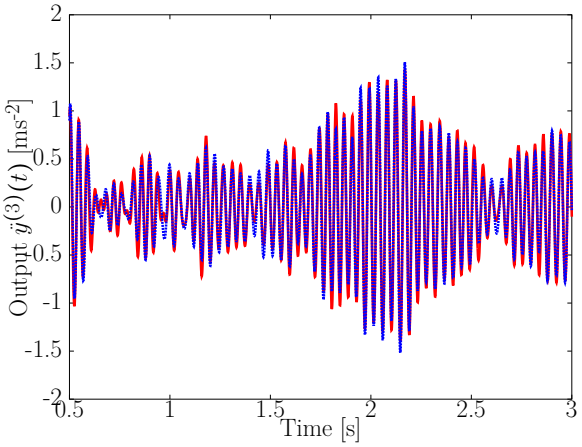

(e) Measured (--) × Predicted (···) response at low level.

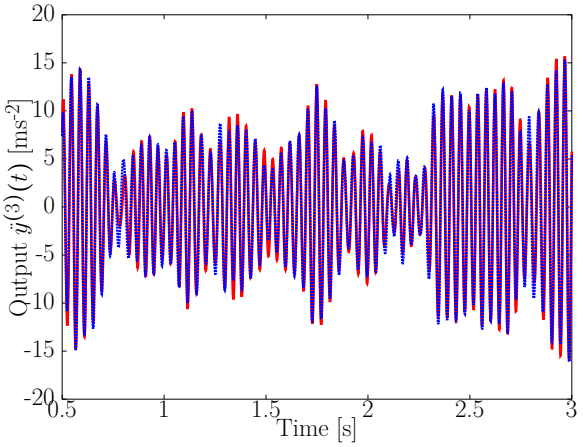

(f) Measured (--) × Predicted (···) response at higher level.

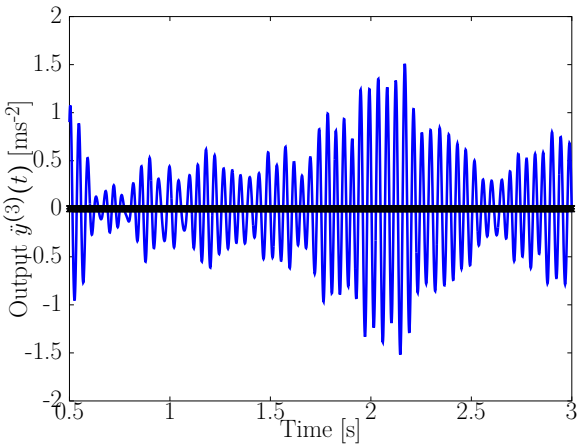

(g) Linear (--), quadratic (*) and cubic (···) contributions.

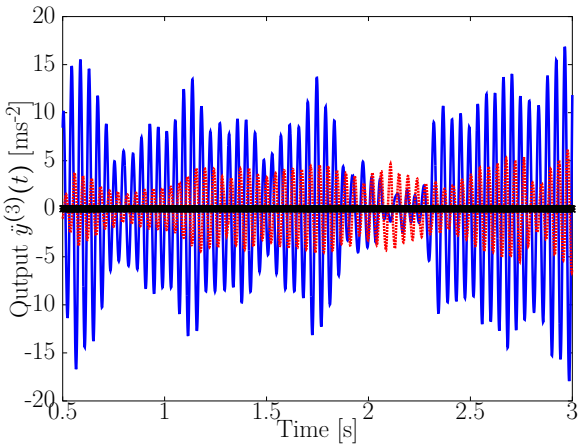

(h) Linear (--), quadratic (*) and cubic (···) contributions.

Source: Prepared by the author.

4.5 Conclusions

This Chapter proposed the application of an alternative and practical methodology through higher-order frequency response functions (HOFRFs) and Volterra series expanded in orthonormal Kautz basis to identify a nonlinear model to reproduce the nonlinear behavior of the magneto-elastic beam. This method leads the problem from spatial space to modal space and provides powerful applicability and benefits in vibrating problems of structural dynamics. Basically, the new representation of HOFRFs allows to analyse inherent properties and natural characteristics of weakly nonlinear systems and they can be simply computed as functions of the conventional FRFs described through an alternative way using the linear modal parameters, natural frequencies, damping factors as well as the mode shapes that are conventionally identified using classical experimental modal analysis.

Based on the results shown, the technique investigated here can be useful in applications for the identification and analysis of weakly nonlinear systems. The HOFRFs and Volterra series based on modal parameters and experimental vibration data can be useful to give information about the nonlinear phenomenon under study, output prediction and parameter estimation of structural dynamics applications. Future steps of this research are concerned with applications involving responses in a wider frequency range of vibration by taking into account multiple mode shapes and output-only signals.

5 Final Remarks

This chapter summarizes briefly the results of the present thesis pointing out the main contributions, advantages and possible limitations. Thus, the chapter is organized as follows. Firstly, it is presented the final remarks highlighting the new results and benefits of each chapter. Afterwards, suggestions for future research topics are carried out.

5.1 Conclusions

Methodologies for analysis, identification and application of Volterra series based on input-output and output-only signals were presented. The algebraic formulation of an extended version of the harmonic probing method via Volterra series expansion to deal with applications where only output signals are available was described in chapter 2. An alternative approach for nonlinear system identification based on output-only signals was presented in chapter 3. A practical methodology for modal analysis of weakly nonlinear system was presented in chapter 4. Thus, the final remarks are listed below:

- The algebraic expressions of the extended Volterra kernels transform were provided as well as their theoretical properties for vibration analysis. It was verified in the Proposition 1 that the framework of extended continuous-time Volterra kernels can be expressed as a combination of the conventional ones similarly to the concept of transmissibility functions. A numerical analysis of a classical two degrees-of-freedom (2DOF) Duffing oscillator showed the effectiveness and potentialities of the extended harmonic probing method. However, it is important to mention that the method was verified only in cases described by weak nonlinearities and might not provide a better understanding of strongly nonlinear systems. Despite this weakness associated to Volterra series expansion, the extended version of the harmonic probing method have shown to be an alternative methodology for analysis of weakly nonlinear systems where only output signals are available.

- The Proposition 2 showed the discrete-time extended Volterra kernels based on output-only data. It was presented an alternative approach for system identification based on discrete-time Volterra series expanded onto orthonormal Kautz basis and output-only data. In this approach at least two output signals measured in different placements are used to compute the multiple convolutions and the excitation signals are not required. It points out the major contribution of this method. The property of separating the polynomial contribution of the response predicted by the model is also a powerful benefit and the presence of harmonics in the response are analysed. The use of orthonormal Kautz filters basis expansion allowed to reduce drastically the large amount of parameters associated to the higher-order kernels and inserted oscillatory behaviour in the nonlinear model identified. The results showed that the modified kernels computed by output-only signals can simulate and predict the linear and nonlinear contributions contained in the responses in a similar way as the conventional Volterra kernels computed with input and output signals. Although this system identification technique is still not able to describe nonlinear systems with strong nonlinearities, it can be used to represent a vast class of applications involving weakly nonlinear systems.

- The new representation of HOFRFs allowed to analyse inherent properties and natural characteristics of weakly nonlinear systems in terms of modal parameters, natural frequencies, damping factors as well as the mode shapes that were conventionally identified by using classical experimental modal analysis. This alternative way of describing these HOFRFs through an algorithm structured by a multi-step excitations have shown the applicability of the method for nonlinearity detection, output prediction, analysis of vibrating tests and parameter estimation of structural dynamics applications. Based on the results shown, the technique investigated showed to be quite useful in applications of identification, analysis and design of weakly nonlinear systems.

5.2 Suggestions for future researches and applications

Future research topics are mentioned below in order to improve the results reached in the present thesis as well as to investigate new hot applications:

- Provide the algebraic expressions for multi-input multi-output systems (MIMO) with multi-degrees-of-freedom (MDOF).

- Extend the concept of transmissibility based on extended higher-order frequency response functions (HOFRFs) and modal parameters aiming problems of structural health monitoring (SHM) for damage detection and location.
- Include the possibility of implementing an adaptive version of the methods presented here for adaptive filtering applications.
- An extension of the methodologies proposed would be very welcome to deal with more applications and to provide a better understanding of the phenomena of interest by taking into account possible uncertainties. The Volterra series were assumed in the present thesis as deterministic approach. However, Volterra kernels and Kautz filters present several uncertainties associated to Kautz parameters and their corresponding coefficients of orthonormal expansion as well. Thus, a study able to consider these issues is very desirable.
- To include random excitations to identify HOFRFs and Volterra models based on operational data.

References

ABED-MERAIN, K. Blind system identification. **Proceedings of the IEEE**, v. 85, n. 8, p. 1310--1322, 1997. Available from: <http://dx.doi.org/10.1109/5.622507>. Access on: 26 Sep. 2013.

ADAMS, D. E. Frequency domain ARX model and multiharmonic FRF estimators for non-linear dynamic systems. **Journal of Sound and Vibration**, London, v. 250, n. 5, p. 935 -- 950, 2002. Available from: <http://www.sciencedirect.com/science/article/pii-/S0022460X01939653>. Access on: 10 Jul. 2014.

ALJANAIDEH, K. F.; BERNSTEIN, D. S. A behavioral equation framework for time-domain transmissibilities. **Automatica**, Kidlington, v. 78, p. 20 -- 24, 2017. ISSN 0005-1098. Available from: <http://www.sciencedirect.com/science/article/pii-/S0005109816304988>. Access on: 10 Feb. 2017.

ALLEMANG, A. J. The modal assurance criterion (mac): Twenty years of use and abuse. **Journal of Sound and Vibration**, London, p. 14--21, 2003. Access on: 15 Jul. 2016.

ALLEN, M. S.; SRACIC, M. W.; CHAUHAN, S.; HANSEN, M. H. Output-only modal analysis of linear time-periodic systems with application to wind turbine simulation data. **Mechanical Systems and Signal Processing**, London, v. 25, n. 4, p. 1174 -- 1191, 2011. Available from: <http://www.sciencedirect.com/science/article/pii-/S0888327011000100>. Access on: 29 Nov. 2016.

AVITABILE, P. Experimental modal analysis. **Sound and vibration**, London, v. 35, n. 1, p. 20--31, 2001. Access on: 5 Jun. 2016.

BANFI, L.; CARASSALE, L. Uncertainties in an application of operational modal analysis. **Model Validation and Uncertainty Quantification, Volume 3: Proceedings of the 34th IMAC, A Conference and Exposition on Structural Dynamics 2016**. Cham: Springer International Publishing, 2016. p. 107--115. Available from: <http://dx.doi.org/10.1007/978-3-319-29754-5_10>. Access on: 15 Dec. 2016.

BEDROSIAN, E.; RICE, S. The output properties of Volterra systems driven by harmonic and gaussian inputs. **Proceedings of the IEEE**, v. 59, p. 1688--1707, 1971. Available from: <http://dx.doi.org/10.1109/PROC.1971.8525>. Access on: 13 Apr. 2015.

BILLINGS, S. Identification of nonlinear systems - a survey. **Control Theory and Applications, IEE Proceedings D**, Stevenage, v. 127, n. 6, p. 272--285, 1980. ISSN 0143-7054. Available from: <http://dx.doi.org/10.1049/ip-d:19800047>. Access on: 9 Oct. 2013.

_____. **Nonlinear system identification: NARMAX methods in the time, frequency, and spatio-temporal domain**. New York: Wiley, 2013.

BILLINGS, S.; FAKHOURI, S. Identification of nonlinear systems using the Wiener model. **Electronics Letters**, Stevenage, v. 13, n. 17, p. 502--504, 1977. Access on: 29 Nov. 2013.

BILLINGS, S.; TSANG, K. Spectral analysis for non-linear systems, part I: Parametric non-linear spectral analysis. **Mechanical Systems and Signal Processing**, London, v. 3, n. 4, p. 319 -- 339, 1989. Available from: <http://www.sciencedirect.com/science-/article/pii/0888327089900411>. Access on: 12 Dec. 2013.

_____. Spectral analysis for non-linear systems, part II: Interpretation of non-linear frequency response functions. **Mechanical Systems and Signal Processing**, London, v. 3, n. 4, p. 341 -- 359, 1989. Available from: <http://www.sciencedirect.com/science-/article/pii/0888327089900423>. Access on: 12 Dec. 2013.

BJÖRSELL, N.; ISAKSSON, M.; HÄNDEL, P.; RÖNNOW, D. Kautz-Volterra modelling of analogue-to-digital converters. **Computer Standards & Interfaces**, Amsterdam, v. 32, n. 3, p. 126 -- 129, 2010. ISSN 0920-5489. Available from: <http://www.sciencedirect.com/science/article/pii/S0920548909000993>. Access on: 21 Feb. 2014.

BJÖRSELL, N.; SUCH · NEK, P.; HÄNDEL, P.; RÖNNOW, D. Measuring Volterra kernels of analog-to-digital converters using a stepped three-tone scan. **IEEE Transactions on Instrumentation and Measurement**, Piscataway, v. 57, n. 4, p. 666--671, 2008. Available from: <http://dx.doi.org/10.1109/TIM.2007.911579>. Access on: 14 Jan. 2014.

BRINCKER, R.; ANDERSEN, P. Ambient response analysis of the heritage court tower building structure. In: **IMAC, 18th, 2000, San Antonio, Texas, USA,: Proceedings of the International Modal Analysis Conference,** [s.n.], 2000. p. 1081-1087. Access on: 03 May 2013.

BRINCKER, R.; ZHANG, L.; ANDERSEN, P. Modal identification of output-only systems using frequency domain decomposition. **Smart Materials and Structures**, Bristol, v. 10, n. 3, p. 441, 2001. Available from: <http://stacks.iop.org/0964-1726/10-/i=3/a=303>. Access on: 30 Jan. 2015.

BROWNJOHN, J.; REYNOLDS, P.; AU, S.; HESTER, D.; BOCIAN, M. Experimental modal analysis of civil structures: State of the art. In: **SHMII - International Conference on Structural Health Monitoring and Intelligent Infrastructure. 7th, 2015, Torino, Italy**. [s.n.], 2015. Available from: <http://hdl.handle.net/10871-/23476>. Access on: 12 Jan. 2016.

CABBOI, A.; AES, F. M.; GENTILE, C.; CUNHA, A. Automated modal identification and tracking: application to an iron arch bridge. **Structural Control and Health Monitoring**, Chichester, v. 24, n. 1, 2017. Available from: <http://dx.doi.org/10.1002-/stc.1854>. Access on: 02 Feb. 2017.

CAFFERTY, S.; TOMLINSON, G. Characterization of automotive dampers using higher order frequency response function. **Journal of Automobile Engineering**, Chenai, v. 211, n. 3, p. 181--203, 1997. Available from: <http://pid.sagepub.com-/content/211/3/181.refs>. Access on: 24 Mar. 2013.

CALDWELL, R. A.; FEENY, B. F. Output-only modal identification of a nonuniform beam by using decomposition methods. **J. Vib. Acoust.**, New York, v. 136, n. 4, 2014. Available from: <10.1115/1.4027243>. Access on: 23 Jul. 2015.

CAMBRAIA, H. N. **Detecção e caracterização de não linearidades em sistemas mecânicos**. Dissertation, Master Degree in Mechanical Engineering - Universidade Estadual de Campinas, Campinas, 1990. Available from: <http://www-.bibliotecadigital.unicamp.br/document/?code=vtls000042385>. Access on: 17 Feb. 2015.

CARASSALE, L.; KAREEM, A. Modeling nonlinear systems by Volterra series. **J. Eng. Mech**, Reston, v. 136, n. 6, p. 801-ñ818., 2010. Available from: <http://dx.doi.org/10-.1061/(ASCE)EM.1943-7889.0000113>. Access on: 04 Jul. 2015.

CAUGHEY, T. K.; O'KELLY, M. E. J. Classical normal modes in damped linear dynamic systems. **J. Appl. Mech**, Tehran, v. 32, n. 3, p. 583--588, 1965. Available from: <http://dx.doi.org/10.1115/1.3627262>. Access on: 28 Aug. 2013.

CHATTERJEE, A. Crack detection in a cantilever beam using harmonic probing and free vibration decay. In: **IMAC, 27, Orlando, Florida, USA**: [s.n.], 2009. Available from: <http://sem-proceedings.com/27i/sem.org-IMAC-XXVII-Conf-s38p004-Crack-Detection-Cantilever-Beam-Using-Harmonic-Probing-Free.pdf>. Access on: 7 Oct. 2013.

_____. Identification and parameter estimation of a bilinear oscillator using Volterra series with harmonic probing. **International Journal of Non-linear Mechanics**, Kidlington, v. 45, n. 1, p. 12--20, 2010. Available from: <http://www.sciencedirect.com-/science/article/pii/S0020746209001632>. Access on: 7 Oct. 2013.

_____. Structural damage assessment in a cantilever beam with a breathing crack using higher order frequency response functions. **Journal of Sound and Vibration**, London, v. 329, n. 16, p. 3325 -- 3334, 2010. Available from: <http://dx.doi.org/10.1016/j.jsv-.2010.02.026>. Access on: 7 Oct. 2013.

_____. Structural damage assessment in a cantilever beam with a breathing crack using higher order frequency response functions. **Journal of Sound and Vibration**, London, v. 329, n. 16, p. 3325 -- 3334, 2010. Available from: <http://www.sciencedirect.com-/science/article/pii/S0022460X10001495>. Access on: 8 Oct. 2013.

_____. Nonlinear dynamics and damage assessment of a cantilever beam with breathing edge crack. **J. Vib. Acoust.**, New York, v. 133, n. 5, p. 051004 (6 pages), 2011. Access on: 10 Oct. 2013.

CHATTERJEE, A.; VYAS, N. Convergence analysis of Volterra series response of nonlinear systems subjected to harmonic excitation. **Journal of Sound and Vibration**, London, v. 236, n. 2, p. 339 -- 358, 2000. Available from: <http:/-/www.sciencedirect.com/science/article/pii/S0022460X00929675>. Access on: 10 Oct. 2013.

CHATTERJEE, A.; VYAS, N. S. Nonlinear parameter estimation in rotor-bearing system using Volterra series and method of harmonic probing. **J. Vib. Acoust.**, New York,

v. 125, n. 3, p. 299--306, 2003. Available from: <http://dx.doi.org/10.1115/1.1547486>. Access on: 8 Oct. 2013.

_____. Non-linear parameter estimation in multi-degree-of-freedom systems using multi-input Volterra series. **Mechanical Systems and Signal Processing**, London, v. 18, n. 3, p. 457 -- 489, 2004. Available from: <http://www.sciencedirect.com/science-/article/pii/S0888327003000165>. Access on: 8 Oct. 2013.

CHEN, S.; BILLINGS, S. A. Representation of non-linear systems: the NARMAX model. **International Journal of Control**, Abingdon, v. 49, n. 3, p. 1013--1032, 1989. Access on: 17 Dec. 2014.

CHEN, W.; LU, Z.; LIN, W.; CHEN, S.; NI, Y.; XIA, Y.; LIAO, W. Theoretical and experimental modal analysis of the guangzhou new TV tower. **Engineering Structures**, Kidlington, v. 33, n. 12, p. 3628 -- 3646, 2011. Available from: <http:/-/www.sciencedirect.com/science/article/pii/S0141029611003129>. Access on: 17 Dec. 2014.

CHENG, C.; PENG, Z.; ZHANG, W.; MENG, G. Volterra-series-based nonlinear system modeling and its engineering applications: A state-of-the-art review. **Mechanical Systems and Signal Processing**, London, v. 87, p. 340--364, 2017. Available from: <http://dx.doi.org/10.1016/j.ymssp.2016.10.029>. Access on: 12 Jan. 2017.

CHENG, C. M.; PENG, Z. K.; ZHANG, W. M.; MENG, G. Wavelet basis expansion-based Volterra kernel function identification through multilevel excitations. **Nonlinear Dynamics**, Dordrecht, v. 76, n. 2, p. 985--999, 2014. ISSN 1573-269X. Available from: <http://dx.doi.org/10.1007/s11071-013-1182-3>. Access on: 03 Mar. 2016.

CHERIF, I.; ABID, S.; FNAIECH, F. Nonlinear blind identification with three-dimensional tensor analysis. **Mathematical Problems in Engineering**, New York, v. 2012, p. 22 pages, Article ID 284815, 2012. Available from: <http://dx.doi.org/10-.1155/2012/284815>. Access on: 18 Aug. 2013.

CHESNÉ, S.; DERAEMAEKER, A. Damage localization using transmissibility functions: A critical review. **Mechanical Systems and Signal Processing**, London, v. 38, n. 2, p. 569 -- 584, 2013. ISSN 0888-3270. Available from: <http://dx.doi.org/10.1016/j-.ymssp.2013.01.020>. Access on: 23 Nov. 2014.

CUNHA, A.; CAETANO, E. Experimental modal analysis of civil engineering structures. **Journal of Sound and Vibration**, London, v. 40, n. 6, p. 12--20, 2006.

CUNHA, T.; LIMA, E.; PEDRO, J. Validation and physical interpretation of the power-amplifier polar Volterra model. **Microwave Theory and Techniques, IEEE Transactions on**, Piscataway, v. 58, n. 12, p. 4012--4021, 2010. Available from: <http://dx.doi.org/10.1109/TMTT.2010.2087347>. Access on: 6 Sep. 2013.

DA SILVA, S. Non-linear model updating of a three-dimensional portal frame based on Wiener series. **International Journal of Non-linear Mechanics**, Kidlington, v. 46, n. 1, p. 312--320, 2011. Available from: <http://dx.doi.org/10.1016/j.ijnonlinmec.2010-.09.014>. Access on: 13 Apr. 2013.

_____. Non-parametric identification of mechanical systems by Kautz filter with multiple poles. **Mechanical Systems and Signal Processing**, London, v. 25, n. 4, p. 1103--1111, 2011. Access on: 27 Mar. 2013.

DA SILVA, S.; COGAN, S.; FOLTÊTE, E. Nonlinear identification in structural dynamics based on Wiener series and Kautz filters. **Mechanical Systems and Signal Processing**, London, v. 24, n. 1, p. 52--58, 2010. Available from: <http://dx.doi.org/10-.1016/j.ymssp.2009.05.017>. Access on: 26 Mar. 2013.

DA SILVA, S.; COGAN, S.; FOLTÊTE, E.; BUFFE, F. Metrics for nonlinear model updating in structural dynamics. **Journal of the Brazilian Society of Mechanical Sciences and Engineering**, Heidelberg, Scielo, v. 31, n. 1, p. 27 -- 34, 2009. Available from: <http://dx.doi.org/10.1590/S1678-58782009000100005>. Access on: 27 Mar. 2013.

DA SILVA, S.; Dias Jr, M.; LOPES Jr, V. Identification of mechanical systems through Kautz filter. **Journal of Vibration and Control**, London, v. 15, n. 6, p. 849--865, 2009. Access on: 29 Mar. 2013.

DIAFERIO, M.; FOTI, D.; MONGELLI, M.; GIANNOCCARO, N. I.; ANDERSEN, P. Operational modal analysis of a historic tower in bari. In: **IMAC, 29, 2011, New York, Proceedings of the 29th IMAC, A Conference on Structural Dynamics, 2011**. New York, NY: Springer New York, 2011. p. 335--342. Available from: <http://dx.doi.org/10.1007/978-1-4419-9316-8_31>. Access on: 13 Apr. 2014.

DZIEDZIECH, K.; STASZEWSKI, W.; UHL, T. Wavelet-based modal analysis for time-variant systems. **Mechanical Systems and Signal Processing**, Kidlington, v. 50-51, p. 323 -- 337, 2015. Available from: <http://www.sciencedirect.com/science-/article/pii/S0888327014001320>. Access on: 17 Jan. 2016.

EWINS, D. J. **Modal testing: theory, practice and application**. Hertordshire: Reasearch Studies, 2000.

FALCO, M.; LIU, M.; NGUYEN, S. H.; CHELIDZE, D. Nonlinear system identification and modeling of a new fatigue testing rig based on inertial forces. **J. Vib. Acoust.**, New York, v. 136, n. 4, p. 041001, 2014. Available from: <http://dx.doi.org/10.1115/1-.4027317>. Access on: 09 Oct. 2015.

FERNANDES, C. A.; FAVIER, G.; MOTA, J. C. M. Blind identification of multiuser nonlinear channels using tensor decomposition and precoding. **Signal Processing**, Amsterdam, v. 89, n. 12, p. 2644 -- 2656, 2009. Special Section: Visual Information Analysis for Security. Available from: <http://www.sciencedirect.com/science/article-/pii/S0165168409002163>. Access on: 25 Apr. 2013.

FRACHEBOURG, A.; KUSTER, F.; GYGAX, P. Practical application of the Volterra series: Modal analysis of higher order. **CIRP Annals - Manufacturing Technology**, Amsterdam, v. 37, n. 1, p. 347 -- 350, 1988. Available from: <http:/-/www.sciencedirect.com/science/article/pii/S0007850607616515>. Access on: 17 Jan. 2016.

GIFFORD, S.; TOMLINSON, G. Recent advances in the application of functional series to non-linear structures. **Journal of Sound and Vibration**, London, v. 135, n. 2, p.

289 -- 317, 1989. Available from: <http://www.sciencedirect.com/science/article/pii-/0022460X8990727X>. Access on: 24 Apr. 2013.

GROSEL, J.; SAWICKI, W.; PAKOS, W. Application of classical and operational modal analysis for examination of engineering structures. **Procedia Engineering**, Amsterdam, v. 91, p. 136 -- 141, 2014. Available from: <http://www.sciencedirect.com-/science/article/pii/S1877705814030537>. Access on: 05 May 2015.

GRUBER, J.; BORDONS, C.; OLIVA, A. Nonlinear MPC for the airflow in a PEM fuel cell using a Volterra series model. **Control Engineering Practice**, Kidlington, v. 20, n. 2, p. 205 -- 217, 2012. ISSN 0967-0661. Available from: <http:-//www.sciencedirect.com/science/article/pii/S0967066111002322>. Access on: 02 Jun. 2013.

GRUBER, J.; RAMIREZ, D.; LIMON, D.; ALAMO, T. Computationally efficient nonlinear min-max model predictive control based on Volterra series models-application to a pilot plant. **Journal of Process Control**, London, v. 23, n. 4, p. 543 -- 560, 2013. ISSN 0959-1524. Available from: <http://www.sciencedirect.com/science/article/pii-/S0959152413000176>. Access on: 13 Jan. 2014.

HANSEN, C.; SHIKI, S. B.; V., L. J.; SILVA, S. da. Non-parametric identification of a non-linear buckled beam using discrete-time Volterra series. In: **International Conference on Structural Dynamics - EURODYN, 9th**. Porto, Portugal.: [s.n.], 2014. p. 2013--2018. Access on: 21 Dez. 2014.

HEUBERGER, P. S.; HOF, P. M. V. D.; WAHLBERG, B. **Modelling and Identification with Rational Orthogonal Basis Functions**. London: Springer, 2005.

HOT, A.; KERSCHEN, G.; FOLTÊTE, E.; COGAN, S. Detection and quantification of non-linear structural behavior using principal component analysis. **Mechanical Systems and Signal Processing**, London, v. 26, n. 0, p. 104 -- 116, 2012. Available from: <http://www.sciencedirect.com/science/article/pii/S0888327011002287>. Access on: 21 Mar. 2013.

IBNKAHLA, M. Statistical analysis of neural network modeling and identification of nonlinear systems with memory. **Signal Processing, IEEE Transactions on**, Piscataway, v. 50, n. 6, p. 1508--1517, 2002. Available from: <http://dx.doi.org/110-.1109/TSP.2002.1003073>. Access on: 02 Nov. 2013.

_____. Nonlinear system identification using neural networks trained with natural gradient descent. **Journal on Applied Signal Processing**, Heidelberg, v. 12, p. 1229--1237, 2003. Available from: <http://dx.doi.org/10.1155/S1110865703306079>. Access on: 22 Jan. 2014.

ISASA, I.; HOT, A.; COGAN, S.; SADOULET-REBOUL, E. Model updating of locally non-linear systems based on multi-harmonic extended constitutive relation error. **Mechanical Systems and Signal Processing**, London, v. 25, n. 7, p. 2413 -- 2425, 2011. Available from: <http://www.sciencedirect.com/science/article/pii-/S0888327011001282>. Access on: 12 Apr. 2013.

JAFARIAN, A.; MEASOOMY, S.; ABBASBANDY, S. Artificial neural networks based modeling for solving Volterra integral equations system. **Applied Soft Computing**, Amsterdam, v. 27, p. 391 -- 398, 2015. Available from: <http:/-/www.sciencedirect.com/science/article/pii/S1568494614005481>. Access on: 22 Nov. 2015.

KAIZER, A. Modeling of the nonlinear response of an electrodynamic loudspeaker by a Volterra series expansion. **Audio Engineering Society**, New York, v. 35, n. 6, p. 421--432, 1987. Available from: <http://www.aes.org/e-lib/browse.cfm?elib=5201>. Access on: 06 May 2013.

KALOUPTSIDIS, N.; KOUKOULAS, P. Blind identification of Volterra-Hammerstein systems. In: **SIEEE WORKSHOP ON STATISTICAL SIGNAL PROCESSING**, [S.I.:s.n.], 2003 p. 202--205. Available from: <http://dx.doi.org/10.1109/SSP.2003-.1289379>. Access on: 02 Feb. 2014.

KAUTZ, W. H. Transient synthesis in the time domain. **IRE Transactions on Circuit Theory**, New York, n. 1, p. 29 -- 39, 1954. Available from: <http://dx.doi.org/10.1109-/TCT.1954.1083588>. Access on: 18 Mar. 2013.

KERSCHEN, G.; PEETERS, M.; GOLINVAL, J. C.; STéPHAN, C. Nonlinear modal analysis of a full-scale aircraft. **Journal of Aircraft**, Reston, v. 50, p. 1409--1419, 2013. Access on: 28 Aug. 2013.

KERSCHEN, G.; WORDEN, K.; VAKAKIS, J. G. A. F. Past, present and future of nonlinear system identification in structural dynamics. **Mechanical Systems and Signal Processing**, London, v. 20, n. 3, p. 505--592, 2006. Available from: <http://www.sciencedirect.com/science/article/pii/S0888327005000828>. Access on: 21 Jul. 2013.

KHOUAJA, A.; KIBANGOU, A.; FAVIER, G. Third-order Volterra kernels complexity reduction using PARAFAC. In: **Control, Communications and Signal Processing**. [S.I.:s.n.], 2004. p. 857--860. Available from: <http://dx.doi.org/10.1109/ISCCSP.2004-.1296581>. Access on: 13 Apr. 2013.

KIM, Y. Prediction of the dynamic response of a slender marine structure under an irregular ocean wave using the NARX-based quadratic Volterra series. **Applied Ocean Research**, Kidlington, v. 49, p. 42--56, 2015. Available from: <http://dx.doi.org/10-.1016/j.apor.2014.11.002> Access on: 24 Jan. 2016.

KORENBERG, M.; HUNTER, I. The identification of nonlinear biological systems: Volterra kernel approaches. **Annals of Biomedical Engineering**, New York, v. 24, n. 4, p. A250--A268, 1996. Available from: <http://dx.doi.org/10.1007/BF02648117>. Access on: 13 Jul. 2014.

KOVACIC IVANA; BRENNAN, M. J. **The Duffing equation: nonlinear oscillators and their behaviour.** [S.l.: s.n.], 2011.

LANG, Z.; PARK, G.; FARRAR, C.; TODD, M.; MAO, Z.; ZHAO, L.; WORDEN, K. Transmissibility of non-linear output frequency response functions with application in detection and location of damage in MDOF structural systems. **International Journal of Non-Linear Mechanics**, Kidlington, v. 46, n. 6, p. 841 -- 853, 2011. Available from:

<http://www.sciencedirect.com/science/article/pii/S0020746211000333>. Access on: 17 Sep. 2013.

LEE, D. Short-term prediction of wind farm output using the recurrent quadratic Volterra model. In: **POWER AND ENERGY SOCIETY GENERAL MEETING**. [S.I.], 2011. New York, IEEE, 2011. p. 1--8. Available from: <http://dx.doi.org/10.1109-/PES.2011.6039128>. Access on: 30 Mar. 2013.

LEE, G. Estimation of non-linear system parameters using higher-order frequency response functions. **Mechanical Systems and Signal Processing**, London, v. 11, n. 2, p. 219 -- 228, 1997. Available from: <http://www.sciencedirect.com/science/article-/pii/S0888327096900801>. Access on: 23 Jul. 2013.

LENAERTS, V.; KERSCHEN, G.; GOLINVAL, J. ECL benchmark: Application of the proper orthogonal decomposition. **Mechanical Systems and Signal Processing**, London, v. 17, n. 1, p. 237 -- 242, 2003. Available from: <http://www.sciencedirect.com-/science/article/pii/S0888327002915657>. Access on: 03 Sep. 2013.

LI, D.; REN, W. X.; HU, Y. D.; YANG, D. Operational modal analysis of structures by stochastic subspace identification with a delay index. **Structural Engineering and Mechanics**, Daejeon, v. 59, n. 1, p. 187--207, 2016. Access on: 28 Dec. 2016.

LJUNG, L. **System identification: theory for the user**. 2nd. ed. [S.l.]: PTR Prentice Hall, 2007.

MAIA, N. M. M.; SILVA, J. M. M.; RIBEIRO, A. M. R. The transmissibility concept in multi-degree-of-freedom systems. **Mechanical Systems and Signal Processing**, London, v. 15, n. 1, p. 129 -- 137, 2001. Available from: <http://dx.doi.org/10.1006-/mssp.2000.1356>. Access on: 12 Dec. 2015.

MAIA, N. M. M.; SILVA, J. M. M. e. **Theoretical and Experimental Modal Analysis**. Taunton: Research Studies, 1997.

MANKTELOW, K. L.; LEAMY, M. J.; RUZZENE, M. Analysis and experimental estimation of nonlinear dispersion in a periodic string. **J. Vib. Acoust**, New York, v. 136, n. 3, p. 031016, 2014. Access on: 03 Feb. 2015.

MASRI, S. F.; CAUGHEY, T. K. A nonparametric identification technique for nonlinear dynamic problems. **ASME. J. Appl. Mech.**, Tehran, v. 46, n. 2, p. 433--447, 1979. Available from: <http://dx.doi.org/10.1115/1.3424568>. Access on: 24 Apr. 2013.

MAYBEE, J. S. Normal and quasi-normal modes in damped linear dynamic systems. **ASME. J. Appl. Mech**, Tehran v. 33, n. 2, p. 413--416, 1966. Available from: <http://dx.doi.org/10.1115/1.3625058>. Access on: 24 Apr. 2013.

MILANESE, A. **Volterra series revisited, with applications in nonlinear structural dynamics and aeroelasticity**. 2009. PhDThesis (Doctorate) --- Clarkson University, Postdam, 2009. Available from: <http://gateway.proquest-.com/openurl%3furl_ver=Z39.88-2004%26res_dat=xri:pqdiss%26rft_val_fmt=info:ofi-/fmt:kev:mtx:dissertation%26rft_dat=xri:pqdiss:3353900>. Access on: 14 Jun. 2013.

MOHAMED, V. O. M.; M'HIRI, R. An approach to polynomial NARX/NARMAX systems identification in a closed-loop with variable structure control. **International Journal of Automation and Computing**, Beijing, v. 5, n. 3, p. 313--318, 2008. Access on: 06 Jan. 2014.

NARAYANAN, S.; POON, H. C. An analysis of distortion in bipolar transistors using integral charge control model and Volterra series. **Circuit Theory, IEEE Transactions on**, New York, v. 20, n. 4, p. 341--351, 1973. Available from: <http://dx.doi.org/10.1109/TCT.1973.1083708>. Access on: 07 Jan. 2014.

NEWMARK, N. M. A method of computation for structural dynamics. **Journal of Engineering Mechanics, ASCE**, New York, v. 85, n. EM3, p. 67--94, 1959. Access on: 06 Jan. 2014.

NOËL, J.; KERSCHEN, G. Frequency-domain subspace identification for nonlinear mechanical systems. **Mechanical Systems and Signal Processing**, London, v. 40, n. 2, p. 701 -- 717, 2013. Available from: <http://www.sciencedirect.com/science/article-/pii/S088832701300318X>. Access on: 26 Dec. 2013.

_____. Nonlinear system identification in structural dynamics: 10 more years of progress. **Mechanical Systems and Signal Processing**, London, v. 83, p. 2 -- 35, 2017. Available from: <http://www.sciencedirect.com/science/article/pii/S088832701630245X>. Access on: 12 Jan. 2017.

NOËL, J.; MARCHESIELLO, S.; KERSCHEN, G. Subspace-based identification of a nonlinear spacecraft in the time and frequency domains. **Mechanical Systems and Signal Processing**, London, v. 43, n. 1-2, p. 217 -- 236, 2014. Available from: <http://www.sciencedirect.com/science/article/pii/S0888327013005578>. Access on: 26 Dec. 2015.

NOËL, J.; RENSON, L.; KERSCHEN, G. Complex dynamics of a nonlinear aerospace structure: Experimental identification and modal interactions. **Journal of Sound and Vibration**, London, v. 333, n. 12, p. 2588 -- 2607, 2014. Available from: <http://www.sciencedirect.com/science/article/pii/S0022460X14000704>. Access on: 16 Dec. 2014.

NOVÁK, A. Identification of nonlinear systems: Volterra series simplification. **Acta Polytechnica**, Prague, v. 47, n. 4-5, p. 72--75, 2007. Available from: <http://ojs.cvut.cz/ojs/index.php/ap/article/view/976>. Access on: 13 Jan. 2014.

OGUNFUNMI, T. **Adaptative nonlinear system identification: The Volterra and Wiener model approaches**. London: Springer, 2007.

OZBEK, M.; RIXEN, D. J. A new analysis methodology for estimating the eigenfrequencies of systems with high modal damping. **Journal of Sound and Vibration**, London, v. 361, p. 290 -- 306, 2016. Available from: <http://www-.sciencedirect.com/science/article/pii/S0022460X15007907>. Access on: 22 Dec. 2016.

PASQUALI, M.; LACARBONARA, W.; MARZOCCA, P. Detection of nonlinearities in plates via higher-order-spectra: Numerical and experimental studies. **J. Vib.**

Acoust., New York, v. 136, n. 4, p. 041015 (13 pages), 2014. Available from: <http://dx.doi.org/10.1115/1.4027625>. Access on: 09 Feb. 2015.

PENG, Z.; LANG, Z. On the convergence of the Volterra-series representation of the Duffing's oscillators subjected to harmonic excitations. **Journal of Sound and Vibration**, London, v. 305, n. 1-2, p. 322 -- 332, 2007. Available from: <http://dx.doi.org/10.1016/j.jsv.2007.03.062>. Access on: 27 Aug. 2013.

PENG, Z.; LANG, Z.; BILLINGS, S.; TOMLINSON, G. Comparisons between harmonic balance and nonlinear output frequency response function in nonlinear system analysis. **Journal of Sound and Vibration**, London, v. 311, n. 1-2, p. 56--73, 2008. Available from: <http://dx.doi.org/10.1016/j.jsv.2007.08.035>. Access on: 12 Jun. 2013.

PLATTEN, M.; WRIGHT, J.; DIMITRIADIS, G.; COOPER, J. Identification of multi-degree of freedom non-linear systems using an extended modal space model. **Mechanical Systems and Signal Processing**, London, v. 23, n. 1, p. 8 -- 29, 2009. Special Issue: Non-linear Structural Dynamics. Available from: <http:/-/www.sciencedirect.com/science/article/pii/S0888327007002610>. Access on: 14 Apr. 2013.

POULIMENOS, A. G.; FASSOIS, S. D. Output-only stochastic identification of a time-varying structure via functional series TARMA models. **Mechanical Systems and Signal Processing**, London, v. 23, n. 4, p. 1180 -- 1204, 2009. Available from: <http://www.sciencedirect.com/science/article/pii/S0888327008002707>. Access on: 04 Jul. 2013.

PRAWIN, J.; RAO, A. R. M. Nonlinear identification of MDOF systems using Volterra series approximation. **Mechanical Systems and Signal Processing**, London, v. 84, Part A, p. 58 -- 77, 2017. Available from: <http://www.sciencedirect.com/science-/article/pii/S0888327016302217>. Access on: 16 Feb. 2017.

RAZ, G. M.; VEEN, B. V. Blind equalization and identification of nonlinear and IIR systems-a least squares approach. **Signal Processing, IEEE Transactions on**, Piscataway, v. 48, n. 1, p. 192--200, 2000. Available from: <http://dx.doi.org/10.1109-/78.815489>. Access on: 16 Jul. 2013.

RIJLAARSDAM, D.; NUIJ, P.; SCHOUKENS, J.; STEINBUCH, M. A comparative overview of frequency domain methods for nonlinear systems. **Mechatronics**, Kidlington, v. 42, p. 11 -- 24, 2017. Available from: <http://www.sciencedirect.com/science/article-/pii/S0957415816301568>. Access on: 16 Feb. 2017.

ROSENBERG, R. The normal modes of nonlinear n-degree-of-freedom system. **American Society of Mechanical Engineers**, Kidlington, v. 29, n. 1, p. 7--14, 1962.

RUGH, W. J. **Nonlinear system theory - The Volterra/Wiener approach**. [S.l.]: University Press, 1981.

SAKELLARIOU, J.; FASSOIS, S. D. Nonlinear arx (narx) based identification and fault detection in a 2 dof system with cubic stiffness. In: **INTERNATIONAL CONFERENCE ON NOISE AND VIBRATIONS ENGINEERING**,

2002, Leuven, Belgium, [s.n.], 2002. p 1--8. Available from: <http://www.smsa-.upatras.gr/publications/2002/2002_Cubic_Stiffness_ISMA.pdf>. Access on: 23 May 2014.

SCHETZEN, M. **The Volterra and Wiener theories of nonlinear systems**. [S.l.]: Wiley, 1980.

SCUSSEL, O.; da Silva, S. Identification of output-only nonlinear mechanical systems using Volterra series. In: **DINAME 2015 - INTERNATIONAL SYMPOSIUM ON DYNAMIC PROBLEMS OF MEHCANICS, 2015** Natal, RN, Brazil: [s.n.], 2015. Access on: 11 Nov. 2015.

_____. Identification of nonlinear mechanical systems: Comparison between harmonic probing and Volterra-Kautz methods. In: **Proceeding Series of the Brazilian Society of Computational and Applied Mathematics**. [s.n.], 2016. v. 4, n. 1. Available from: <http://dx.doi.org/10.5540/03.2016.004.01.0080>. Access on: 21 Nov. 2015.

_____. Output-only identification of nonlinear systems via Volterra series. **ASME. J. Vib. Acoust.**, New York, v. 138, n. 4, p. 041012--041012 (13 pages), 2016. Available from: <http://dx.doi.org/10.1115/1.4033458>. Access on: 21 Oct. 2016.

_____. The harmonic probing method for output-only nonlinear mechanical systems. **Journal of the Brazilian Society of Mechanical Sciences and Engineering**, Heidelberg, p. 1--13, 2017. ISSN 1806-3691. Available from: <http://dx.doi.org/10.1007-/s40430-017-0723-y>. Access on: 02 Mar. 2017.

SCUSSEL, O.; DA SILVA, S.; VASCONCELOS, G. J. Q.; VILLANI, L. G. G.; SHIKI, S. B. Identification of mechanical systems through Volterra series - study of benchmark cases. In: **Proceeding Series of the Brazilian Society of Computational and Applied Mathematics**. [s.n.], 2013. v. 1, n. 1. Available from: <http://dx.doi.org/10.5540/03.2013.001.01.0020>. Access on: 12 Jan. 2014.

SCUSSEL, O.; SILVA, A. A.; da Silva, S. Modeling of the dynamics of a gyroscope using Volterra series. In: **IBERO-LATIN AMERICAN CONGRESS ON COMPUTATIONAL METHODS IN ENGINEERING (CILAMCE). Proceedings**, 34, PirenÛpolis, Go, Brasil. [s.n.], 2013. Access on: 07 Apr. 2014.

SHAW, S.; PIERRE, C. Normal modes for non-linear vibratory systems. **Journal of Sound and Vibration**, London, v. 164, n. 1, p. 85 -- 124, 1993. Available from: <http://www.sciencedirect.com/science/article/pii/S0022460X83711983>. Access on: 12 Mar. 2014.

_____. Normal modes of vibration for non-linear continuous systems. **Journal of Sound and Vibration**, London, v. 169, n. 3, p. 319 -- 347, 1994. Available from: <http://www.sciencedirect.com/science/article/pii/S0022460X84710212>. Access on: 12 Mar. 2014.

SHIKI, S. B. **Application of Volterra series in nonlinear mechanical system identification and in structural health monitoring problems**. 2016. 115 p. PhDThesis (Doctorate) --- UNESP - Universidade Estadual Paulista Júlio de Mesquita Filho, Faculdade de Engenharia, March 2016. Access on: 12 apr. 2016.

SHIKI, S. B.; DA SILVA, S.; TODD, M. D. On the application of discrete-time Volterra series for the damage detection problem in initially nonlinear systems. **Structural Health Monitoring**, London, v. 16, n. 1, p. 62--78, 2017. Available from: <http://dx.doi.org/10.1177/1475921716662142>. Access on: 26 Feb. 2017.

SHIKI, S. B.; HANSEN, C.; DA SILVA, S. Nonlinear features identified by Volterra series for damage detection in a buckled beam. **MATEC WEB OF CONFERENCES, INTERNATIONAL CONFERENCE ON STRUCTURAL NONLINEAR DYNAMICS AND DIAGNOSIS (CSNDD14)**, 2nd, 2014. Agadir, Morocco: [s.n.], 2014. p. 02003. Available from: <http://dx.doi.org/10.1051/matecconf/20141602003>. Access on: 16 Mar. 2015.

SHIKI, S. B.; LOPES Jr, V.; DA SILVA, S. Model updating of the non-linear vibrating structures through Volterra series and proper orthogonal decomposition. In: **INTERNATIONAL CONFERENCE ON NOISE AND VIBRATION ENGINEERING ? ISMA**, 2012, Leuven, Belgium: [s.n.], 2012. Access on: 16 Mar. 2015.

_____. Identification of nonlinear structures using discrete-time Volterra series. **Journal of the Brazilian Society of Mechanical Sciences and Engineering**, Berlin Heidelberg, v. 36, n. 3, p. 523--532, 2014. Available from: <http://dx.doi.org/10.1007-/s40430-013-0088-9>. Access on: 17 Mar. 2015.

SHIKI, S. B.; SAMUEL, D.; SANTOS, F. L. M.; PEETERS, B. Characterization of the nonlinear behavior of a f-16 aircraft using discrete-time Volterra series. In: **INTERNATIONAL CONFERENCE ON NOISE AND VIBRATION ENGINEERING ? ISMA**, 2014, Leuven, Belgium: [s.n.], 2014. Access on: 16 Mar. 2015.

SILVA, W. Identification of nonlinear aeroelastic systems based on the Volterra theory: Progress and opportunities. **Nonlinear Dynamics**, Dordrecht, v. 39, p. 25--62, 2005. Available from: <http://dx.doi.org/10.1007/s11071-005-1907-z>. Access on: 03 May 2013.

SJÖBERG, J.; ZHANG, Q.; LJUNG, L.; BENVENISTE, A.; DEYLON, B.; GLORENNEC, P.; HJALMARSSON, H.; JUDITSKY, A. Nonlinear black-box modeling in system identification: a unified overview. **Automatica**, Kidlington, v. 31, n. 12, p. 1691 -- 1724, 1995. Available from: <http://www.sciencedirect.com/science/article/pii-/0005109895001208>. Access on: 12 May 2013.

SPIRIDONAKOS, M.; FASSOIS, S. Parametric identification of a time-varying structure based on vector vibration response measurements. **Mechanical Systems and Signal Processing**, London, v. 23, n. 6, p. 2029 -- 2048, 2009. Special Issue: Inverse Problems. Available from: <http://www.sciencedirect.com/science/article/pii-/S0888327008003099>. Access on: 12 May 2013.

STORER, D.; TOMLINSON, G. Recent developments in the measurement and interpretation of higher order transfer functions from non-linear structures. **Mechanical Systems and Signal Processing**, London, v. 7, n. 2, p. 173 -- 189, 1993. Available from: <http://www.sciencedirect.com/science/article/pii/S088832708371006X>. Access on: 22 Apr. 2013.

STORER, D. M. **Dynamic analysis of non-linear structures using higher order frequency response functions**. PhDThesis (Doctorate) --- University of Manchester, 1991. Available from: <http://www3.imperial.ac.uk/pls/portallive/docs/1/40377701-.PDF>. Access on: 23 Sep. 2014.

TAN, H.-Z.; ABOULNASR, T. Tom-based blind identification of nonlinear Volterra systems. **Instrumentation and Measurement, IEEE Transactions on**, Piscataway, v. 55, n. 1, p. 300--310, 2006. Available from: <http://dx.doi.org/10.1109/TIM.2005-.861496>. Access on: 23 Jan. 2015.

TAN, H.-Z.; HUANG, Y.; FU, J. Blind identification of sparse Volterra systems. **International Journal of Adaptive Control and Signal Processing**, Chichester, John Wiley & Sons, Ltd., v. 22, n. 7, p. 652--662, 2008. Available from: <http://dx.doi-.org/10.1002/acs.1011>. Access on: 07 Aug. 2013.

TANG, B.; BRENNAN, M.; JR, V. L.; SILVA, S. da; RAMLAN, R. Using nonlinear jumps to estimate cubic stiffness nonlinearity: An experimental study. **Proceedings of the Institution of Mechanical Engineers, Part C: Journal of Mechanical Engineering Science**, 2015. Available from: <http://pic.sagepub.com/content/early-/2015/09/15/0954406215606746.abstract>.

TANG, D.; WANG, Z.; YUE, Q.; SHI, Z.; FENG, J. Modal analysis of multi-degree-of-freedom dynamic system based on non-stationary response data. **Journal of Sound and Vibration**, London, v. 347, p. 139 -- 149, 2015. Available from: <http://www.sciencedirect.com/science/article/pii/S0022460X1500142X>. Access on: 14 Jan. 2016.

TANG, H.; LIAO, Y.; CAO, J.; XIE, H. Fault diagnosis approach based on Volterra models. **Mechanical Systems and Signal Processing**, London, v. 24, n. 4, p. 1099 -- 1113, 2010. Available from: <http://www.sciencedirect.com/science/article/pii-/S0888327009002611>. Access on: 26 Apr. 2013.

TAWFIQ, I.; VINH, T. Contribution to the extension of modal analysis to non-linear structure using Volterra funcitonal series. **Mechanical Systems and Signal Processing**, Lonond, v. 17, n. 2, p. 379 -- 407, 2003. Available from: <http:/-/www.sciencedirect.com/science/article/pii/S0888327002914998>. Access on: 23 Sep. 2014.

THOUVEREZ, F. A new convergence criteria of volterra series for harmonic inputs. In: **IMAC, INTERNATIONAL MODAL ANALYSIS CONFERENCE**, 16, 1998, Santa Barbara, CA, USA: [s.n.], 1998.

THOUVEREZ, F.; JEZEQUEL, L. Identification of NARMAX models on a modal base. **Journal of Sound and Vibration**, London, v. 189, n. 2, p. 193 -- 213, 1996. Available from: <http://www.sciencedirect.com/science/article/pii/S0022460X96900152>. Access on: 12 Jan. 2014.

TOMLINSON, G.; MANSON, G.; LEE, G. A simple criterion for establishing an upper limit to the harmonic excitation level of the Duffing oscillator using the Volterra series. **Journal of Sound and Vibration**, London, v. 190, n. 5, p. 751 -- 762, 1996. Available from: <http://www.sciencedirect.com/science/article/pii/S0022460X96900917>. Access on: 20 Jan. 2014.

VAERENBERGH, S. V.; VÍA, J.; SANTAMARÍA, I. Adaptive kernel canonical correlation analysis algorithms for nonparametric identification of Wiener and Hammerstein systems. **EURASIP J. Adv. Signal Process**, New York, v. 2008, p. 123:1--123:13, 2008. Available from: <http://dx.doi.org/10.1155/2008/875351>. Access on: 10 Apr. 2015.

VAKAKIS, A. Non-linear normal modes (nnms) and their applications in vibration theory: An overview. **Mechanical Systems and Signal Processing**, London, v. 11, n. 1, p. 3 -- 22, 1997. Available from: <http://www.sciencedirect.com/science/article/pii/S0888327096999999>. Access on: 13 Jul. 2014.

VIRGIN, L. **Introduction to experimental nonlinear dynamics: a case study in mechanical vibration**. 1st. ed. Cambridge University Press, 2000. ISBN 9780521779319. Available from: <http://books.google.com.br/books?id=L8dLzjTpyhAC>. Access on: 13 Jul. 2014.

VOLTERRA, V. **Theory of functionals and of integral and integro-differential equations**. [S.l.]: Dover Publications, 1959.

WAHLBERG, B. System identification using Kautz models. **IEEE Tansactions On Automatic Control**, Piscataway, v. 39, n. 6, p. 1276 -- 1282, 1994. Available from: <http://dx.doi.org/10.1109/9.293196>. Access on: 2 Jul. 2014.

WEIJTJENS, W.; SITTER, G. D.; DEVRIENDT, C.; GUILLAUME, P. Operational modal parameter estimation of MIMO systems using transmissibility functions. **Automatica**, Kidlington, v. 50, n. 2, p. 559 -- 564, 2014. Available from: <http://dx.doi.org/10.1016/j.automatica.2013.11.021>. Access on: 04 Dec. 2014.

WIENER, N. **Nonlinear problems in randon theory**. New York: Wiley, 1958.

WILLS, A.; SCHÖN, T. B.; LJUNG, L.; NINNESS, B. Identification of Hammerstein-Wiener models. **Automatica**, Kidlington, v. 49, n. 1, p. 70 -- 81, 2013. Available from: <http://www.sciencedirect.com/science/article/pii/S0005109812004815>. Access on: 12 Feb. 2014.

WORDEN, K.; GREEN, P. A machine learning approach to nonlinear modal analysis. **Mechanical Systems and Signal Processing**, London, v. 84, Part B, p. 34 -- 53, 2017. Recent advances in nonlinear system identification. Available from: <http://www.sciencedirect.com/science/article/pii/S0888327016300681>. Access on: 04 Feb. 2017.

WORDEN, K.; HICKEY, D.; HAROON, M.; ADAMS, D. E. Nonlinear system identification of automotive dampers: A time and frequency-domain analysis. **Mechanical Systems and Signal Processing**, v. 23, n. 1, p. 104 -- 126, 2009. Special Issue: Non-linear Structural Dynamics. Available from: <http://www.sciencedirect.com/science/article/pii/S0888327008000630>. Access on: 10 Aug. 2014.

WORDEN, K.; MANSON, G. A Volterra series approximation to the coherence of the duffing oscillator. **Journal of Sound and Vibration**, London, v. 286, n. 3, p. 529 -- 547, 2005. ISSN 0022-460X. Available from: <http://www.sciencedirect.com/science/article/pii/S0022460X04008399>. Access on: 21 Jun. 2014.

WORDEN, K.; MANSON, G.; TOMLINSON, G. A harmonic probing algorithm for the multi-input Volterra series. **Journal of Sound and Vibration**, London, v. 201, n. 1, p. 67 -- 84, 1997. ISSN 0022-460X. Available from: <http://www-.sciencedirect.com/science/article/pii/S0022460X96907464>. Access on: 10 Aug. 2014.

WORDEN, K.; TOMLINSON, G. R. **Nonlinearity in Structural Dynamics**. London: Institute of Physics, 2001.

XIA, X.; ZHOU, J.; XIAO, J.; XIAO, H. A novel identification method of Volterra series in rotor-bearing system for fault diagnosis. **Mechanical Systems and Signal Processing**, London, v. 66-67, p. 557 -- 567, 2016. Available from: <http:/-/www.sciencedirect.com/science/article/pii/S0888327015002277>. Access on: 18 Oct. 2016.

XU, G.; LIU, H.; TONG, L.; KAILATH, T. A least-squares approach to blind channel identification. **Signal Processing, IEEE Transactions on**, Piscataway, v. 43, n. 12, p. 2982--2993, 1995.

XU, Y.; KO, J.; YU, Z. Modal analysis of tower-cable system of tsing ma long suspension bridge. **Engineering Structures**, Kidlington, v. 19, n. 10, p. 857 -- 867, 1997. Available from: <http://www.sciencedirect.com/science/article/pii/S0141029697001582>. Access on: 10 Apr. 2013.

XUE, Z.-P.; LI, M.; JIA, H.-G. Modal method for dynamics analysis of cantilever type structures at large rotational deformations. **International Journal of Mechanical Sciences**, Kidlington, v. 93, p. 22 -- 31, 2015. Available from: <http://www-.sciencedirect.com/science/article/pii/S0020740315000041>. Access on: 13 Apr. 2016.

YANG, S.; ALLEN, M. S. Output-only modal analysis using continuous-scan laser doppler vibrometry and application to a 20 kW wind turbine. **Mechanical Systems and Signal Processing**, London, v. 31, p. 228 -- 245, 2012. Available from: <http://www.sciencedirect.com/science/article/pii/S0888327012001392>. Access on: 07 Jun. 2013.

YANG, Y.; NAGARAJAIAH, S. Output-only modal identification with limited sensors using sparse component analysis. **Journal of Sound and Vibration**, v. 332, n. 19, p. 4741 -- 4765, 2013. Available from: <http://www.sciencedirect.com/science/article/pii-/S0022460X13003210>. Access on: 22 May 2014.

ZHANG, B.; BILLINGS, S. Volterra series truncation and kernel estimation of nonlinear systems in the frequency domain. **Mechanical Systems and Signal Processing**, London, v. 84, Part A, p. 39 -- 57, 2017. Available from: <http:/-/www.sciencedirect.com/science/article/pii/S0888327016302333>. Access on: 25 Feb. 2017

ZHANG, Q.; SUKI, B.; WESTWICK, D.; LUTCHEN, K. Factors affecting Volterra kernel estimation: Emphasis on lung tissue viscoelasticity. **Annals of Biomedical Engineering**, New York, v. 26, n. 1, p. 103--116, 1998. Available from: <http://www.ncbi.nlm.nih.gov/pubmed/10355555>. Access on: 10 Apr. 2013.

ZHAO, X. Y.; LANG, Z. Q.; PARK, G.; FARRAR, C. R.; TODD, M. D.; MAO, Z.; WORDEN, K. A new transmissibility analysis method for detection and location of damage via nonlinear features in mdof structural systems. **IEEE/ASME Transactions on Mechatronics**, Piscataway, v. 20, n. 4, p. 1933--1947, 2015. Available from: <http://dx.doi.org/10.1109/TMECH.2014.2359419>. Access on: 03 Nov. 2016

ZOU, T.; ZHANG, J.; PANG, J.; LI, C.; LIU, B.; JIA, W.; WANG, Y.; XU, C. The structure modal analysis and engineering application of the passenger car driver's seat system. In: _____. **Proceedings of SAE-China Congress 2015: Selected Papers**. Singapore: Springer Singapore, 2016. p. 349--363. Available from: <http://dx.doi.org/10.1007/978-981-287-978-3_32>. Access on: 13 Dec. 2016

ZWOLSKI, J.; BIEŃ, J. Modal analysis of bridge structures by means of forced vibration tests. **Journal of Civil Engineering and Management**, Vilnius, v. 17, n. 4, p. 590--599, 2011. Available from: <http://dx.doi.org/10.3846/13923730.2011.632489>. Access on: 07 Jul. 2014

Appendix A - Algebraic Expressions of HOFRFs

This appendix shows the algebraic expressions for the higher-order frequency response functions (HOFRFs) of the nonlinear part of Eq. (75) from Chapter 4 and eighteen specific case studies are described. For such cases, it is considered different locations of the nonlinear restoring forces involving stiffness components. Tables 4 and 5 show six cases where the nonlinear restoring forces are described by cubic springs. As mentioned before, the operator $\Delta^{(2)}(t) = y^{(2)}(t) - y^{(1)}(t)$ denotes the nonlinear component of stiffness between the masses 1 and 2.

Tables 6 and 7 show the cases where the nonlinear restoring forces are characterized by cubic dampers only. In such cases $\dot{\Delta}^{(2)}(t) = \dot{y}^{(2)}(t) - \dot{y}^{(1)}(t)$ is the nonlinear component of damping. Additionally, the cases involving both cubic dampers and springs are showed in Tabs. 8 and 9.

Table 4 – HOFRFs of a Duffing 2DOF oscillator characterized by cubic springs.

Cases	Higher-order FRFs
I	$\mathcal{H}_3^{(1)}(\omega,\omega,\omega) = -\beta[\mathcal{H}_1^{(1)}(\omega)]^3\mathcal{H}_1^{(1)}(3\omega)$ $\mathcal{H}_3^{(2)}(\omega,\omega,\omega) = 0$
II	$\mathcal{H}_3^{(1)}(\omega,\omega,\omega) = -\beta[\mathcal{H}_1^{(2)}(\omega) - \mathcal{H}_1^{(1)}(\omega)]^3\mathcal{H}_1^{(1)}(3\omega)$ $\mathcal{H}_3^{(2)}(\omega,\omega,\omega) = \beta[\mathcal{H}_1^{(2)}(\omega) - \mathcal{H}_1^{(1)}(\omega)]^3\mathcal{H}_1^{(2)}(3\omega)$
III	$\mathcal{H}_3^{(1)}(\omega,\omega,\omega) = 0$ $\mathcal{H}_3^{(2)}(\omega,\omega,\omega) = -\beta[\mathcal{H}_1^{(2)}(\omega)]^3\mathcal{H}_1^{(2)}(3\omega)$
IV	$\mathcal{H}_3^{(1)}(\omega,\omega,\omega) = -\beta[[\mathcal{H}_1^{(1)}(\omega)]^3 + [\mathcal{H}_1^{(2)}(\omega) - \mathcal{H}_1^{(1)}(\omega)]^3]\mathcal{H}_1^{(1)}(3\omega)$ $\mathcal{H}_3^{(2)}(\omega,\omega,\omega) = \beta[\mathcal{H}_1^{(2)}(\omega) - \mathcal{H}_1^{(1)}(\omega)]^3\mathcal{H}_1^{(2)}(3\omega)$
V	$\mathcal{H}_3^{(1)}(\omega,\omega,\omega) = -\beta[\mathcal{H}_1^{(1)}(\omega)]^3\mathcal{H}_1^{(1)}(3\omega)$ $\mathcal{H}_3^{(2)}(\omega,\omega,\omega) = -\beta[\mathcal{H}_1^{(2)}(\omega)]^3\mathcal{H}_1^{(2)}(3\omega)$
VI	$\mathcal{H}_3^{(1)}(\omega,\omega,\omega) = -\beta[[\mathcal{H}_1^{(1)}(\omega)]^3 + [\mathcal{H}_1^{(2)}(\omega) - \mathcal{H}_1^{(1)}(\omega)]^3]\mathcal{H}_1^{(1)}(3\omega)$ $\mathcal{H}_3^{(2)}(\omega,\omega,\omega) = -\beta[[\mathcal{H}_1^{(2)}(\omega)]^3 - [\mathcal{H}_1^{(2)}(\omega) - \mathcal{H}_1^{(1)}(\omega)]^3]\mathcal{H}_1^{(2)}(3\omega)$

Table 5 – Nonlinear components a Duffing 2DOF oscillator characterized by cubic springs.

Cases	Nonlinear force $\{\boldsymbol{F}_{nl}(\boldsymbol{y})\}$	Location of nonlinear component
I	$\begin{Bmatrix} \beta(y^{(1)}(t))^3 \\ 0 \end{Bmatrix}$	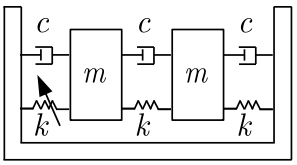
II	$\begin{Bmatrix} \beta(\Delta^{(2)}(t))^3 \\ -\beta(\Delta^{(2)}(t))^3 \end{Bmatrix}$	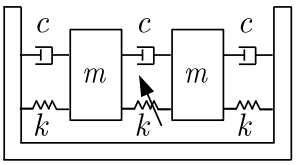
III	$\begin{Bmatrix} 0 \\ \beta(y^{(2)}(t))^3 \end{Bmatrix}$	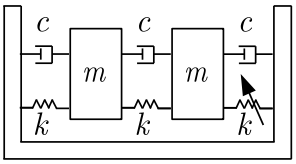
IV	$\begin{Bmatrix} \beta(y^{(1)}(t))^3 + \beta(\Delta^{(2)}(t))^3 \\ -\beta(\Delta^{(2)}(t))^3 \end{Bmatrix}$	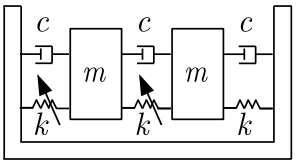
V	$\begin{Bmatrix} \beta(y^{(1)}(t))^3 \\ \beta(y^{(2)}(t))^3 \end{Bmatrix}$	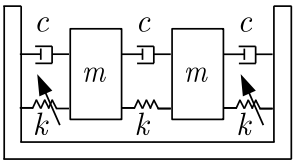
VI	$\begin{Bmatrix} \beta(y^{(1)}(t))^3 + \beta(\Delta^{(2)}(t))^3 \\ \beta(y^{(2)}(t))^3 - \beta(\Delta^{(2)}(t))^3 \end{Bmatrix}$	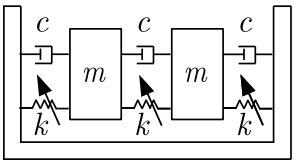

Table 6 – HOFRFs of a Duffing 2DOF oscillator characterized by cubic dampers.

Cases	Higher-order FRFs
VII	$\mathcal{H}_3^{(1)}(\omega,\omega,\omega) = j\omega^3\gamma[\mathcal{H}_1^{(1)}(\omega)]^3\mathcal{H}_1^{(1)}(3\omega)$ $\mathcal{H}_3^{(2)}(\omega,\omega,\omega) = 0$
VIII	$\mathcal{H}_3^{(1)}(\omega,\omega,\omega) = -j\omega^3\gamma[\mathcal{H}_1^{(2)}(\omega) - \mathcal{H}_1^{(1)}(\omega)]^3\mathcal{H}_1^{(1)}(3\omega)$ $\mathcal{H}_3^{(2)}(\omega,\omega,\omega) = -j\omega^3\gamma[\mathcal{H}_1^{(2)}(\omega) - \mathcal{H}_1^{(1)}(\omega)]^3\mathcal{H}_1^{(2)}(3\omega)$
IX	$\mathcal{H}_3^{(1)}(\omega,\omega,\omega) = 0$ $\mathcal{H}_3^{(2)}(\omega,\omega,\omega) = j\omega^3\gamma[\mathcal{H}_1^{(2)}(\omega)]^3\mathcal{H}_1^{(2)}(3\omega)$
X	$\mathcal{H}_3^{(1)}(\omega,\omega,\omega) = j\omega^3\gamma[[\mathcal{H}_1^{(1)}(\omega)]^3 + [\mathcal{H}_1^{(2)}(\omega) - \mathcal{H}_1^{(1)}(\omega)]^3]\mathcal{H}_1^{(1)}(3\omega)$ $\mathcal{H}_3^{(2)}(\omega,\omega,\omega) = -j\omega^3\gamma[\mathcal{H}_1^{(2)}(\omega) - \mathcal{H}_1^{(1)}(\omega)]^3\mathcal{H}_1^{(2)}(3\omega)$
XI	$\mathcal{H}_3^{(1)}(\omega,\omega,\omega) = j\omega^3\gamma[\mathcal{H}_1^{(1)}(\omega)]^3\mathcal{H}_1^{(1)}(3\omega)$ $\mathcal{H}_3^{(2)}(\omega,\omega,\omega) = j\omega^3\gamma[\mathcal{H}_1^{(2)}(\omega)]^3\mathcal{H}_1^{(2)}(3\omega)$
XII	$\mathcal{H}_3^{(1)}(\omega,\omega,\omega) = j\omega^3\gamma[[\mathcal{H}_1^{(1)}(\omega)]^3 + [\mathcal{H}_1^{(2)}(\omega) - \mathcal{H}_1^{(1)}(\omega)]^3]\mathcal{H}_1^{(1)}(3\omega)$ $\mathcal{H}_3^{(2)}(\omega,\omega,\omega) = j\omega^3\gamma[[\mathcal{H}_1^{(2)}(\omega)]^3 - [\mathcal{H}_1^{(2)}(\omega) - \mathcal{H}_1^{(1)}(\omega)]^3]\mathcal{H}_1^{(2)}(3\omega)$

Table 7 – Nonlinear components a Duffing 2DOF oscillator characterized by cubic dampers.

Cases	Nonlinear force $\{\boldsymbol{F}_{nl}(\dot{\boldsymbol{y}})\}$	Location of nonlinear component
VII	$\begin{Bmatrix}\gamma(\dot{y}^{(1)}(t))^3 \\ 0\end{Bmatrix}$	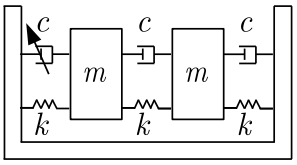
VIII	$\begin{Bmatrix}\gamma(\dot{\Delta}^{(2)})^3 \\ -\gamma(\dot{\Delta}^{(2)})^3\end{Bmatrix}$	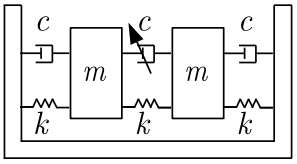
IX	$\begin{Bmatrix}0 \\ \gamma(\dot{y}^{(2)}(t))^3\end{Bmatrix}$	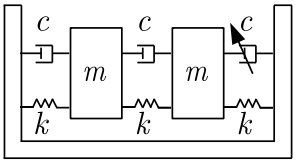
X	$\begin{Bmatrix}\gamma(\dot{y}^{(1)}(t))^3+\gamma(\dot{\Delta}^{(2)})^3 \\ -\gamma(\dot{\Delta}^{(2)})^3\end{Bmatrix}$	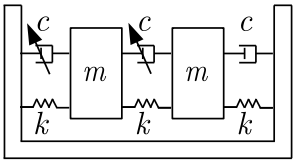
XI	$\begin{Bmatrix}\gamma(\dot{y}^{(1)}(t))^3 \\ \gamma(\dot{y}^{(2)}(t))^3\end{Bmatrix}$	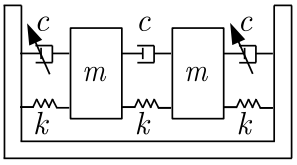
XII	$\begin{Bmatrix}\gamma(\dot{y}^{(1)}(t))^3+\gamma(\dot{\Delta}^{(2)})^3 \\ \gamma(\dot{y}^{(2)}(t))^3-\gamma(\dot{\Delta}^{(2)})^3\end{Bmatrix}$	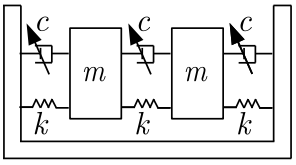

Table 8 – HOFRFs of a Duffing 2DOF oscillator characterized by both cubic springs and dampers.

Cases	Higher-order FRFs
XIII	$\mathcal{H}_3^{(1)}(\omega,\omega,\omega) = (\beta - j\omega^3\gamma)[\mathcal{H}_1^{(1)}(\omega)]^3\mathcal{H}_1^{(1)}(3\omega)$ $\mathcal{H}_3^{(2)}(\omega,\omega,\omega) = 0$
XIV	$\mathcal{H}_3^{(1)}(\omega,\omega,\omega) = -(\beta - j\omega^3\gamma)[\mathcal{H}_1^{(2)}(\omega) - \mathcal{H}_1^{(1)}(\omega)]^3\mathcal{H}_1^{(1)}(3\omega)$ $\mathcal{H}_3^{(2)}(\omega,\omega,\omega) = -(\beta - j\omega^3\gamma)[\mathcal{H}_1^{(2)}(\omega) - \mathcal{H}_1^{(1)}(\omega)]^3\mathcal{H}_1^{(2)}(3\omega)$
XV	$\mathcal{H}_3^{(1)}(\omega,\omega,\omega) = 0$ $\mathcal{H}_3^{(2)}(\omega,\omega,\omega) = (\beta - j\omega^3\gamma)[\mathcal{H}_1^{(2)}(\omega)]^3\mathcal{H}_1^{(2)}(3\omega)$
XVI	$\mathcal{H}_3^{(1)}(\omega,\omega,\omega) = (\beta - j\omega^3\gamma)[[\mathcal{H}_1^{(1)}(\omega)]^3 + [\mathcal{H}_1^{(2)}(\omega) - \mathcal{H}_1^{(1)}(\omega)]^3]\mathcal{H}_1^{(1)}(3\omega)$ $\mathcal{H}_3^{(2)}(\omega,\omega,\omega) = -(\beta - j\omega^3\gamma)[\mathcal{H}_1^{(2)}(\omega) - \mathcal{H}_1^{(1)}(\omega)]^3\mathcal{H}_1^{(2)}(3\omega)$
XVII	$\mathcal{H}_3^{(1)}(\omega,\omega,\omega) = (\beta - j\omega^3\gamma)[\mathcal{H}_1^{(1)}(\omega)]^3\mathcal{H}_1^{(1)}(3\omega)$ $\mathcal{H}_3^{(2)}(\omega,\omega,\omega) = (\beta - j\omega^3\gamma)[\mathcal{H}_1^{(2)}(\omega)]^3\mathcal{H}_1^{(2)}(3\omega)$
XVIII	$\mathcal{H}_3^{(1)}(\omega,\omega,\omega) = (\beta - j\omega^3\gamma)[[\mathcal{H}_1^{(1)}(\omega)]^3 + [\mathcal{H}_1^{(2)}(\omega) - \mathcal{H}_1^{(1)}(\omega)]^3]\mathcal{H}_1^{(1)}(3\omega)$ $\mathcal{H}_3^{(2)}(\omega,\omega,\omega) = (\beta - j\omega^3\gamma)[[\mathcal{H}_1^{(2)}(\omega)]^3 - [\mathcal{H}_1^{(2)}(\omega) - \mathcal{H}_1^{(1)}(\omega)]^3]\mathcal{H}_1^{(2)}(3\omega)$

Table 9 – Nonlinear Duffing 2DOF oscillator characterized by cubic dampers and springs.

Cases	Nonlinear force $\{\boldsymbol{F}_{nl}(\boldsymbol{y},\dot{\boldsymbol{y}})\}$	Location of nonlinear force
XIII	$\begin{Bmatrix}\beta(y^{(1)}(t))^3+\gamma(\dot{y}^{(1)}(t))^3\\ 0\end{Bmatrix}$	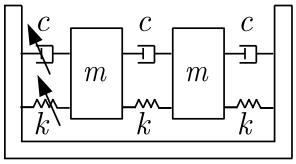
XIV	$\begin{Bmatrix}\beta(y^{(1)}(t))^3+\gamma(\dot{y}^{(1)}(t))^3+\beta(\Delta^{(2)}(t))^3+\gamma(\dot{\Delta}^{(2)}(t))^3\\ -\beta(\Delta^{(2)}(t))^3-\gamma(\dot{\Delta}^{(2)}(t))^3\end{Bmatrix}$	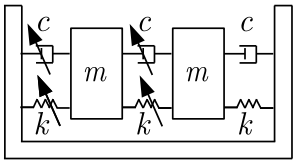
XV	$\begin{Bmatrix}\beta(y^{(1)}(t))^3+\beta(\Delta^{(2)}(t))^3+\gamma(\dot{\Delta}^{(2)}(t))^3\\ -\beta(\Delta^{(2)}(t))^3-\gamma(\dot{\Delta}^{(2)}(t))^3+\gamma(\dot{y}^{(2)}(t))^3\end{Bmatrix}$	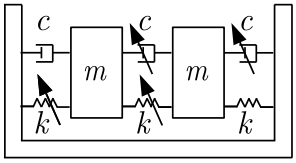
XVI	$\begin{Bmatrix}\gamma(\dot{y}^{(1)}(t))^3+\beta(\Delta^{(2)}(t))^3+\gamma(\dot{\Delta}^{(2)}(t))^3\\ \beta(y^{(1)}(t))^3-\beta(\Delta^{(2)}(t))^3-\gamma(\dot{\Delta}^{(2)}(t))^3\end{Bmatrix}$	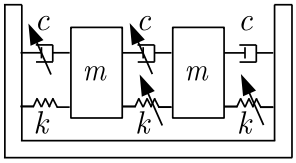
XVII	$\begin{Bmatrix}\beta(\Delta^{(2)}(t))^3+\gamma(\dot{\Delta}^{(2)}(t))^3\\ -\beta(\Delta^{(2)}(t))^3-\gamma(\dot{\Delta}^{(2)}(t))^3\end{Bmatrix}$	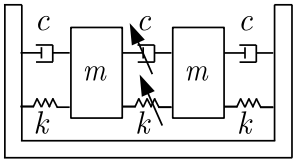
XVIII	$\begin{Bmatrix}\beta(y^{(1)}(t))^3+\gamma(\dot{y}^{(1)}(t))^3+\beta(\Delta^{(2)}(t))^3+\gamma(\dot{\Delta}^{(2)}(t))^3\\ \beta(y^{(2)}(t))^3+\gamma(\dot{y}^{(2)}(t))^3-\beta(\Delta^{(2)}(t))^3-\gamma(\dot{\Delta}^{(2)}(t))^3\end{Bmatrix}$